ANKARA YILDIRIM BEYAZIT UNIVERSITY

GRADUATE SCHOOL OF NATURAL AND APPLIED SCIENCES

DESIGN AND STRUCTURAL ANALYSIS OF UNIQUE LATTICE STRUCTURE WITH NEGATIVE POISSON'S RATIO

M.Sc. Thesis by

İbrahim AKSOY

Department of Mechanical Engineering

July, 2022

ANKARA

DESIGN AND STRUCTURAL ANALYSIS OF UNIQUE LATTICE STRUCTURE WITH NEGATIVE POISSON'S RATIO

A Thesis Submitted to

The Graduate School of Natural and Applied Sciences of

Ankara Yıldırım Beyazıt University

In Partial Fulfillment of the Requirements for the Degree of Master of Science in Mechanical Engineering, Department of Mechanical Engineering

by

İbrahim AKSOY

July, 2022

ANKARA

M.Sc. THESIS EXAMINATION RESULT FORM

We have read the thesis entitled **"DESIGN AND STRUCTURAL ANALYSIS OF UNIQUE LATTICE STRUCTURE WITH NEGATIVE POISSON'S RATIO"** completed by **İBRAHİM AKSOY** under the supervision of **ASSOC. PROF. DR. İHSAN TOKTAŞ** and we certify that in our opinion it is fully adequate, in scope and in quality, as a thesis for the degree of Master of Science.

Assoc. Prof. Dr. İhsan TOKTAŞ

Supervisor

Assist. Prof. Dr. Mostafa RANJBAR

Jury Member

Prof. Dr. Murat Tolga ÖZKAN

Jury Member

Prof. Dr. Sadettin ORHAN

Director

Graduate School of Natural and Applied Sciences

ETHICAL DECLARATION

I hereby declare that, in this thesis which has been prepared in accordance with the Thesis Writing Manual of Graduate School of Natural and Applied Sciences,

- All data, information and documents are obtained in the framework of academic and ethical rules,
- All information, documents and assessments are presented in accordance with scientific ethics and morals,
- All the materials that have been utilized are fully cited and referenced,
- No change has been made on the utilized materials,
- All the works presented are original,

and in any contrary case of above statements, I accept to renounce all my legal rights.

Date: 21.07.2022 **Signature:** ……..

Name & Surname: İbrahim AKSOY

ACKNOWLEDGMENTS

Firstly, I would like to express my sincere gratitude to my supervisor, Assoc. Prof. Dr. İhsan TOKTAŞ who does not spare his knowledge, experience and support so that I improve in the best way during my undergraduate and graduate education, I will take an example his energy, hard work, humanitarian and academic principles.

I am grateful to all the staff of my second home, which ensures us to study in peace at Ankara Yıldırım Beyazıt University, of which I am proud to be a member and student.

Finally, I must express my profound appreciations to my dear Mother and Father, who have always been by my side since I was born, who did not spare any material and moral sacrifices, who are still constantly watching my way, and whose rights I will never be able to repay.

2022, 21 July **İbrahim AKSOY**

DESIGN AND STRUCTURAL ANALYSIS OF UNIQUE LATTICE STRUCTURE WITH NEGATIVE POISSON'S RATIO

ABSTRACT

The positive Poisson's ratio is one of the common and characteristic features of most materials. Materials with a negative Poisson's ratio are called auxetic materials. Materials with auxetic behavior are rare in nature. Auxetic materials, unlike normal materials, contract in compression and expand in tension, due to the negative Poisson's ratios. Materials with negative Poisson's ratio have energy absorbency, fracture strength, thermal shock resistance, etc. properties are expected to be high. For this reason, it is planned to be used in many fields such as biomedicine, defense industry and aviation.

Structural analysis was run according to the thickness and angle parameters of the unique lattice structure with negative Poisson's ratio determined in the first part of the study. Poisson's ratios of 15 different lattice structures in total were calculated according to 3 different thicknesses and 5 different angles. The lowest Poisson's ratio was found to be -0.70. Then, geometric improvements were made with two different methods by keeping the mass of the lattice structure with the lowest Poisson's ratio constant and the improvements were modeled numerically. As a result of the applied improvements, finite element analysis was performed again and the Poisson's ratios of the lattice structures with two different methods were calculated as -0.78 and -0.73. Finally, in order to compare the mechanical properties of three different lattice structures, modal, static structural and explicit dynamics analyzes were carried out using the finite element method. According to the results of the analysis made after the new numerical model was applied, it was observed that there was a significant decrease in the stresses on the lattice structure.

As a result; It has been concluded that the stresses of auxetic geometries with different lattices can be reduced by mathematical models developed with special formulas.

Keywords: Auxetic structure, negative Poisson's ratio, lattice structure, structural analysis, geometric improvement, mathematical modelling.

NEGATİF POISSON ORANINA SAHİP ÖZGÜN LATİS YAPI TASARIMI VE YAPISAL ANALİZİ

ÖZ

Pozitif Poisson oranı çoğu malzemenin ortak ve karakteristik özelliklerinden biridir. Negatif Poisson oranına sahip malzemeler ise daha sınırlı sayıda olup auxetic malzeme olarak isimlendirilir. Auxetic davranış gösteren malzemeler, Poisson oranlarının negatif olmaları sebebiyle normal malzemelerden farklı olarak basma işleminde daralır, çekme işleminde ise genişler. Negatif Poisson oranına sahip malzemelerin enerji emiciliği, kırılma dayanımı, termal şok dayanımı vb. özelliklerinin yüksek olması beklenir. Bu sebeple biyomedikal, savunma sanayi ve havacılık gibi birçok alanda kullanılması planlanmaktadır.

Çalışmanın ilk bölümünde, belirlenen negatif Poisson oranına sahip özgün latis yapıların kalınlık ve açı parametrelerine göre yapısal analizleri yapılmıştır. 3 farklı kalınlık ve 5 farklı açıya göre toplamda 15 farklı latis yapının Poisson oranları hesaplanmıştır. En düşük Poisson oranı -0,70 olarak bulunmuştur. Ardından, en düşük Poisson oranına sahip latis yapının kütlesi sabit tutularak iki farklı yöntem ile geometrik iyileştirmeler yapılmış ve yapılan iyileştirmeler nümerik olarak modellenmiştir. Uygulanan iyileştirmeler sonucunda tekrar sonlu elemanlar analizi yapılmış ve iki farklı geometrik iyileştirme yöntemi uygulanan latis yapıların Poisson oranları -0,78 ve -0,73 olarak hesaplanmıştır. Son olarak elde edilen üç farklı latis yapıların mekanik özelliklerinin karşılaştırılması amacıyla sonlu elemanlar yöntemi ile modal, static structural ve explicit dynamics analizleri yapılmıştır. Yeni nümerik model uygulandıktan sonra yapılan analiz sonuçlarına göre latis yapının üzerinde oluşan gerilmelerde ciddi miktarda azalma olduğu gözlemlenmiştir.

Sonuç olarak; farklı desenlere sahip auxetic geometrilerin gerilimlerinin, kendilerine özel formüllerle geliştirilecek matematiksel modellemelerle azaltılabileceği kanısına varılmıştır.

Anahtar Kelimeler: Auxetic yapı, negatif Poisson oranı, latis yapı, yapısal analiz, geometrik iyileştirme, matematiksel modelleme.

CONTENTS

M.Sc. THESIS EXAMINATION RESULT FORM ii
ETHICAL DECLARATION iii
ACKNOWLEDGMENTS iv
ABSTRACT v
ÖZ vi
CONTENTS vii
NOMENCLATURE x
LIST OF TABLES xii
LIST OF FIGURES xiii
CHAPTER 1 – INTRODUCTION 1
1.1 Overview 1
1.2 Literature Review 2
1.3 Justification of the Study 12
1.4 Aim and Objectives of the Thesis 13
1.5 Outline of Thesis 13
1.6 Lattice Structure Details to be Investigated in the Study 14
CHAPTER 2 – MATERIAL AND METHOD 18
2.1 Calculation of Poisson's Ratio of the Lattice Structure According to Variable Parameters 18
2.1.1 Model Details 18
2.1.1.1 Unit Cell Demonstration 18
2.1.1.2 Lattice Structure Demonstration 19
2.1.1.3 Matrix Demonstration 20
2.1.2 Analysis Settings 20
2.1.2.1 Analysis Geometry Informations 22
2.1.2.2 Solid Model Information 23
2.1.2.3 Material Properties 24
2.1.2.4 Contact Algorithms 25
2.1.2.5 Mesh Details 25
2.1.2.6 Boundary Conditions and Loads 28
2.1.3 Analysis Resutls 28
2.1.3.1 Calculation of the Poisson's Ratio 28

2.1.3.2 Comparison of Poisson's Ratios 30
2.1.4 Section Evaluation and Preparation for the Next Section..... 31
2.2 Geometric Improvement of Lattice Structure with the Lowest Poisson Ratio. 33
2.2.1 Overview..... 33
2.2.2 Geometric Improvements and Modeling 33
2.2.2.1 Unit Cell and Laticce Structure Demonstration 33
2.2.2.2 Structural Improvement 34
2.2.2.3 Mathematical Modeling of Improvement 35
2.2.2.4 Improved Unit Cell Mathematical Equation 40
2.2.2.5 Mechanical Comparison of Unit Cells 41
2.2.3 Model Details of Improved Unique Lattice Structures..... 42
2.2.3.1 Unit Cell Demonstration 42
2.2.3.2 Lattice Structure Demonstration 43
2.2.3.3 Matrix Demonstration 44
2.2.4 Analysis Settings 45
2.2.4.1 Analysis Geometry Information..... 45
2.2.4.2 Solid Model Information..... 45
2.2.4.3 Material Properties..... 46
2.2.4.4 Contact Algorithms 46
2.2.4.5 Mesh Details..... 47
2.2.4.6 Boundary Conditions and Loads 48
2.2.5 Analysis Results..... 49
2.2.5.1 Calculation of Poisson's Ratio 49
2.2.5.2 Comparison of Poisson's Ratios 49
2.2.6 Section Evaluation and Preparation for the Next Section..... 49
2.3 Comparison of Obtained Lattice Structures with Structural Analysis 52
2.3.1 Overview..... 52
2.3.2 Analysis Settings 52
2.3.2.1 Analysis Geometry Information..... 52
2.3.2.2 Solid Model Information..... 53
2.3.2.3 Material Properties..... 55
2.3.2.4 Contact Algorithms 55
2.3.2.5 Mesh Details..... 55
2.3.3 Modal Analysis for Geometries..... 56

2.3.3.1 Modal Analysis Settings 56
2.3.3.2 Modal Analysis Results 57
2.3.4 Static Structural Analysis for Geometries 61
2.3.4.1 Static Structural Analysis Settings 61
2.3.4.2 Static Structural Analysis Results 61
2.3.5 Explicit Dynamics Analysis for Geometries 66
2.3.5.1 Explicit Dynamics Analysis Settings 67
2.3.5.2 Explicit Dynamics Analysis Resutls 67
2.3.6 Section Evaluation 70
CHAPTER 3 – RESULTS AND DISCUSSION 72
3.1 Calculation of Poisson's Ratio of Lattice Structure According to Variable Parameters 72
3.2 Geometric Improvement of Lattice Structure with the Lowest Poisson Ratio. 75
3.3 Comparison of Obtained Lattice Structures with Structural Analysis 79
CHAPTER 4 – CONCLUSION AND RECOMMENDATIONS 82
REFERENCES 85
CURRICULUM VITAE 90

NOMENCLATURE

Roman Letter Symbols

G	Shear modulus, GPa
K	Bulk modulus, N/ m^2
E	Young's modulus, GPa
V	Volume, m^3
σ_y	Yield Strength, MPa
σ_u	Ultimate Strength, MPa
ε_1	Axial Strain, mm/mm
ε_2	Lateral Strain, mm/mm
L_1	Final Length, mm
L_0	Initial Length, mm
ΔL	Lenght Difference, mm
ΔV	Volume Difference, m^3
V_{UC}	Unit Cell Volume, mm^3

Greek Letter Symbols

$\boldsymbol{\nu}$	Poisson's ratio
$\boldsymbol{\varepsilon}$	Strain, mm/mm
Δ	Difference
ρ	Density, kg/ m^3

Subscripts

max	Maximum
m	Mean
t	Thickness, mm
α	Angle, °

Acronyms

FEA	Finite element analysis
FEM	Finite element method
DVH	Doubble V Head

DUH	Doubble U Head
FDM	Fused Deposition Modeling
RCA	Re-entrant chiral auxetic

LIST OF TABLES

Table 1.1 Poisson's ratios of some materials 2
Table 1.2 Calculation of Poisson's ratio..... 16
Table 2.1 Analysis details by parameters..... 23
Table 2.2 AL6061-T6 mechanical properties..... 25
Table 2.3 Mesh details..... 26
Table 2.4 Element quality factor scale for mesh..... 27
Table 2.5 Aspect ratio factor scale for mesh..... 27
Table 2.6 Poisson's ratios lattice structures 30
Table 2.7 Results of first iteration..... 37
Table 2.8 Results of second iteration 38
Table 2.9 Results of third ıteration..... 38
Table 2.10 Unit cell mass details..... 42
Table 2.11 Mesh details..... 48
Table 2.12 Mass and Poisson's ratios of lattice structures..... 51
Table 2.13 Mesh details..... 56
Table 2.14 Modal analysis frequencies 57
Table 2.15 Equivalent stress and total displacement results 62
Table 2.16 Explicit dynamic analysis results 67
Table 3.1 Results of analysis for Poisson's ratio calculation..... 74
Table 3.2 Equivalent stress of analyzes..... 75
Table 3.3 Poisson's ratio and unit cell volume change 78
Table 3.4 Results of Analysis for Poisson's ratio calculation..... 78
Table 3.5 Stress change and Poisson's ratio for static analysis..... 80
Table 3.6 Stress change and Poisson's ratio for explicit dynamics analysis..... 80

LIST OF FIGURES

Figure 1.1 Poisson's ratio demonstration 3
Figure 1.2 Auxetic behaviour(a), non-auxetic behaviour(b) 3
Figure 1.3 Foam with auxetic structure 4
Figure 1.4 Synclastic (auxetic) (a), anticlastic (non-auxetic) (b) 5
Figure 1.5 Response to shock force; non-auxetic (a), auxetic (b) 6
Figure 1.6 Non-auxetic vessel (a), auxetic vessel (b) 7
Figure 1.7 Neck movements adaptation of auxetic structures 8
Figure 1.8 Sport helmet with auxetic foam 8
Figure 1.9 DVH model (a), DUH model (b) 9
Figure 1.10 Sandwich panel with auxetic structure 9
Figure 1.11 Auxetic model (a), reinforced auxetic model (b) 10
Figure 1.12 Non-auxetic cyclinder (a), auxetic cyclinder (b) 11
Figure 1.13 Mısri mosque's altar 14
Figure 1.14 Lattice structure demonstration 14
Figure 1.15 Matrix geometries of the lattice structure 15
Figure 1.16 Free body diagram of matrix geometry 16
Figure 2.1 Unit cell (4-pointed star) 19
Figure 2.2 Forming of lattice structure 19
Figure 2.3 Matrix demonstration 20
Figure 2.4 Interface of analysis screen 21
Figure 2.5 Setting summary of analysis 21
Figure 2.6 Unit cell analysis geometry 22
Figure 2.7 Limits of parameters demonstration 23
Figure 2.8 Analysis solid model 24
Figure 2.9 Unit cell demonstration of the special case 24
Figure 2.10 Example of mesh demonstration 25
Figure 2.11 Free body diagram 28
Figure 2.12 Directional deformation path demonstration 29
Figure 2.13 Poisson's ratio results for group 1 31
Figure 2.14 Poisson's ratio results for group 2 32
Figure 2.15 Poisson's ratio results for group 3 32
Figure 2.16 Creation of a lattice structure from the unit cell 33

Figure 2.17 Geometric improvement applied with first method - 1..... 34
Figure 2.18 Geometric improvement applied with first method - 2..... 34
Figure 2.19 Geometric improvement applied with second method 35
Figure 2.20 Unit cell start and end points demonstration 36
Figure 2.21 Different equations model 1 36
Figure 2.22 Different equations model 2 37
Figure 2.23 Horizontal axis sinus curve equation..... 39
Figure 2.24 Geometric improved lattice structure 40
Figure 2.25 Geometrically improved unit cell 40
Figure 2.26 Unit cell 1 (a), unit cell 2 (b), unit cell 3 (c)..... 41
Figure 2.27 Improved unit cell 1..... 43
Figure 2.28 Improved unit cell 2..... 43
Figure 2.29 Improved lattice structure 1 43
Figure 2.30 Improved lattice structure 2 44
Figure 2.31 Improved matrix 1 44
Figure 2.32 Improved matrix 2 45
Figure 2.33 Analysis geometries..... 46
Figure 2.34 Example of contact algorithm..... 47
Figure 2.35 Example mesh form demonstration 47
Figure 2.36 Free body diagram 48
Figure 2.37 Unit cell of normal geometry..... 50
Figure 2.38 Unit cell of ımproved geometry 1..... 50
Figure 2.39 Unit cell of ımproved geometry 2..... 50
Figure 2.40 Structural analysis unit cell details 53
Figure 2.41 Static structural and modal analysis solid models 53
Figure 2.42 Explicit dynamics analysis matrix of normal geometry 54
Figure 2.43 Explicit dynamics analysis matrix of improved geometry 1 54
Figure 2.44 Explicit dynamics analysis matrix of improved geometry 2 55
Figure 2.45 Modal analysis free body diagram..... 57
Figure 2.46 Normal geometry mode 1 deformation..... 58
Figure 2.47 Normal geometry mode 1 deformation..... 58
Figure 2.48 Improved geometry 1 mode 1 deformation 59
Figure 2.49 Improved geometry 1 mode 6 deformation 59
Figure 2.50 Improved geometry 2 mode 1 deformation 60

Figure 2.51 Improved geometry 2 mode 10 deformation 60
Figure 2.52 Static analysis free body diagram 61
Figure 2.53 Normal geometry equivalent stress..... 62
Figure 2.54 Normal geometry equivalent stress..... 63
Figure 2.55 Before deformation (a), after deformation (b) 63
Figure 2.56 Improved geometry 1 equivalent stress 64
Figure 2.57 Improved geometry 1 equivalent stress 64
Figure 2.58 Before deformation (a), after deformation (b) 65
Figure 2.59 Improved geometry 2 equivalent stress 65
Figure 2.60 Improved geometry 2 equivalent stress 66
Figure 2.61 Before deformation (a), after deformation (b) 66
Figure 2.62 Normal geometry equivalent stress details 68
Figure 2.63 Normal geometry deformation..... 68
Figure 2.64 Improved geometry 1 equivalent stress 69
Figure 2.65 Improved geometry 1 deformastion..... 69
Figure 2.66 Improved 2. geometry equivalent stress 70
Figure 2.67 Improved 2. geometry deformation 70
Figure 3.1 Parameters of unit cell 73
Figure 3.2 Unit Cell, lattice structure and matrix geometry..... 73
Figure 3.3 Optimum unit cell demonstration 75
Figure 3.4 Center and edge points are fixed..... 76
Figure 3.5 Improvement equation demonstration 77
Figure 3.6 Unit cells demonstration 78

CHAPTER 1

INTRODUCTION

1.1 Overview

Various materials with different mechanical properties are used in industry. Many parameters are effective when choosing materials according to the usage area. However, one of the most important parameters is the relationship between strength and lightness. It is possible to obtain materials with superior properties by adding additional properties to conventional materials. The need for efficient materials, which is increasing day by day, can be met by adding additional features to existing materials.

Various methods are available to add additional properties to materials. Controlling the lattice structures of materials is one of these methods. By controlling the lattice structures, it can be estimated how the material will react or deform against the forces to be applied. Materials with negative Poisson's ratio (Auxetic) can obtained by controlling the lattice structures.

The positive Poisson's ratio is one of the common and characteristic features of most materials. Materials with auxetic behavior are more limited in nature. Unlike normal materials, auxetic materials contract in compression and expand in tension, unlike normal materials, due to the negative Poisson's ratios. From another point of view, condensation occurs due to the narrowing in the lateral axis due to the negative Poisson's ratio in the regions exposed to the compression force.

In this study, the auxetic behavior of the structures due to their unique deformation feature was studied. In the study, it has been proven that a lattice structure that has not been examined before in the literature has a negative Poisson's ratio, and this lattice structure is focused on. The advantages and disadvantages of the original lattice structure were analyzed using the finite element method.

1.2 Literature Review

What is the Poisson's Ratio?

Poisson's ratio is the measurement ratio of the deformation of the structure caused by the force applied to the structure. This is the ratio of the vertical displacement to the horizontal displacement, which occurs as a result of the force applied on the vertical axis to the structure (it can be summarized as the ratio of the amount of expansion to the amount of contraction).

Table 1.1 Poisson's ratios of some materials [1,2]

Material	Poisson Ratio's (ν)
Aluminum	0.33
Copper	0.36
Ice	0.33
Steel	0.3
Cast Iron	0.30
Epoxy Resin	0.40
Rubber	0.5
Polystyrene	0.34
Polyvinylchloride	0.35

This ratio is symbolized by the symbol ν (nu) and is unitless because it is mm/mm. Poisson's ratios for most materials found on Earth have been calculated as 0 to 0.5 [3], so this value is positive for most materials. However, this value is generally concentrated between 0.25 and 0.35 in solids [3]. This ratio was proposed and named by the French physicist Simeon Poisson.

An example calculation of the Poisson's ratio is shown in Figure 1.1. By dividing the displacements in the vertical and horizontal axes by the initial lengths of the axes, the strains in the axes are obtained. Poisson's ratio is the negative of the ratio of these two values to each other [3].

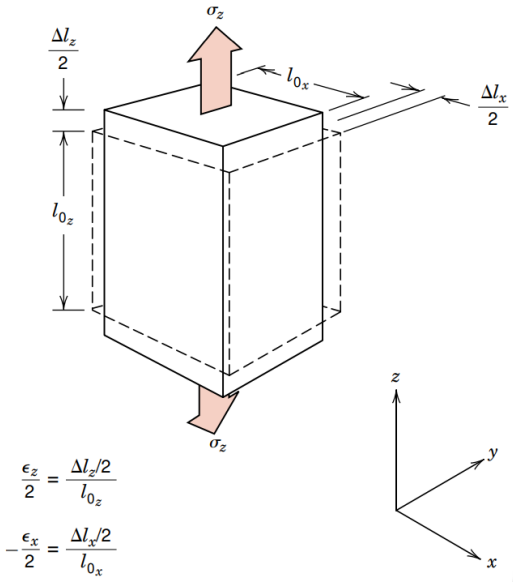


Figure 1.1 Poisson's ratio demonstration [3]

Negative Poisson's Ratio and Auxetic Structures

Although most of the materials used in the industry have a positive Poisson's ratio, there are materials with a negative Poisson's ratio. Theoretically, the Poisson's ratio of isotropic materials can be between -1 and 0.5 [4]. Materials with a negative Poisson's ratio are called auxetic materials, and these materials can be produced artificially as well as naturally. Normally, auxetic structures can be obtained by changing the lattice structures of materials with positive Poisson's ratio [5]. Auxetic structures expand in tensile processes and contract in compression processes due to the negative Poisson's ratio they have.

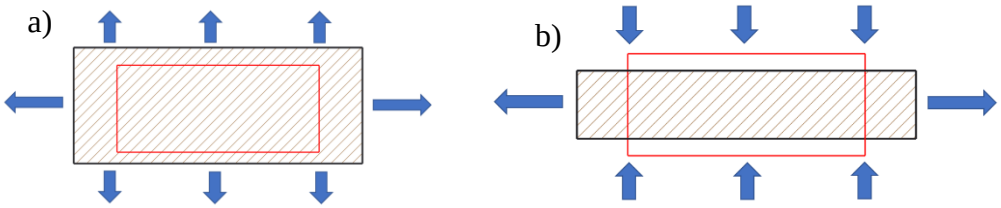


Figure 1.2 Auxetic behaviour (a), non-auxetic behaviour (b)

History of Auxetic Structures

The word auxetic is derived from the Greek word 'auxetikos' and Evans et al used this term for the first time in 1991 [6]. As a word, it means inclined to expand. In the early 1900s, the first natural molecular structure material discovered to have an auxetic structure is iron sulfide with a Poisson's ratio of -0.14 [7]. In later studies, it was determined that $YBa_2Cu_3O_7$ (Yttrium barium copper oxide) material also has a negative Poisson's ratio [8]. Also, examples of natural auxetic structures are arsenic [9] and cadmium [10].

In the 1900s, besides finding auxetic materials in nature, studies were carried out on artificially producing structures with negative Poisson's ratios. The first material that was subsequently given auxetic behavior was applied by Rod Lakes on a foam in the 1980s. The first lattice structure with a negative Poisson's ratio was made by Gibson et al using silicone rubber in two dimensions [11,12].



Figure 1.3 Foam with auxetic structure [13]

Classification of Auxetic Materials

Auxetic materials can be classified as natural and artificial. Also, classification was made according to material sizes [14]. Natural auxetic materials are limited in number compared to artificial ones. It is possible to obtain artificial auxetic material with a change in the lattice structure.

Example of natural auxetic materials is the spongy structure of the human tibia. Williams et al. In his study by creating a finite element model to examine the bone, he stated that the human tibia is negative [15]. Auxetic behavior has been detected in studies on various animal skins. In studies on cat skin, salamander skin and cow udder skin, the Poisson's ratio was calculated to be negative [16-18].

In the literature, it is generally studied on artificially created auxetic structures. The first artificial auxetic lattice structure was designed by Gibson in 1982 in the form of a two-dimensional honeycomb [19]. Later, auxetic behavior of polyurethane foams was observed at compression and temperature [11]. Apart from these studies, many artificial auxetic materials have been studied until today.

Properties of Auxetic Structures

Auxetic structures have a unique deformation tendency due to their negative Poisson's ratio. This makes auxetic structures superior to normal materials in some areas.

First of all, synclastic behavior can be given as an example of these superior features. Synclatic can be explained as the deformation behavior of the structure exposed to bending force [20]. Structures with synclastic behavior take the shape of a dome when deformed, while anticlastic structures tend to become cylindrical, and when subjected to uniaxial bending force, they tend to bend in the opposite direction from the edges. Auxetic structures show synclastic behavior when subjected to bending force. Thanks to these features, they can be used in surface applications with various forms.

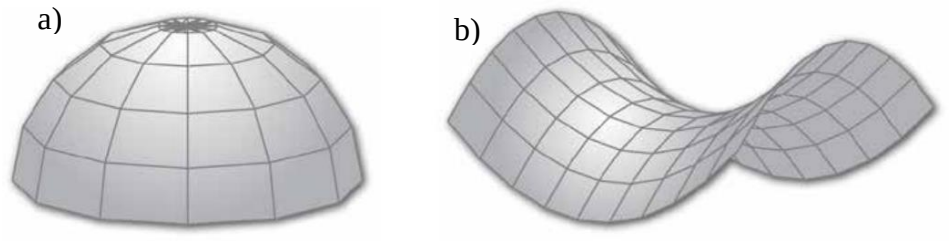


Figure 1.4 Synclastic (auxetic) (a), anticlastic (non-auxetic) (b) [21]

In auxetic structures, it comes to the forefront compared to other structures due to its indentation resistance. When the auxetic structures are exposed to the local compression force, they contract and condensation occurs in the area where the force is applied [22]. When the applied local forces are removed, the material returns to its original state. Thanks to these features, it can be preferred in applications where shock absorption is important [23,24].

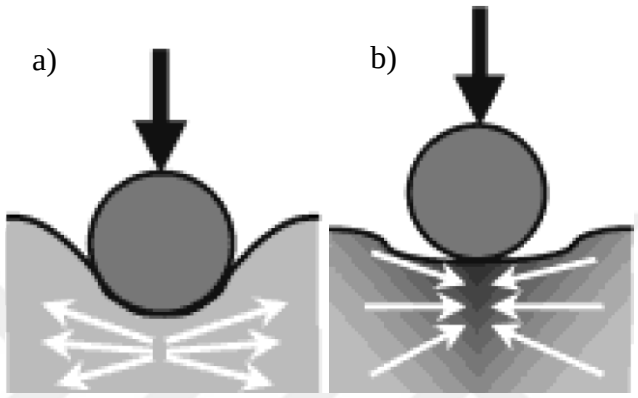


Figure 1.5 Response to shock force; non-auxetic (a), auxetic (b) [25]

One of the other features of NPR structures is their resistance to shear stresses [26]. Under the influence of bending and shear stresses, shear stress occurs on the structure and in the inner parts of the structure. The relationship between the elastic modulus, shear modulus, bulk modulus and Poisson's ratio parameters used in the elasticity calculation is as shown in the equation below.

$$G = \frac{E}{2\times(1+v)} \tag{1.1}$$

$$K = \frac{E}{3\times(1-2v)} \tag{1.2}$$

The range of Poisson's ratio that isotropic linear elastic materials can have is between -1 and 0.5 in three-dimensional cases. In two dimensions, this range increases between -1 and 1 [4]. As the Poisson’s ratio increases, the bulk modulus increases relative to the shear modulus. However, as the Poisson’s ratio decreases, the shear modulus becomes much higher than the bulk modulus. In this case, the structure is easily deformed, but the shear stress is increased.

According to the studies, the fracture toughness of some NPR materials was determined by high experiments. When the traditional foam with polyurethane-polyester material and NPR foam are compared, the fracture toughness of foams with NPR structure is higher [27].

Scope of Application

Material selection according to the field of use in materials used in the industry is generally taken into account by the parameters of strength, lightness and cost. The responses and deformations of NPR structures obtained by adding additional features to conventional materials against forces can be seen beforehand and they can be preferred due to their superior properties compared to other materials with positive Poisson's ratio. For this reason, NPR structures are used in various fields in the industry and are planned to be used in new fields.

The first example of the usage areas of auxetic structures can be given in the biomedical sector. It is used in components placed in the body, stents and tissues. In a study, a blood vessel produced with traditional materials and a blood vessel with NPR were compared. According to the results obtained, it has been suggested that the vein made of traditional material becomes thinner at the edges and poses a danger when the blood pressure rises. However, when the blood vessel with NPR structure is examined, the thickness does not decrease due to the auxetic behavior of the structure in places where blood pressure rises [25].

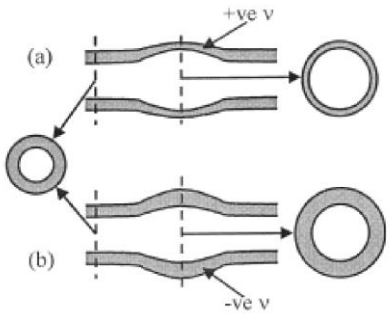


Figure 1.6 Non-auxetic vessel (a), auxetic vessel (b)

It can be used in surface coating applications due to its synclastic feature. In a study using NPR structure, a personalized neck collar design was made. A design that limits the movement to the desired extent due to its NPR structure and does not sweat due to its hollow structure has been proposed.

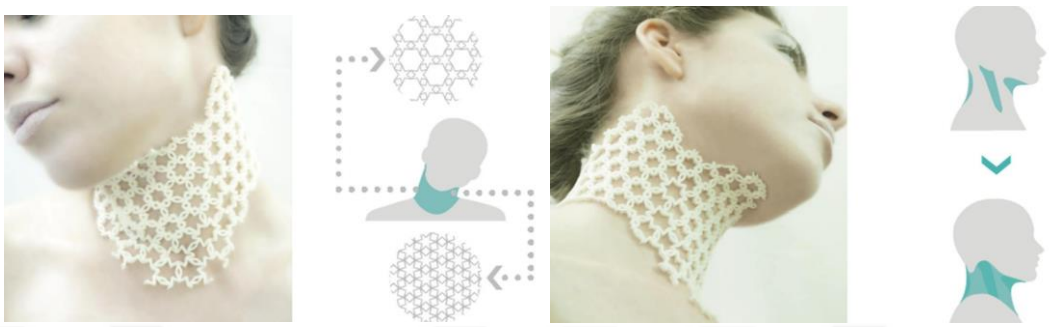


Figure 1.7 Neck movements adaptation of auxetic structures [28]

Products with NPR structure are also planned to be used in the field of sports. Due to the superior shock absorption properties of auxetic structures, it has been shown that helmets obtained from NPR structure significantly reduce trauma at the time of impact [29,30].



Figure 1.8 Sport helmet with auxetic foam [30]

Various studies have been carried out for the use of NPR structures in the field of textiles. By using the shock absorption and synclastic properties of the auxetic behavior, the curtain used against explosions has been developed [31].

Auxetic Structure Reviews

Many studies have been carried out to examine, develop and investigate the properties of Auxetic. Yang H. et al. examined the double arrowhead structure previously used in the literature and brought the double-V geometry to the double-U structure. The obtained geometries were produced by the additive manufacturing method. He stated that the obtained double-V-headed structure has a lower Poisson's ratio and higher collapse voltage than the double-V-headed structure [32].

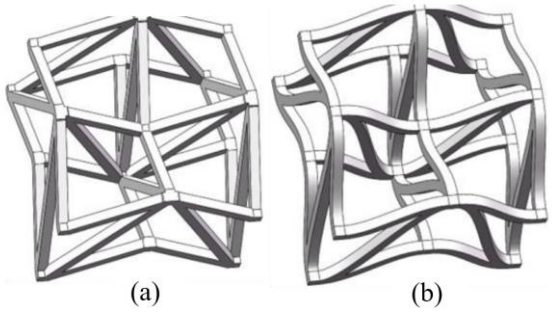


Figure 1.9 DVH model (a), DUH model (b) [32]

Ranjbar et al. investigated the vibroacoustic behavior of auxetic structures with finite element analysis. He investigated the mechanical properties of anti-tetrachiral and auxetic hexagonal structures and the natural frequencies of panels formed with auxetic structures. It has been determined that the geometry and thickness of the sandwich panel structures prepared using the auxetic structure effect the radiated sound power. The structure was optimized by changing the dimensions of the created unit cell. Thus, the frequency of the first modes of the structure is increased. The auxetic hexagonal structure is proposed to reduce structure-borne radiated noise in the low frequency ranges [33].

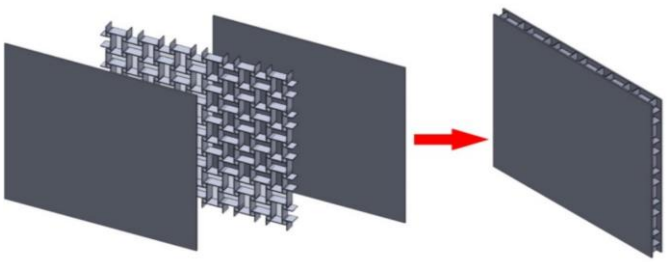


Figure 1.10 Sandwich panel with auxetic structure [33]

In another study to develop structures with NPR structure, re-entrant honeycomb and double arrowhead structure were used. Support columns were added to pass through the middle of these structures. Structural analyzes of the new geometries obtained were performed. According to the calculated results, the strength was significantly increased and it was determined that there was no change in the Poisson's ratio. The results obtained have been confirmed by experiments [34].

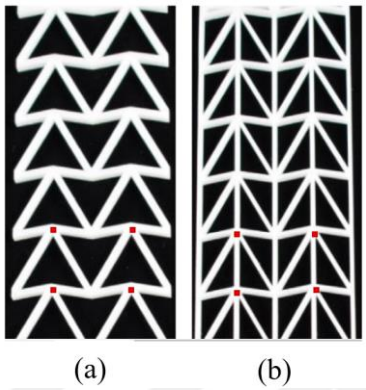


Figure 1.11 Auxetic model (a), reinforced auxetic model (b) [34]

Honeycomb, re-entrant honeycomb and double arrowhead structure were designed for the production of shock absorbing pads planned to be used in the human body. Design, analysis and experimentation were carried out. The results showed that the auxetic material can be effective in reducing shock forces [35].

Gao and Liao were inspired by foam filled structures in their study. The energy absorption properties of a thin-walled structure filled with a double-arrow NPR structure were investigated. The increase in energy absorption ability using gradient configurations has been theoretically calculated and confirmed by analysis [36].

In their study, Alomarah et al. investigated 4 different auxetic structures, RCA, tetrachiral, re-entrant honeycomb and anti-tetrachiral honeycomb structures, numerically and experimentally. The RCA structure was found to outperform other honeycomb types in terms of strength and specific energy absorption [37].

In another study, which observed the shock absorption properties of NPR, auxetic structures were examined in terms of axial collision and energy absorption. Re-entrant geometry and honeycomb geometry found in the literature were used as lattice geometry. The samples were produced as cylinders by using metal powder by additive manufacturing method. In low energy impacts, the auxetic structure shows higher specific energy absorption. Also, during axial collision, the structure becomes denser and the deformation slows down significantly [38].

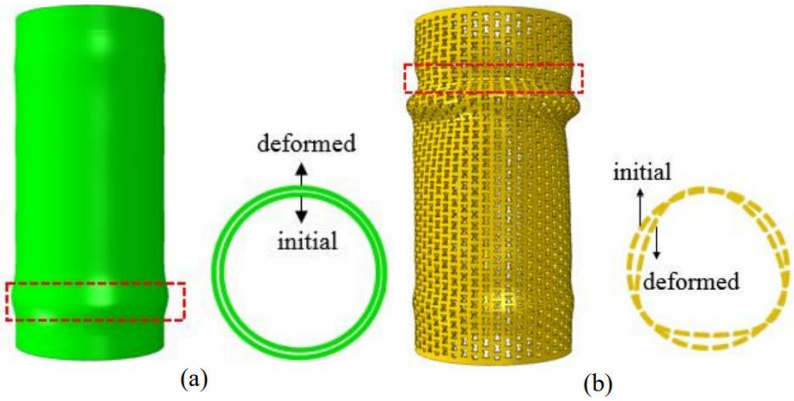


Figure 1.12 Non-auxetic cyclinder (a), auxetic cyclinder (b) [38]

In a study to increase the stiffness and strength of auxetic structures, fiber-reinforced polymers are used. The double-headed arrow found in the literature was used. It includes experimental, theoretical and analytical work. The results showed that the stiffness of the composite auxetic structure is much higher than that of the metal structure. Auxetic structures made using Fiber Reinforced Polymer are much higher performance [39].

Alomarah et al. hexagonal honeycomb and re-entry honeycomb structures are studied as out-of-plane and in-plane. Additive manufacturing method with FDM method was used for sample production. Deformation, stress-strain curve and energy absorptions were investigated. The energy absorption efficiency has been shown to be higher for the RCA structure than for the other two structures [40].

Johnston's work includes examining the structures found in the literature, two auxetic and one non-auxetic, in terms of material diversity. Different materials are used on the walls and corners. Samples were produced by the additive manufacturing method and

tested experimentally. He found that monomaterial structures offer the highest performance where they absorb the most energy [41].

Shokri Rad et al. investigated unit cell configurations by experimental and numerical methods to measure the energy absorption of various auxetic structures under quasi-static and dynamic forces. Auxetic structures can withstand high quasi-static axial impact loads. For this reason, their energy absorption capacity and impact resistance are superior to structures with positive Poisson's ratios [42].

Shepherd examined 4 different structures in his study. Three of these structures are auxetic and one of them is non-auxetic. The structures were produced by the additive manufacturing method. Hammer drop test with different structures was performed on the samples. The impact situation commonly encountered in sports has been simulated. FEM analyzes were confirmed by experiments. He stated that it can be simulated by FEM analysis without the need to produce experimental prototypes [43].

Nafaji investigated the behavior of auxetic structures under low velocity axial loading. Three different auxetic structures were used in the experiment and were produced by the numerical additive manufacturing method. Information about the energy absorption and fracture mechanisms of all three structures is given [44].

In the study, auxetic structure was developed for the first time by using composite materials. Five different auxetic structures were developed including glass fibers, polyester filaments and epoxy resin. Tensile test was applied on the samples. According to the results obtained, the Poisson's ratio was found to be between -0.3 and -5.2 [45].

1.3 Justification of the Study

Most materials found on Earth have a positive Poisson's ratio. There are a limited number of materials with a negative Poisson's ratio. However, structures with a negative Poisson's ratio can be artificially produced. Auxetic structures have different deformation tendencies compared to normal materials. Due to this tendency, it has many advantages over normal materials.

Due to their unique properties, auxetic structures have become popular in recent years and different studies are being carried out on them. The reason for starting the study is to examine the parameters affecting the Poisson's ratio in future studies, to improve the Poisson's ratio by keeping the mass constant, and even to improve the strength of the structures with geometric improvements. These improvements will be modeled numerically and will lead to geometric improvement in future studies.

1.4 Aim and Objectives of the Thesis

The study aims to design a unique lattice structure optimized with geometric improvements, which will be useful in various auxetic building applications. In order to design the original optimum lattice structure, the following steps will be followed to create a lattice structure with a unit cell, which has not been examined before in the literature;

- Modeling of the original unit cell
- Calculation of Poisson's ratios of the unit cell according to various parameters
- Applying geometric improvements of the structure with the lowest Poisson's ratio and creating a mathematical model of the improvements made.
- Comparison of the first unit cell examined and the unit cells whose geometric improvements were completed with structural analysis

1.5 Outline of Thesis

In the first part of the study, the subject studied was explained in detail and the reason for starting the study, its aims and objectives were mentioned. In the second part, the method used to design the optimum original lattice structure is explained. In the third part, the results obtained are evaluated. In the last section, the results were evaluated and a summary was created. In the last part, recommendations and conclusions was presented.

1.6 Lattice Structure Details to be Investigated in the Study

The lattice structure to be used in the study was inspired by the patterns found in the altar of the Afyonkarahisar Misri mosque which was built by Evliya Kasım Pasha in 1478 [46].

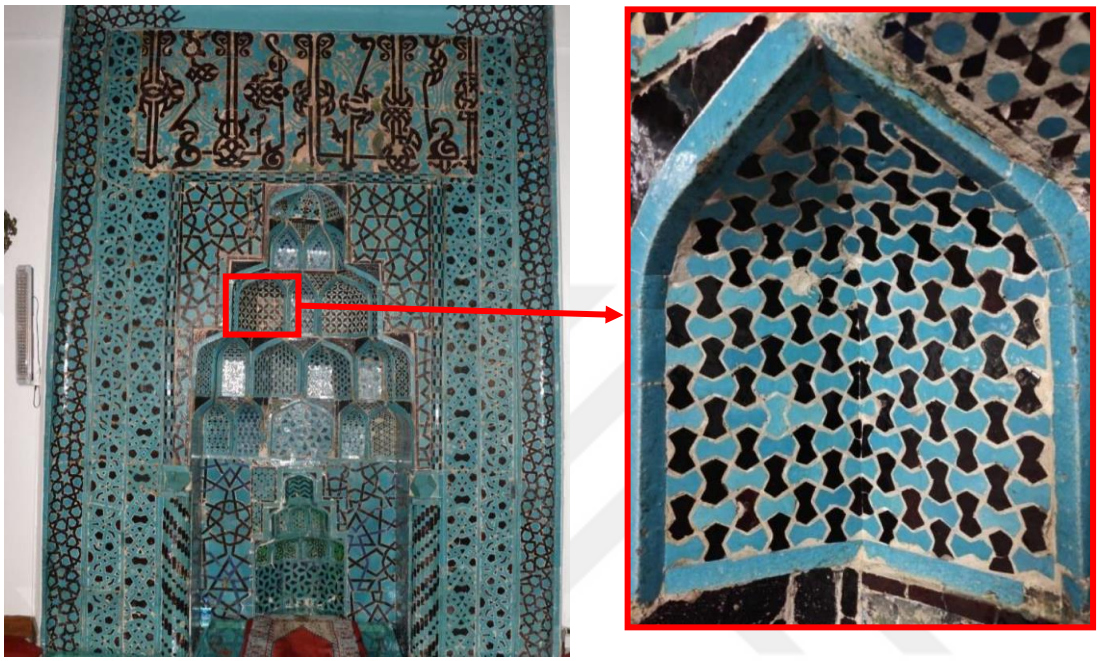


Figure 1.13 Mısri mosque's altar

There has been no previous study on the auxetic behavior of the unit cell to be examined. The original dimensions of the lattice structure to be studied are given in Figure 1.13.

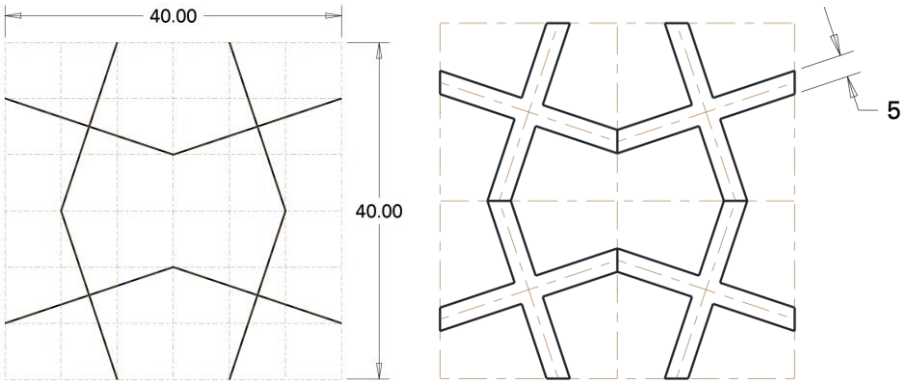


Figure 1.14 Lattice structure demonstration

The unit cell studied does not mean much by itself. The horizontal and vertical axes of the unit cell are symmetrically taken and all unit cells are combined to form a lattice structure. In order to check the suitability of the lattice structure for the work to be done, first of all, the auxetic behavior was examined by calculating the Poisson's ratio. Poisson's ratio calculation will be done with the analysis program Ansys Workbench version 19.2, which uses the FEM. Matrix geometry was created by combining lattice structures for finite element analysis.

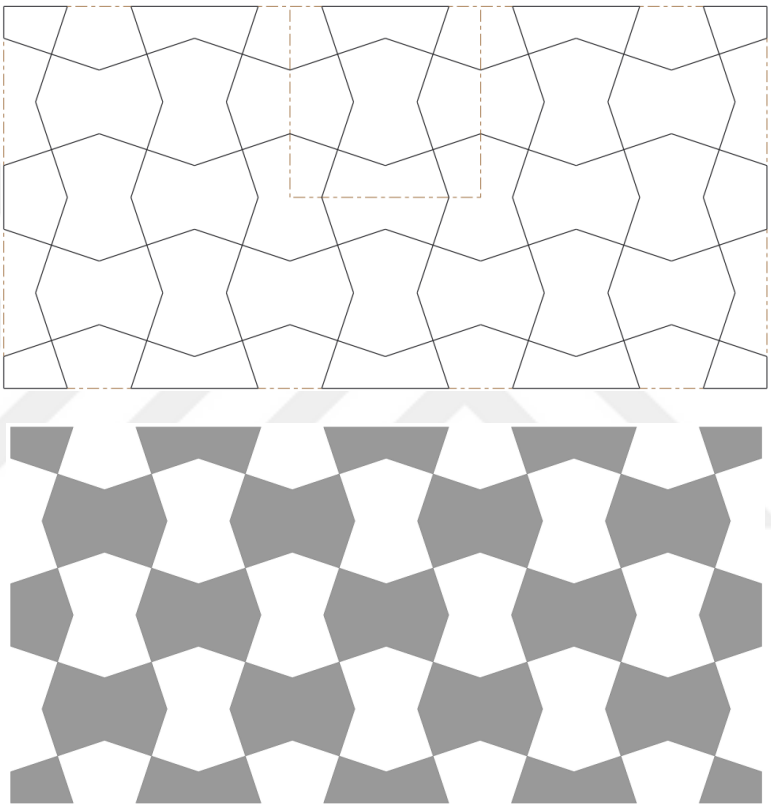


Figure 1.15 Matrix geometries of the lattice structure

AL6061-T6 (Table 2.2) was chosen as the material in the completed analysis to calculate the Poisson's ratio. In contact algorithms, all links are implemented as inseparable link 'bonded'. The default method of the program is selected when applying the mesh structure. All elements are dimensioned as 2 mm as mesh dimensions. As a boundary condition, 'fixed support' was applied from 5 surfaces of the lower grap bar. Finally, 1 mm tension is defined as the loading.

While calculating the Poisson's ratio, the ratio of the displacement on the vertical axis to the amount of displacement on the horizontal axis is used. To calculate these rates, the 'deformation probe' and 'directional deformation' tools included in the program were used.

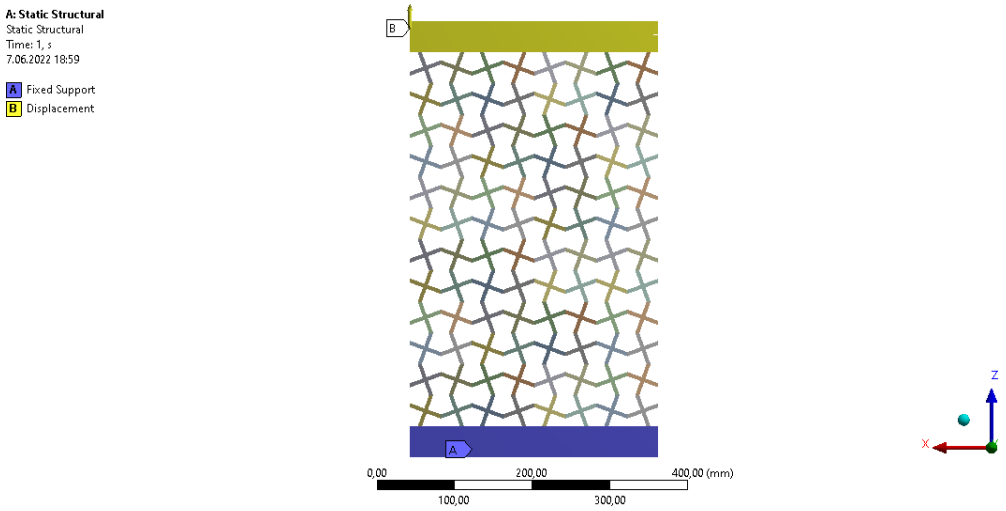


Figure 1.16 Free body diagram of matrix geometry

According to the results of the completed analysis, the displacement in the z-axis was found to be 1 mm, and the total length was 480 mm. The displacement in the x-axis is calculated by the program as a total of 0.243 mm, and the total length in the horizontal axis is 200 mm.

According to the results obtained, the Poisson's ratio of the lattice structure was calculated as -0.58. It has been revealed that the determined lattice structure is auxetic. The structure is suitable for working.

Table 1.2 Calculation of Poisson's ratio

ΔL_y	L_{y_1}	ΔL_x	L_{x_1}	**Poisson's Ratio, v**
480	1.00	200	0.243	-0.58

In the study, the measurements were revised. The unit cell outer dimensions have been updated as 10×10×10 mm. The angle made by the two line segments of the unit cell with each other is kept constant. The angles of the edge thicknesses and the line segments with the normal axis have been made parametric. By changing these values, the geometry with the lowest Poisson’s ratio will be found.

CHAPTER 2

MATERIAL AND METHOD

Under this title, it consists of a total of 3 parts; determination of the optimum lattice structure according to variable parameters, geometric improvement of the determined optimum lattice structure, and comparison of the improved geometries and other geometry with analysis. All the details are given in the chapter.

2.1 Calculation of Poisson's Ratio of the Lattice Structure According to Variable Parameters

In the first part of this chapter, there is the unit cell of the determined figure and the lattice structure obtained by combining the unit cells. In this section, analyzes to be made using the finite element method will focus on the Poisson's Ratio of the unique lattice structure. Two different parameters, thickness and angle with the nominal axis, are assigned to the determined unit cell dimensions. Thus, the effect of these parameters on the Poisson's ratio will be examined. The details of the design to be studied, the settings of the analyzes to be made to find the Poisson's ratio of these designs and the results of these analyzes are explained in this section.

2.1.1 Model Details

A lattice structure is formed by combining unit cells. However, it is not possible to analyze directly the created lattice structure. For this reason, unit cell, lattice structure and matrix geometry designs were made. While designing, Creo Parametric 5.0.4.0 student version was used.

2.1.1.1 Unit Cell Demonstration

The figure to be examined was determined as a 4-pointed inclined star. The outer dimensions of the unit cell are given in Figure 2.1. The unit cell consists of 10×10 mm, the depth is 10 mm. The control volume of the unit cell is designed to be a cube.

However, the analyzes and calculations will be made with reference to two axes, horizontal and vertical axis.

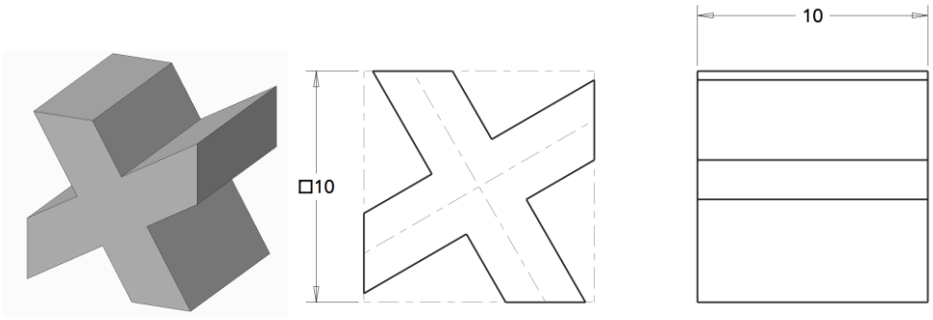


Figure 2.1 Unit cell (4-pointed star)

2.1.1.2 Lattice Structure Demonstration

Unit cells cannot be included in calculations or analysis as single. In order to complete calculations and analyzes, unit cells must be combined to form a lattice structure. 4 unit cells are needed to form the lattice structure by combining the unit cells. When the symmetry of the unit cells in the horizontal and vertical axes is taken, a lattice structure is formed. The appearance of the formed lattice structure is given in Figure 2.2.

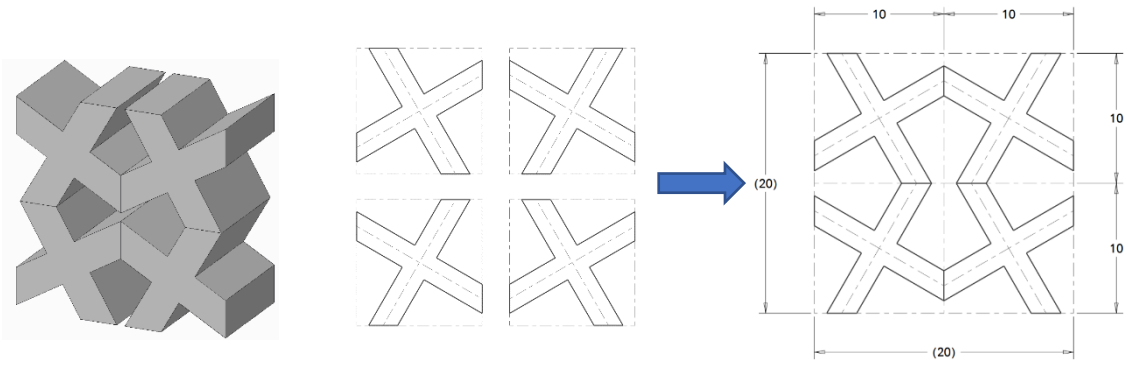


Figure 2.2 Forming of lattice structure

2.1.1.3 Matrix Demonstration

In order to better understand, examine and analyze the figure, the matrix model shown in Figure 2.3 was created by combining the lattice structures shown in Figure 2.2. The model to be analyzed is 80×120×10 mm in size. The unit cell dimensions indicated in Figure 2.1 will change with the analysis. Details are given in the analysis section.

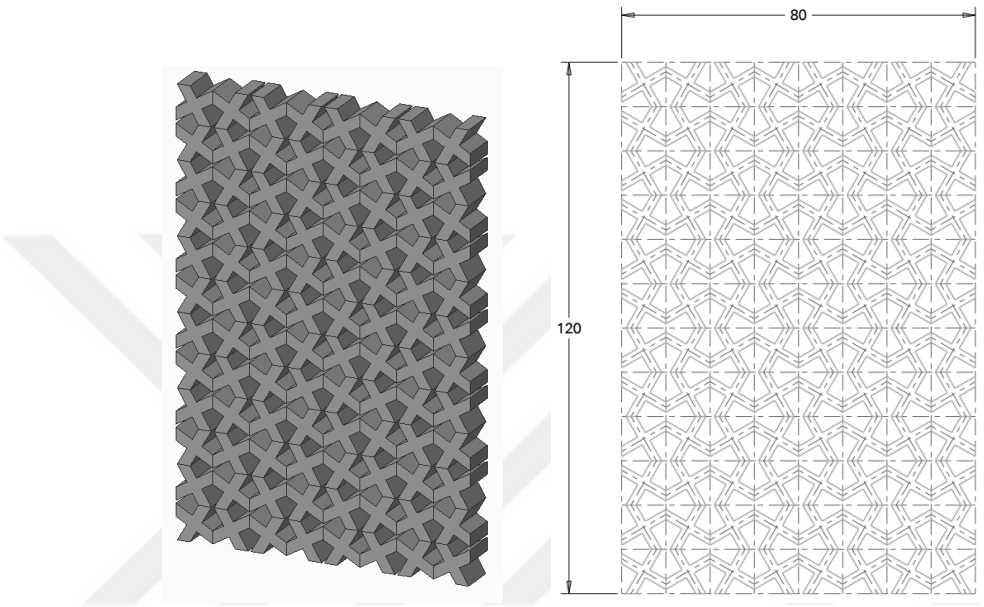


Figure 2.3 Matrix demonstration

2.1.2 Analysis Settings

This part of the study includes the effect of the thickness and angle change of the determined lattice structure on the Poisson's ratio. An analysis simulation program using the finite element method was used while calculating the Poisson's ratio. Analysis preparations and settings are given in detail in the section.

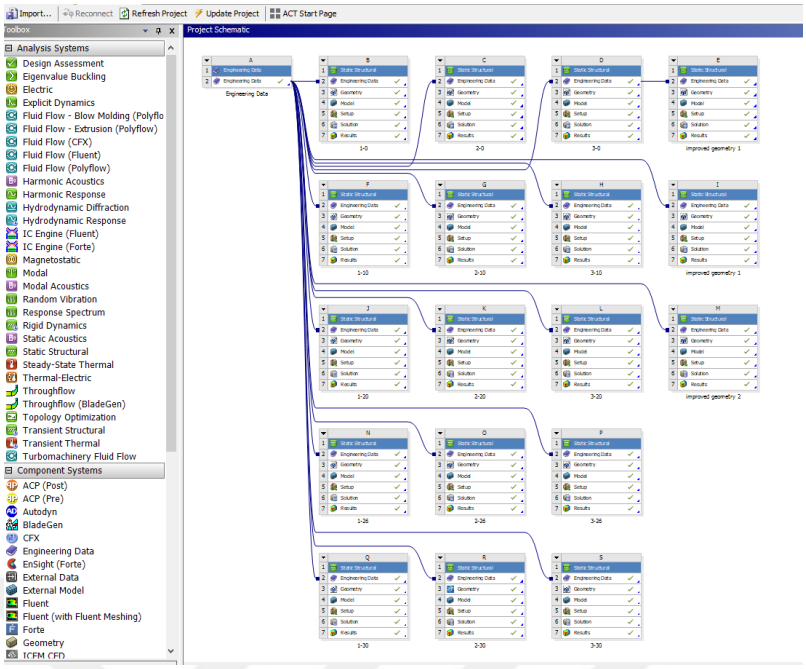


Figure 2.4 Interface of analysis screen

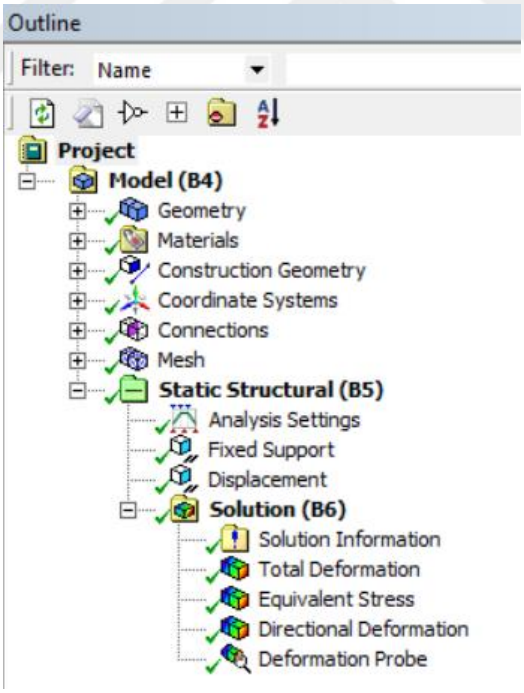


Figure 2.5 Setting summary of analysis

2.1.2.1 Analysis Geometry Informations

In order to examine the Poisson's Ratio of the unique lattice structure, two different parameters, α and t, were created (Figure 2.6). A total of 15 analyzes were run by defining 3 different values for the t parameter as 1 mm, 2 mm and 3 mm, and for the α parameter as 0°, 10°, 20°, 26.52°, and 30°. The boundaries are as follows according to the unique lattice structure created. When it is desired to run the analysis at thicker or higher angles, the lattice structure joins at the corners and this situation directly changes the result. Before these analyzes were made, three groups were formed according to the t value. Comparisons were made in two different ways, first within the group and then between the groups. The α and t values and group details used for the 15 analyzes are given in Table 2.1.

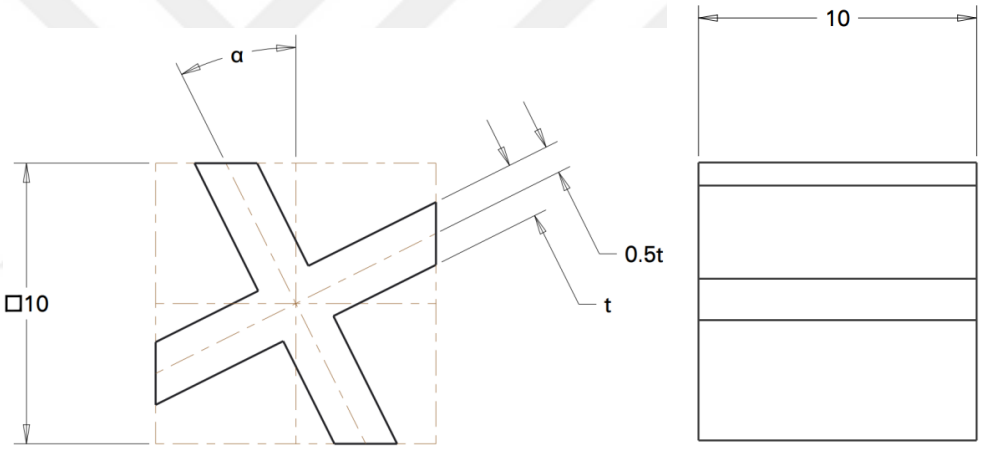


Figure 2.6 Unit cell analysis geometry

While creating the parameters, the thickness was applied between 1 and 3 mm. The angle is between 0 and 30 degrees. When a thickness greater than 3 mm is selected, the geometry merges. For this reason, the maximum thickness is accepted as 3 mm. The maximum angle is determined as 30. If the angle is chosen higher, the lattice structure is combined again and this situation disrupts the auxetic behavior, the original of the geometry is distorted (Figure 2.7).

The lowest 0 degrees was chosen as the angle. When a negative value is given, the geometry becomes the same again. The thickness was determined as 1 mm in order not to weaken the strength and not to increase the production costs.

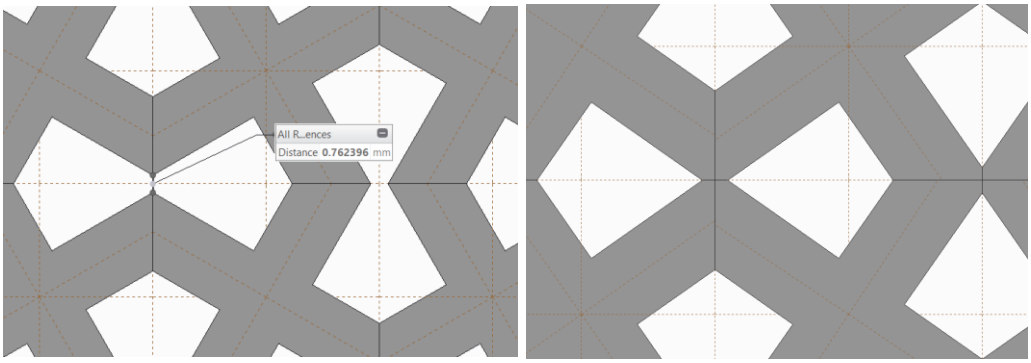


Figure 2.7 Limits of parameters demonstration

Table 2.1 Analysis details by parameters

	Analysis No	***t* (mm)**	***α* (°)**
1. Group	1	1	0
	2	1	10
	3	1	20
	4	1	26.52
	5	1	30
2. Group	6	2	0
	7	2	10
	8	2	20
	9	2	26.5
	10	2	30
3. Group	11	3	0
	12	3	10
	13	3	20
	14	3	26.52
	15	3	30

2.1.2.2 Solid Model Information

In order to distribute balanced the boundary conditions and initial conditions to be given in the analysis, a 80×20×10 mm grap bar was added to the upper and lower limits of the analysis model. Thus, the outer dimensions of the model to be analyzed were 80×160×10 mm. The analysis floor model consists of a total of 96 unit cells and 2 grap bars for all geometries.

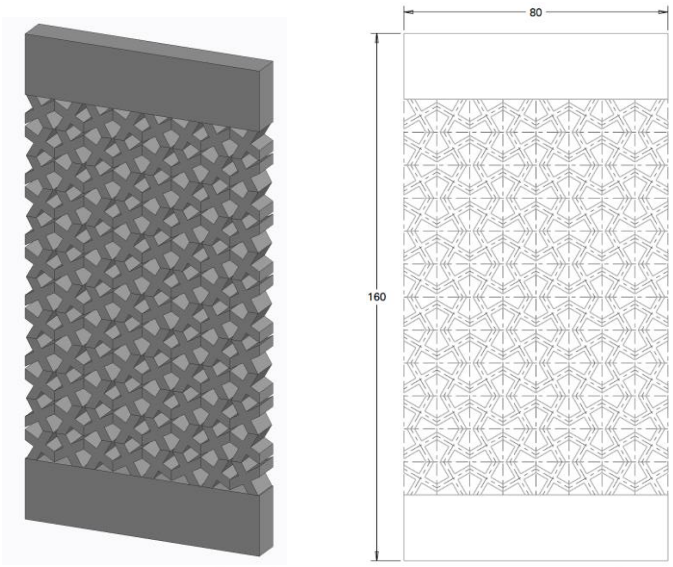


Figure 2.8 Analysis solid model

Special Case 26.52°

When the α value is 26.52°, the distance of the unit cell's axis to the horizontal and vertical axis is equal (Figure 2.9). Therefore, 26.52° will be examined separately.

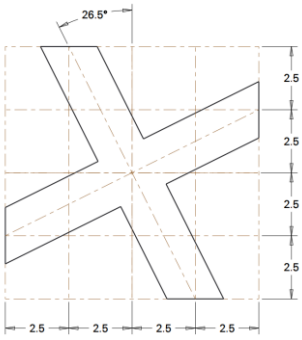


Figure 2.9 Unit cell demonstration of the special case

2.1.2.3 Material Properties

In the first group analysis, Aluminum 6061-T6, which is used extensively in many fields such as defense and automotive, was assigned to all parts as a material. Detailed mechanical properties of the determined material are given in Table 2.2.

Table 2.2 AL6061-T6 mechanical properties [47]

Material	$\boldsymbol{\rho}$	$\boldsymbol{E}$	$\boldsymbol{v}$	$\boldsymbol{\sigma_y}$	$\boldsymbol{\sigma_u}$
AL6061-T6	2700	68.9	0.33	276	310

2.1.2.4 Contact Algorithms

As stated in Section 2.1.2.2, all samples consist of 24 lattice structures (96 unit cells) and 2 bars. All of these parts are connected to each other with a "Bonded" (Inseparable) connection. A node has 6 degrees of freedom in total, with the inseparable connection, the degree of freedom of the unit cells among themselves is reduced to zero. The structure moves as a single part. The default settings of the program for other settings of contact algorithms are not changed.

2.1.2.5 Mesh Details

Method assignment is not made while creating the mesh. The mesh size of the lattice structures is 0.5 mm, and the mesh size of the analysis bars is 2 mm. Element Quality and Aspect Ratio from mesh metric tools were used to check the mesh quality. The number of elements and nodes forming the mesh are given in Table 2.3. As an example mesh form, images from analysis number 8 are given in Figure 2.10. The above mentioned settings were applied for all other analyses.

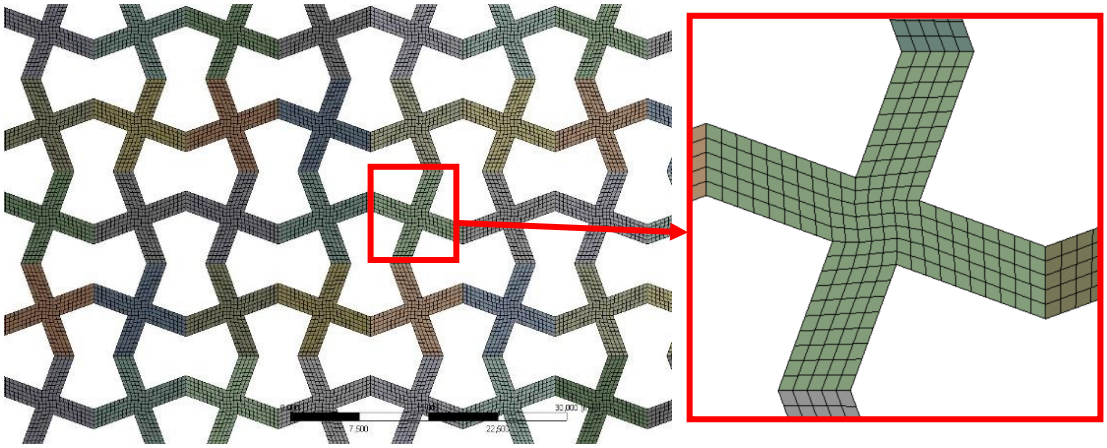


Figure 2.10 Example of mesh demonstration

Table 2.3 Mesh details

Analysis No	*t* (mm)	*α* (°)	Node Number	Element Number	Element Quality (m)	Aspect Ratio (max)
1	1	0	867706	149920	1	1
2	1	10	1273978	242080	0.884	1.619
3	1	20	1393402	265120	0.876	1.600
4	1	26.52	1393402	265120	0.850	1.607
5	1	30	1458426	278624	0.783	1.755
6	2	0	1409530	280480	1	1
7	2	10	1847674	380320	0.958	1.289
8	2	20	1963162	405280	0.917	1.322
9	2	26.5	2146330	443680	0.903	1.305
10	2	30	2146330	443680	0.891	1.311
11	3	0	1887610	395680	1	1
12	3	10	2357626	503200	0.977	1.187
13	3	20	2504986	535840	0.949	1.210
14	3	26.52	2668282	572320	0.913	1.243
15	3	30	520954	100000	0.872	1.473

Mesh Quality Evaluation

One of the most important factors directly affecting the accuracy of the analysis is the mesh quality. Mesh quality must be checked for each analysis performed. Mesh quality control can be done with the mesh metric tool included in the program. As a result of the analyzes to be made in this section, the Poisson's Ratio calculation is made. The deformation tool is used to calculate the Poisson's Ratio. For this reason, Element Quality and Aspect Ratio calculation methods in the mesh metric tool were used when questioning the element quality. Element Quality and Aspect Ratio values are shared for 15 analyzes performed in Table 2.4 and Table 2.5. According to the results obtained

from the mesh metric tool, the element quality is very close to the ideal mesh structure. Depending on the quality of the element, there will be no deviation in the analysis results.

Element Quality

The Element Quality factor is one of the mesh form quality factors that should be looked at first in the analysis. Element quality is the ratio of the volume of a mesh element to the edge length of that mesh element. The value in the element quality factor is between 0 and 1, mesh elements with a value of 1 are considered perfect according to the element quality parameter. The rating bar according to the element quality factor is given in Table 2.4.

Table 2.4 Element quality factor scale for mesh [47]

Unacceptable	Bad	Acceptable	Good	Very Good	Excellent
0.00-0.25	0.25-0.40	0.40-0.50	0.50-0.70	0.70-0.95	0.95-1.00

Aspect Ratio

Aspect ratio value represents the aspect ratio of a mesh element. The longest side in the element is proportional to the shortest side. The aspect ratio value of the ideal mesh element is 1. For Aspect ratio, when checking Aspect ratio, the maximum value is taken as reference, not the average value. The rating bar for aspect ratio is given in Table 2.5.

Table 2.5 Aspect ratio factor scale for mesh [47]

Excellent	Very Good	Good	Acceptable	Bad	Unacceptable
1.0-2.0	2.0-4.0	4.0-8.0	8.0-10.0	10.0-20.0	20-∞

2.1.2.6 *Boundary Conditions and Loads*

Fixed Support is defined on the 5 surfaces of the lower grap bar as boundary conditions. The sample weight is neglected. While loading, all of the analysis results were adjusted to be in the elastic region. Accordingly, a displacement in the z-axis of 0.1 mm is defined as the loading. During the analysis, the "free body diagram" of analysis number 8 is given in Figure 2.11 as an example. All boundary conditions and loadings are the same in all 15 analyzes performed.

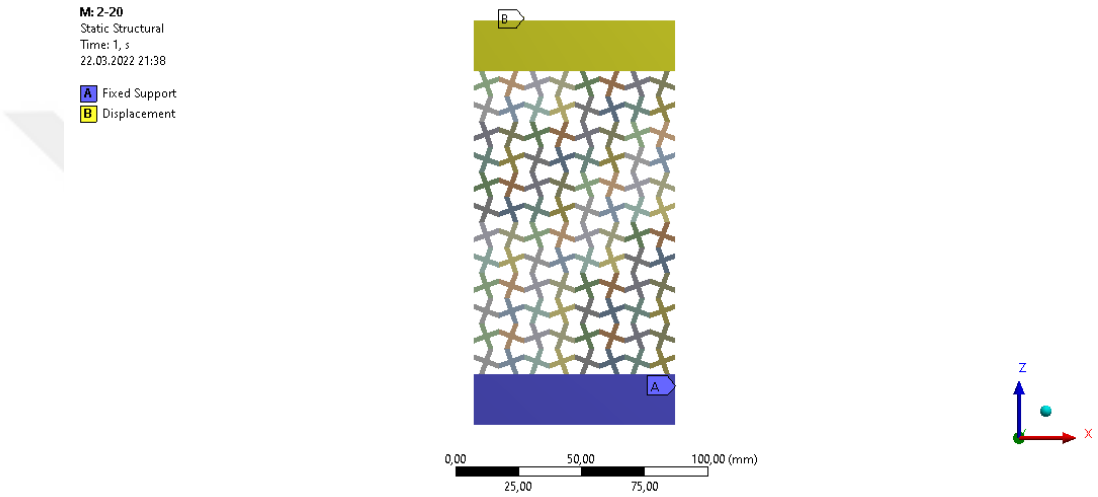


Figure 2.11 Free body diagram

2.1.3 Analysis Resutls

The settings of the analyzes were explained in detail in the previous section. In this section, the results of the completed analyzes and the Poisson's atios calculated with these results are included.

2.1.3.1 Calculation of the Poisson's Ratio

While calculating the Poisson's ratio of the sample, the Deformation Probe and Directional Deformation tool in the software were used. With these tools it will show the displacement occurring in the vertical and horizontal axes.

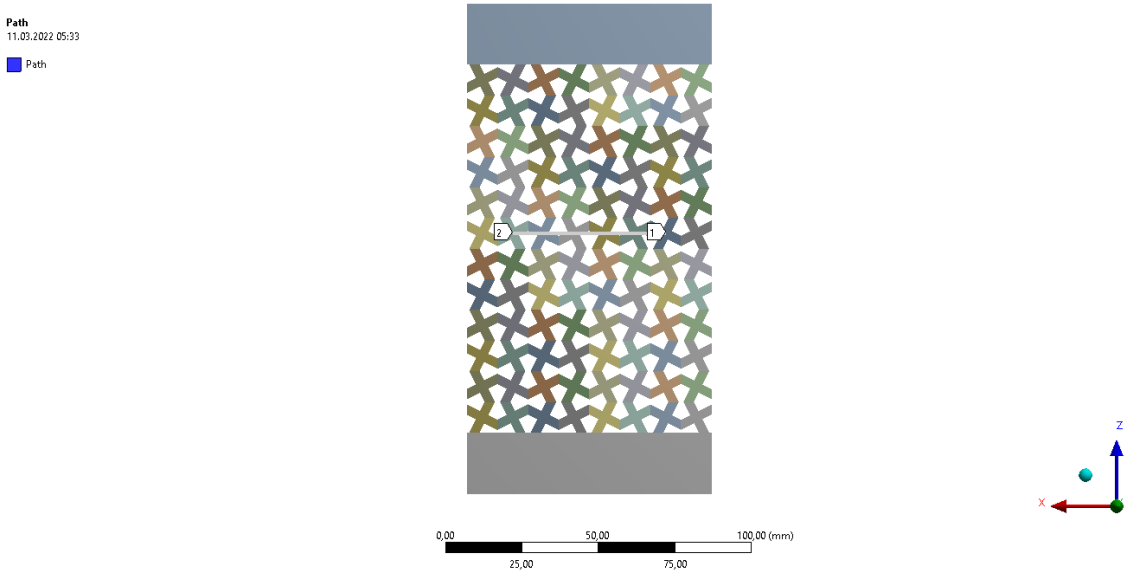


Figure 2.12 Directional deformation path demonstration

In order to apply the Poisson's ratio formula, the displacements in the Z-axis and X-axis were calculated using the analysis program. The displacement in the Z axis is obtained by subtracting the displacement of the grap bar (Z2-Z1). The total displacement in the X axis is the total displacement in the +X and -X directions on the X axis (X1+X2). While calculating the displacement in the X-axis, the middle part of the geometry was taken as reference, since the edges can move freely. Considering all these criteria, the Poisson's ratio calculation of Analysis 10 is given below. Poisson's ratio calculation is done in the same way in all analyzes.

Poisson's ratio calculation;

$$\nu = -\frac{\varepsilon_2}{\varepsilon_1} \tag{2.1}$$

$$\varepsilon = \frac{\Delta L}{L_0} = \frac{L_1 - L_0}{L_0} \tag{2.2}$$

$$\varepsilon_1 = \varepsilon_Z = \frac{\Delta L}{L_0} = \frac{L_{z_1} - L_{z_0}}{L_{z_0}} = \frac{(120.09999\ \text{mm}) - (120\ \text{mm})}{120\ \text{mm}}$$

$$= 0.00083325\ \text{mm/mm}$$

$$\varepsilon_2 = \varepsilon_X = \frac{\Delta L}{L_0} = \frac{L_{x_1} + L_{x_0}}{L_{x_0}} \tag{2.3}$$

$$= \frac{(50.0258\ mm) - (50\ mm)}{50\ mm} = 0.00051616\ mm/mm$$

$$\nu = -\frac{\varepsilon_2}{\varepsilon_1} = -\frac{0.00051616}{0.00083325} \quad \nu = -0.62$$

2.1.3.2 Comparison of Poisson's Ratios

The results of the 15 completed analyzes were made according to the calculation given in the section 2.1.3.1. Calculation of the Poisson's Ratio. All analysis results calculated according to the analysis results are given in Table 2.6.

Table 2.6 Poisson's ratios lattice structures

	Analysis No	***t* (mm)**	***α* (°)**	***ν***
1. Group	1	1	0	0.03
	2	1	10	-0.45
	3	1	20	-0.65
	4	1	26.52	-0.69
	5	1	30	-0.70
2. Group	6	2	0	0.07
	7	2	10	-0.18
	8	2	20	-0.46
	9	2	26.5	-0.58
	10	2	30	-0.62
3. Group	11	3	0	0.12
	12	3	10	-0.03
	13	3	20	-0.28
	14	3	26.52	-0.42
	15	3	30	-0.48

2.1.4 Section Evaluation and Preparation for the Next Section

Before the analysis, three groups were formed according to the t value (thickness). A total of 15 different analysis models were run under the same conditions, with 5 different angle values as reference in each group, and two different Strain results were obtained in each analysis, in the Z and X axes. With these results, the Poisson's ratio was calculated. Comparisons were made in two different ways, first within the group and then between the groups.

In the first group, the largest Poisson's ratio was 0.03, while the smallest Poisson's ratio was -0.70. The biggest difference between the two lattice structures is 0.73. The biggest difference compared to other groups is when t=1 mm. The variation of the Poisson's ratio decreases as the angle increases. 0 degree lattice geometry is non-auxetic. However, the highest Poisson's ratio variation after 0 degrees is between 0 and 10 degrees. It was observed that as the thickness increased, the Poisson's ratio change became more balanced, moving closer to linear rather than polynomial. The lowest Poisson's ratio is -0.70 with t=1mm and α=30°.

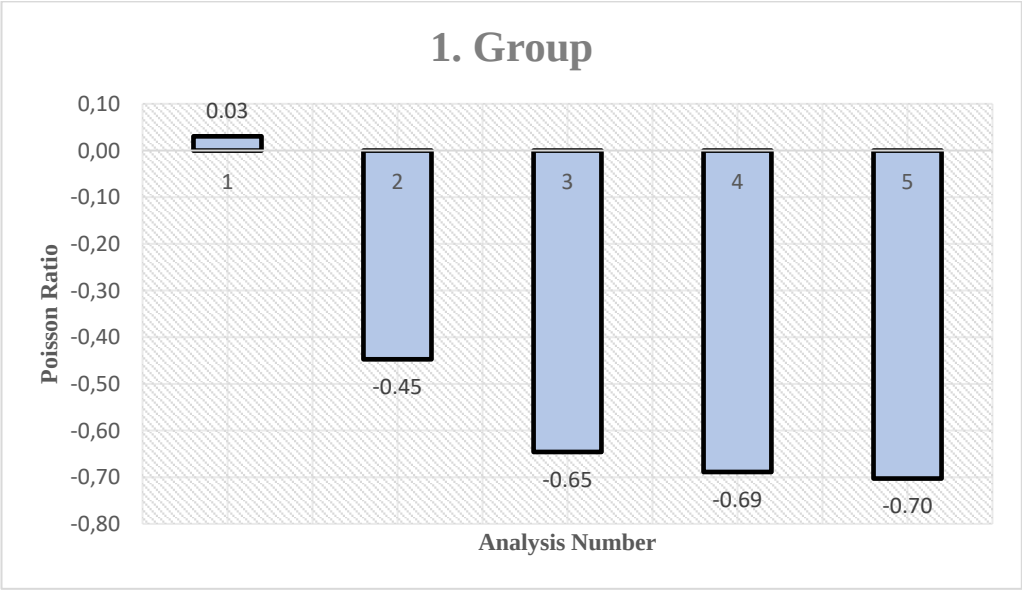


Figure 2.13 Poisson's ratio results for group 1

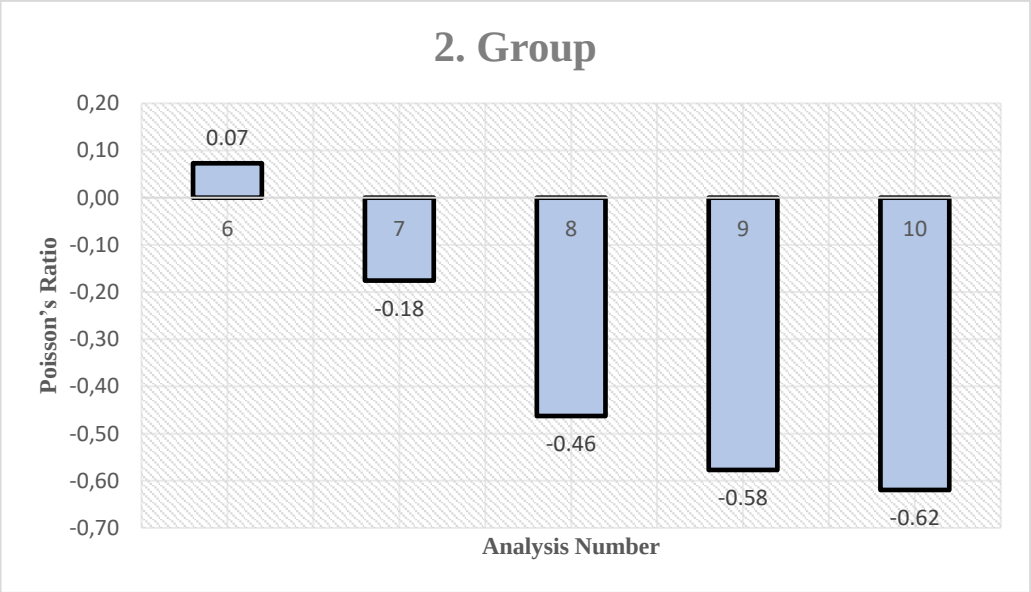


Figure 2.14 Poisson**'s** ratio results for group 2

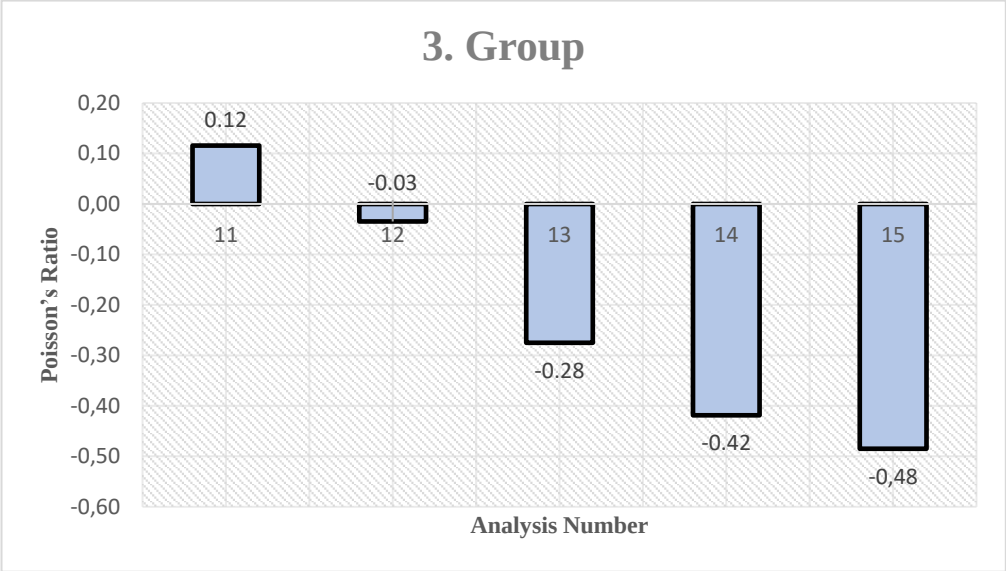


Figure 2.15 Poisson**'s** ratio results for group 3

2.2 Geometric Improvement of Lattice Structure with the Lowest Poisson's Ratio

2.2.1 Overview

In this section, geometric improvements of the lattice structure with the lowest Poisson's ratio will be made according to the 15 analysis results completed in the first section. At the end of the first section, the lowest Poisson ratio was calculated as -0.70 with t=1mm and α=30° (Analysis 5). Various geometric improvements will be made for the lattice structure with t=1mm and α=30°. While making these improvements, the lattice structure mass of the geometry will be kept constant. Poisson's ratio will be improved.

2.2.2 Geometric Improvements and Modeling

Two different geometric improvement methods will be applied to the determined lattice structure. The mathematical model of the improvements will be created and explained in the chapter.

2.2.2.1 Unit Cell and Laticce Structure Demonstration

The unit cell and lattice structure details of the original lattice structure with t=1 mm and α=30° Poisson's ratio -0.70 are given in Figure 2.16.

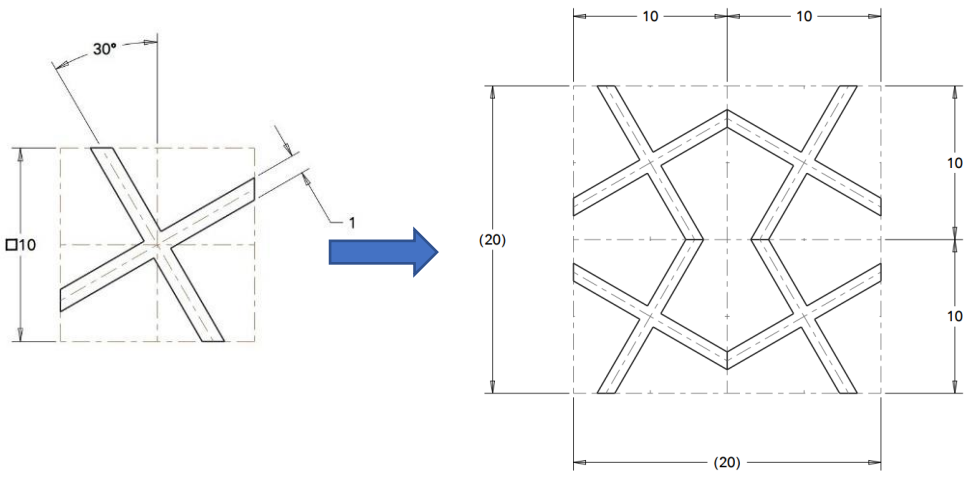


Figure 2.16 Creation of a lattice structure from the unit cell

2.2.2.2 Structural Improvement

Improvements to the determined lattice geometry will be made using two different methods. As a result of both methods, the Poisson's ratio and mass of the lattice structure will be kept constant. In both cases, it is aimed to reduce the stress level on the lattice structure.

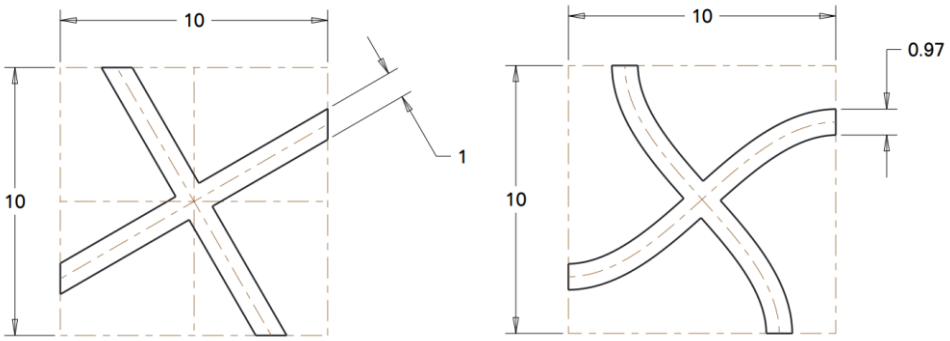


Figure 2.17 Geometric improvement applied with first method - 1

In the first method, while the unit cells are forming the lattice structure, the points where they are connected to each other and the center point of the unit cell are kept constant and a sinus curve is formed. The thickness of the unit cell was reduced from 1 mm to 0.97 mm to keep the total mass constant.

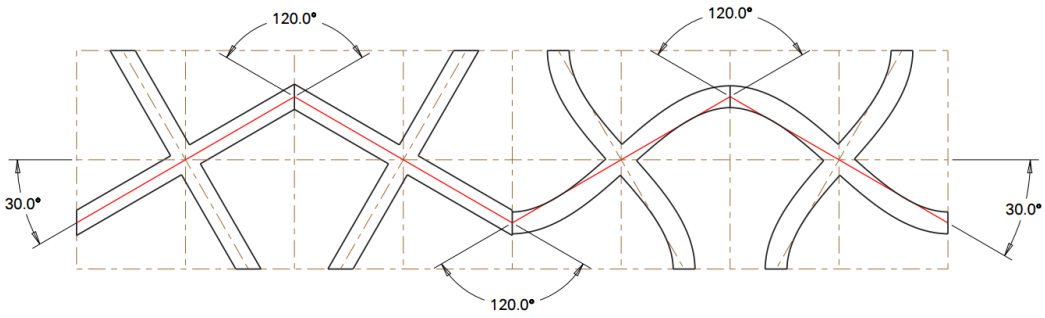


Figure 2.18 Geometric improvement applied with first method - 2

While applying the second method, reinforcement columns were added in addition to the first improvement, which was prepared according to the sinus curves formed on the horizontal and vertical axes. The thickness has been updated to 0.7 mm so that the total mass is the same as the previous two lattice structures.

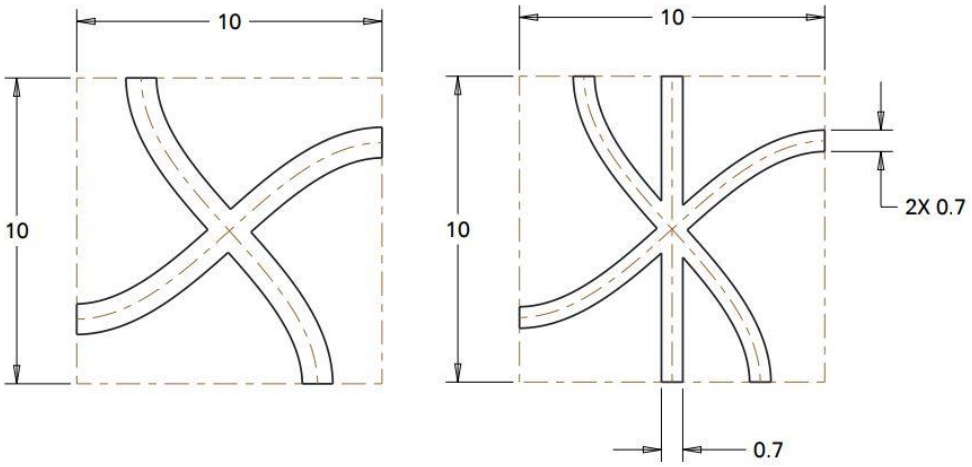


Figure 2.19 Geometric improvement applied with second method

2.2.2.3 Mathematical Modeling of Improvement

In the analyzes made, it has been observed that there are high stresses at the sharp corners. While improving the solid model, the sharp corners were eliminated by creating a new geometry according to the sinus curve in the first method. While constructing the sinus curve, the central and corner locations of the unit cell to be improved were kept constant (Figure 2.20).

While creating the mathematical model, firstly, the measurements of the center and connection points of the unit cell to be improved were taken. The distance of all joints to the center is 2.89 mm, the distances to the edge are 2.11 mm. While creating the lattice structure, the lattice structure connection point positions will be kept constant.

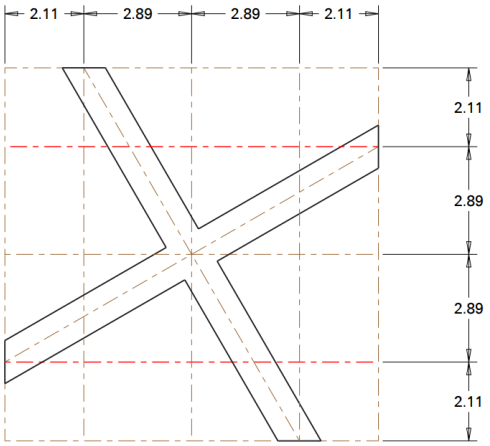
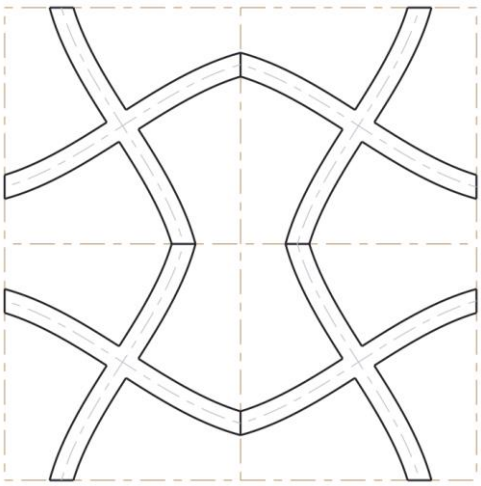


Figure 2.20 Unit cell start and end points demonstration

The center point was taken as a reference while creating the equation. While creating the lattice structure and matrix geometry, the coefficient of the sinus function was accepted as 2.89 so that the distance from the vertex to the center was 2.89 mm.

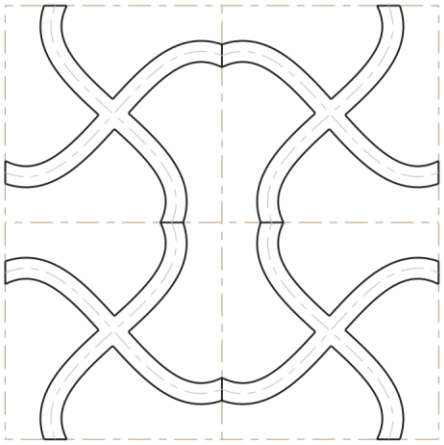
In order to form the lattice structure, unit cells must be combined. The coefficient must be determined so that the combined unit cells can be made exactly tangent to each other. The coefficient will be done with iterations by changing the value in the sinus. Iteration will continue until the result is 2.89 mm. The non-converged sample lattice structure representations obtained during the iterations are given in Figure 2.21 and Figure 2.22.



$$-5 \le y \le 5; \quad x = 2.89 \times \sin\left[\left(\frac{40}{\pi}\right) \times y\right]$$

$$-5 \le x \le 5; \quad y = 2.89 \times \sin\left[\left(\frac{40}{\pi}\right) \times x\right]$$

Figure 2.21 Different equations model 1



$$-5 \le y \le 5; \quad x = 2.89 \times \sin\left[\left(\frac{70}{\pi}\right) \times y\right]$$

$$-5 \le x \le 5; \quad y = 2.89 \times \sin\left[\left(\frac{70}{\pi}\right) \times x\right]$$

Figure 2.22 Different equations model 2

The connection curves of the lattice structure formed by combining the unit cells must be tangential to each other. For this reason, the sinus coefficient is converged until the coefficient value is obtained at the unit cell boundary of the determined equation. Converge results are given in Table 2.7.

Table 2.7 Results of first iteration

1. Iteration Results		
No	**Coefficient**	**Results**
1	0	0
2	10	0.792
3	20	1.524
4	30	2.139
5	40	2.59
6	50	2.842
7	60	2.877
8	70	2.691
9	80	2.298
10	90	1.73

During the first iteration, the values from 0 to 90 were increased by 10 points and taken as the sinus value in the equation. According to the result obtained from the first iteration, it was understood that the coefficient in the sinus was between 50 and 60. Iteration will be done again by increasing 1 point.

Table 2.8 Results of second iteration

2. Iteration Results		
No	**Coefficient**	**Results**
1	51	2.856
2	52	2.867
3	53	2.876
4	54	2.883
5	55	2.887
6	56	2.89
7	57	2.89
8	58	2.888
9	59	2.883
10	60	2.877

As a result of the second iteration completed, the desired value of 2.89 was found to be between 56.00 and 57.00. For this reason, the third iteration will be done between these two values by increasing 0.1 points.

Table 2.9 Results of third ıteration

3. Iteration Results		
No	**Coefficient**	**Results**
1	56	2.88966
2	56.1	2.88978
3	56.2	2.88986
4	56.3	2.88993
5	56.4	2.88998
6	**56.5**	**2.89**
7	56.6	2.88998
8	56.7	2.88997
9	56.8	2.88993
10	56.9	2.88986

According to the last iteration completed, it was determined that the desired coefficient to be used in the sinus was 56.5. With the iterations, the mathematical model has been

100% converged. The equation of the sinus curve for the horizontal axis is given in Figure 2.23. The same method was also applied for the vertical axis.

$$y = 2.89 \times \sin\left[\left(\frac{56.5}{\pi}\right) \times x\right]$$

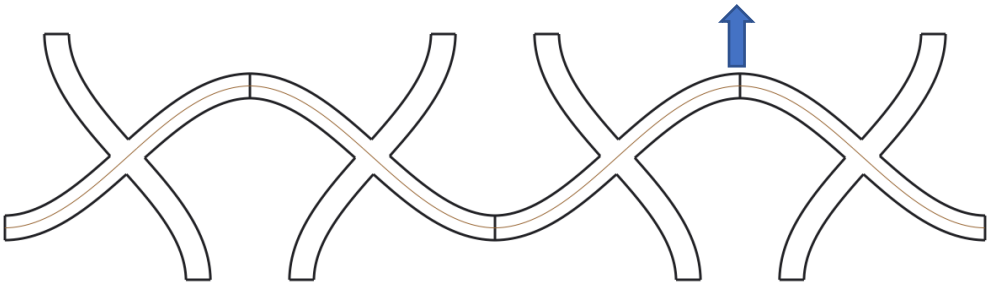


Figure 2.23 Horizontal axis sinus curve equation

Mathematical modeling;

The unit cell consists of two different curves. The formula for these curves is as follows:

$$-5 \leq y \leq 5; \quad x = 2.89 \times \sin\left[\left(\frac{56.5}{\pi}\right) \times y\right] \tag{2.4}$$

$$-5 \leq x \leq 5; \quad y = 2.89 \times \sin\left[\left(\frac{56.6}{\pi}\right) \times x\right] \tag{2.5}$$

When both equations are combined, the unit cell is formed. In order to make the structure more robust, a support column was added by applying method 2. Reinforced unique lattice structure was created by combining the improved unit cells.

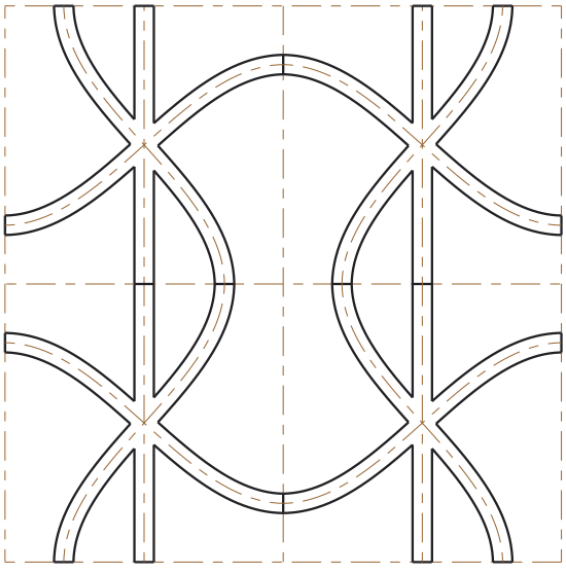


Figure 2.24 Geometric improved lattice structure

2.2.2.4 Improved Unit Cell Mathematical Equation

The unit cell on which improvement has been made is given below. Three different formulas are applied to form the unit cell.

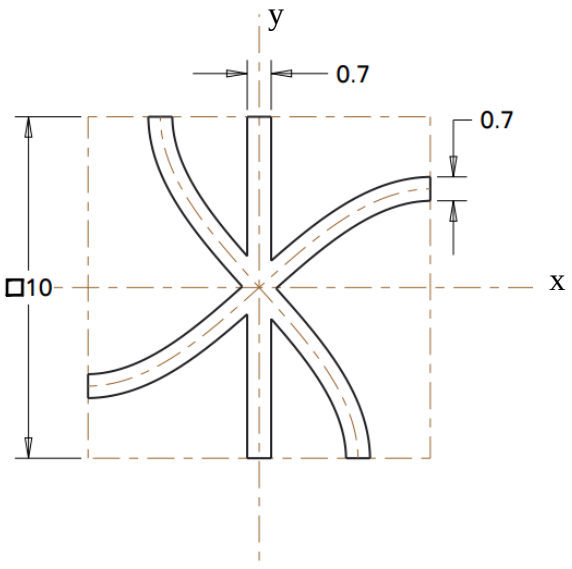


Figure 2.25 Geometrically improved unit cell

Unit Cell Mathematical Modeling;

When the three given equations are combined, the unit cell given in Figure 2.25 is obtained.

$$-5 \leq y \leq 5; \quad x = 2.89 \times \sin\left[\left(\frac{56.5}{\pi}\right) \times y\right] \tag{2.6}$$

$$-5 \leq x \leq 5; \quad y = 2.89 \times \sin\left[\left(\frac{56.5}{\pi}\right) \times x\right] \tag{2.7}$$

$$-5 \leq y \leq 5; \quad x = 0 \tag{2.8}$$

2.2.2.5 Mechanical Comparison of Unit Cells

Two different geometric improvements were made to the lattice structure with the lowest Poisson's ratio obtained at the end of the first chapter. Like this; A total of three different unit cells were obtained: normal unit cell, unit cell in which only the first method was applied, and unit cell in which both methods were applied. These unit cells are named as unit cell 1, unit cell 2 and unit cell 3 respectively.

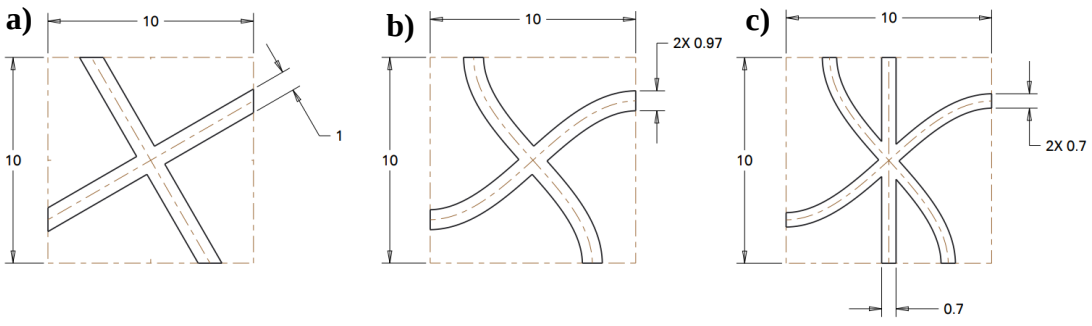


Figure 2.26 Unit cell 1 (a), unit cell 2 (b), unit cell 3 (c)

AL 6061-T6, which is frequently used in many fields such as aerospace and defense industry, is used as material. The mechanical properties of the material used are given in section 2.1.2.3. These mechanical properties were taken as reference when

calculating the mass of the unit cells. Mass information of unit cells is given in Table 2.10.

Table 2.10 Unit cell mass details

	$\boldsymbol{V\ (m^3)}$	$\boldsymbol{\rho\ (\frac{kg}{m^3})}$	$\boldsymbol{m\ (g)}$
Unit Cell 1	2.21×10^{-6}	2700	5.97
Unit Cell 2	2.20×10^{-6}	2700	5.94
Unit Cell 3	2.21×10^{-6}	2700	5.97

The mass of the normal unit cell is calculated as 5.97g. The improved first unit cell is 5.94g. There is approximately 0.5% difference between them. The unit cell mass does not change when the support column is added.

2.2.3 Model Details of Improved Unique Lattice Structures

The unit cell, lattice structure and analysis geometry details of the determined geometry are given in the previous sections. In this section, the model details of the first improved geometry and the improved second geometry will be given. Creo Parametric 5.0.4.0 was used as solid model program.

2.2.3.1 Unit Cell Demonstration

After the geometric improvements were completed, two different unit cells were created. The outer dimensions of these unit cells were taken as 10×10×10 mm.

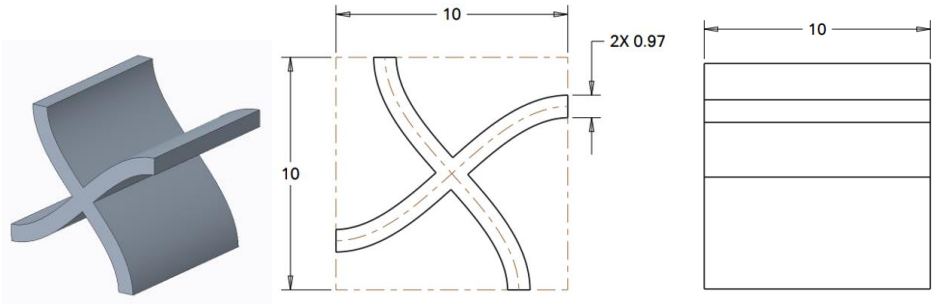


Figure 2.27 Improved unit cell 1

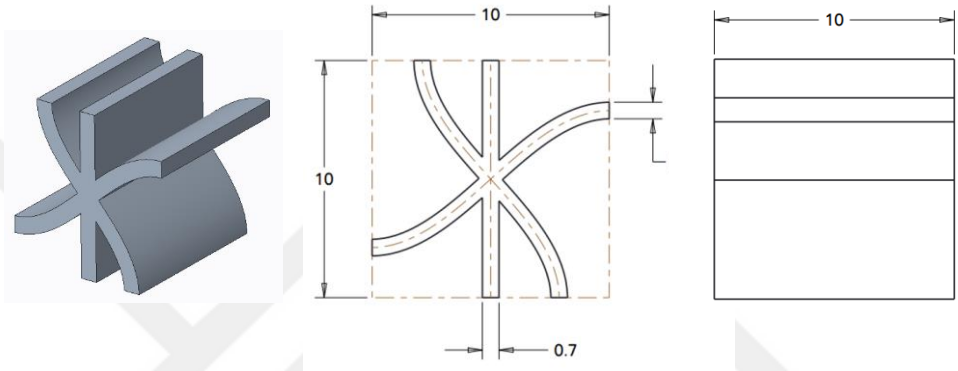


Figure 2.28 Improved unit cell 2

2.2.3.2 Lattice Structure Demonstration

After the improvements made, the unit cells forming the lattice structures section 2.1.1.2. It is assembled symmetrically with respect to the x and y axes. The lattice structure representation for both lattice structures created is given in Figure 2.29 and Figure 2.30.

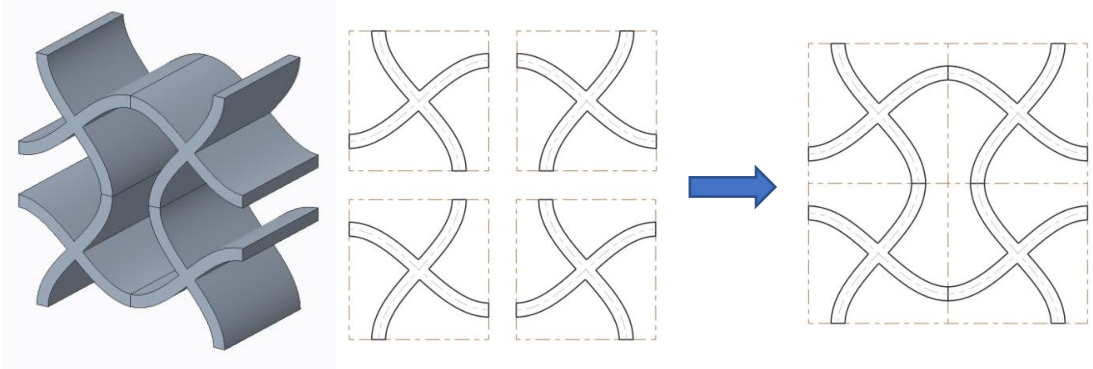


Figure 2.29 Improved lattice structure 1

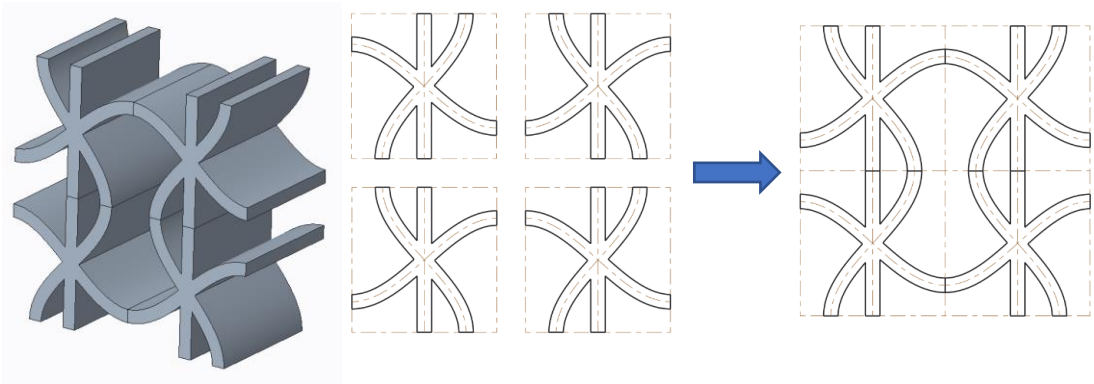


Figure 2.30 Improved lattice structure 2

2.2.3.3 Matrix Demonstration

Before the analysis of the improved geometries, the lattice structures were combined to form the matrix geometry. Model dimensions to be analyzed, section 2.1.1.3. The matrix geometry models to be analyzed for both improved geometries are given in Figure 2.31 and Figure 2.32.

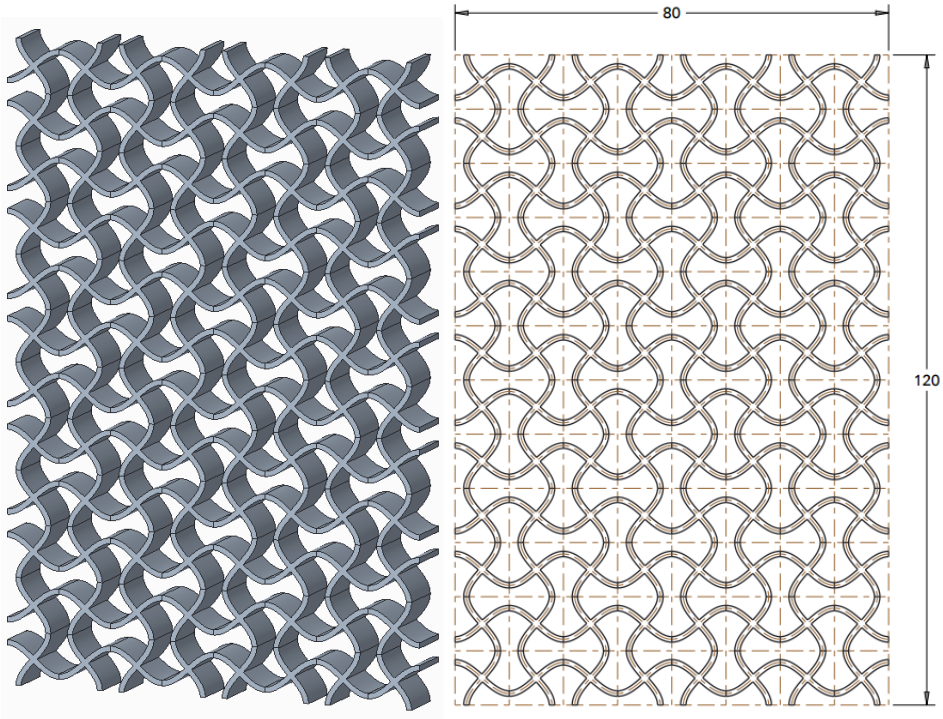


Figure 2.31 Improved matrix 1

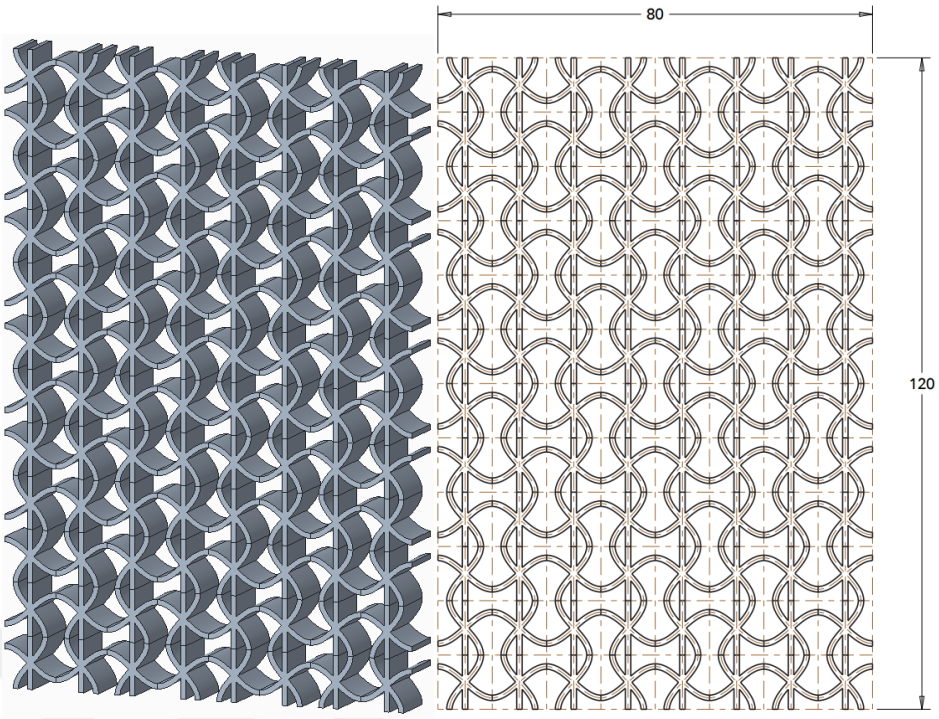


Figure 2.32 Improved matrix 2

2.2.4 Analysis Settings

In this section, the structural analysis settings of two different lattice structures will be given. According to the analysis results, the Poisson's ratios of the geometries will be calculated. An analysis program that works with the finite element method will be used during the analysis. Details of the analysis are given in detail in the section. For other settings not shown, the program's default settings are used.

2.2.4.1 Analysis Geometry Information

As a result of two different improvements applied to the determined geometry, two different lattice structures were created. Details of the geometries to be analyzed are given in section 2.2.3.

2.2.4.2 Solid Model Information

In order for the load and boundary condition points defined in the analysis to be balanced, a grap bar is added to the lower and upper limits of the assembly model. The external dimensions of the analysis geometry with the grapa bar were 80×160×10 mm.

In analysis geometry, lattice structures consist of 4 rows and 6 columns. Thus, it consists of a total of 24 lattice structures and 2 grap bars.

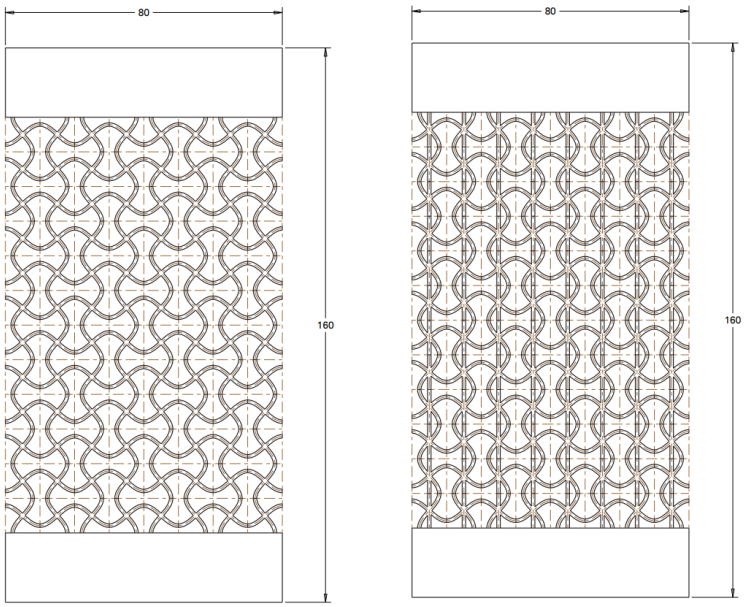


Figure 2.33 Analysis geometries

2.2.4.3 Material Properties

Aluminum 6061-T6 was assigned as the material to all unit cells and grap bars in the analysis models, as in the first group analyses. The properties of the material are given in Table 2.2 in detail.

2.2.4.4 Contact Algorithms

All components in the analysis geometries are connected to each other at the contact points with a "Bonded" (inseparable) connection. During the analysis, the geometry will move together as a single part. An example contact algorithm is given in Figure 2-29.

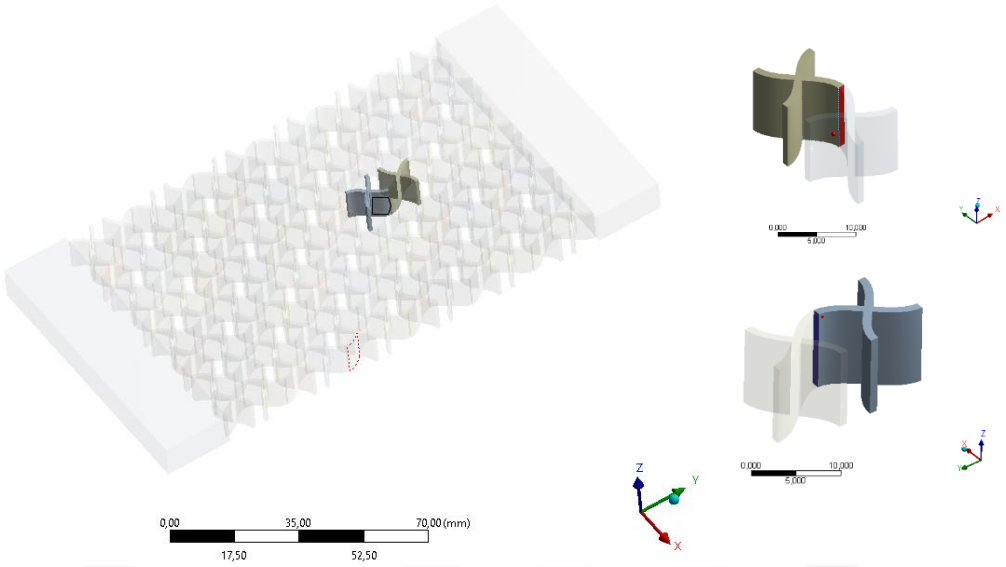


Figure 2.34 Example of contact algorithm

2.2.4.5 *Mesh Details*

The mesh size of the unit cells is 0.5 mm, and the mesh size of the grap bars is 2 mm. No special method has been assigned as a method, the default method has been used. Element Quality and Aspect Ratio values were checked as used in the previous sections to check the element quality.

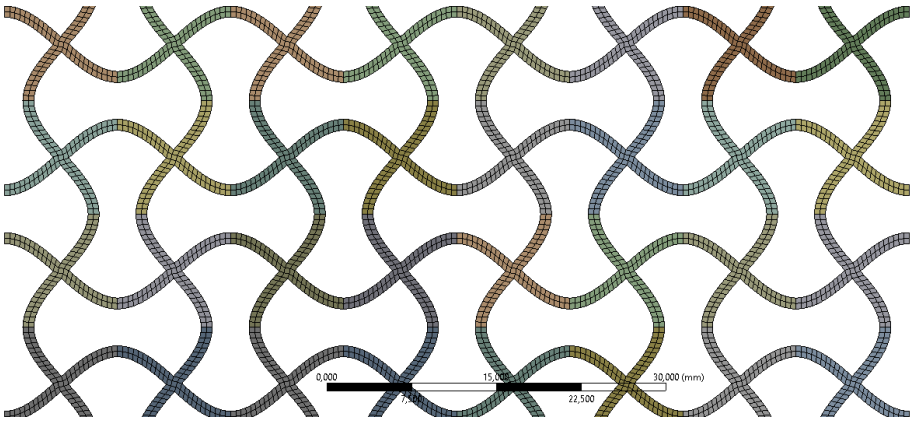


Figure 2.35 Example mesh form demonstration

Mesh form directly affects the analysis results. Element Quality and Aspect Ratio in the mesh metric tool included in the program have been confirmed for network structure control. The results obtained are given in Table 2.11.

Table 2.11 Mesh details

Analysis Model	Node Number	Element Number	Element Quality (m)	Aspect Ratio (max)
Improved Geometry 1	1094554	190240	0.92719	1.307
Improved Geometry 2	1456666	251680	0.88399	2.047

2.2.4.6 Boundary Conditions and Loads

All boundary conditions and loadings were applied from the upper and lower grab bars added to the analysis geometry. Fixed Support is applied to the 5 surfaces of the lower grap bar as a boundary condition. While loading, it was applied to the 5 surfaces of the upper grap bar evenly, 0.1 mm, from the y-axis. The free body diagram of the analysis geometry is given in Figure 2.36.

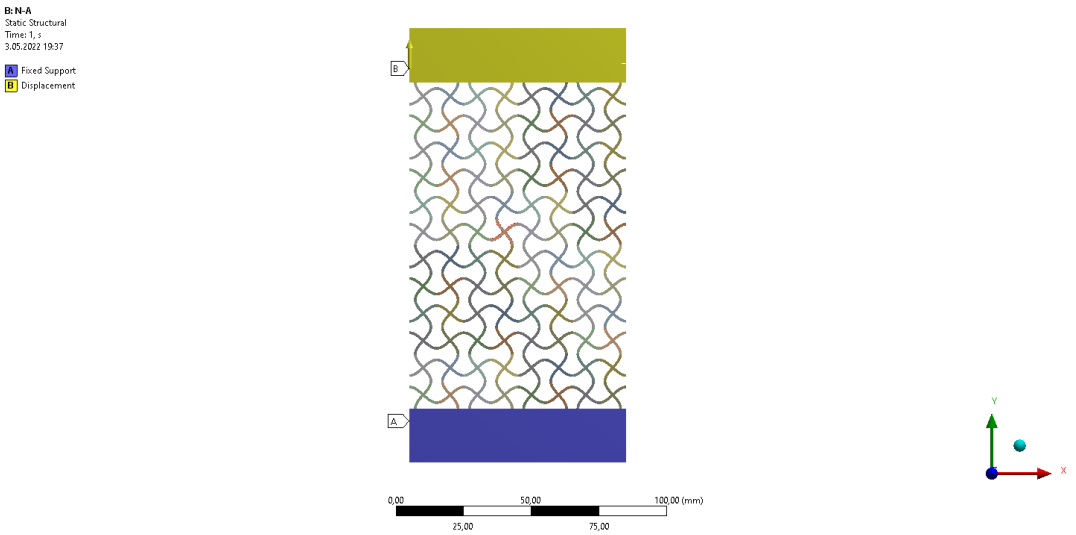


Figure 2.36 Free body diagram

2.2.5 Analysis Results

Completed analysis settings are described in detail in the previous section. All settings not detailed are default settings. In this section, the results of the analysis and the Poisson's ratios calculated according to these results are included.

2.2.5.1 Calculation of Poisson's Ratio

According to the results of the analysis, the method used in section 2.1.3.1 was used while calculating the Poisson's ratio. Calculation was made according to the deformation probe results in the program.

Poisson's is the ratio of vertical displacement to horizontal displacement. All of the accounts are given in detail in section 2.1.3.1.

2.2.5.2 Comparison of Poisson's Ratios

Poisson's ratios were calculated according to the results of both analyzes run. The Poisson's ratio for the improved 1st lattice structure was found to be -0.78. For the improved 2nd geometry supported by the column, the Poisson's ratio was calculated as -0.73. In the previous section, the Poisson's ratio of normal geometry was calculated as -0.70.

2.2.6 Section Evaluation and Preparation for the Next Section

According to the analysis results of the original lattice structure, which was completed by defining various angles and thicknesses in the previous section, it was revealed that the lowest Poisson's ratio was -0.70, with t=1mm and $\alpha=30°$. In this section, it is aimed to make two different improvements in order to reduce the stress on this determined lattice structure.

In the first method, the mass was kept constant and the sinus curve was formed without changing the center and edge contact points, and the sharp corners on the structure were eliminated. In the second method, in addition to the first method, support columns are added to the unit cell. Unit cell thicknesses have been revised so that the lattice masses do not change. The external dimensions of the unit cell have not been changed

and the Poisson's ratio has been kept constant. A mathematical model of the unit cells with geometric improvements was created. This mathematical equation was taken as reference while creating the unit cell design, lattice structure and assembly geometry.

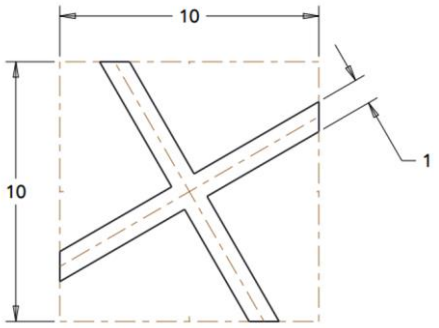


Figure 2.37 Unit cell of normal geometry

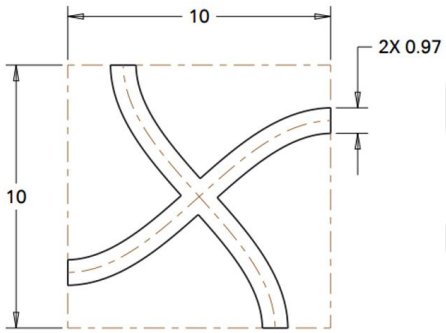


Figure 2.38 Unit cell of ımproved geometry 1

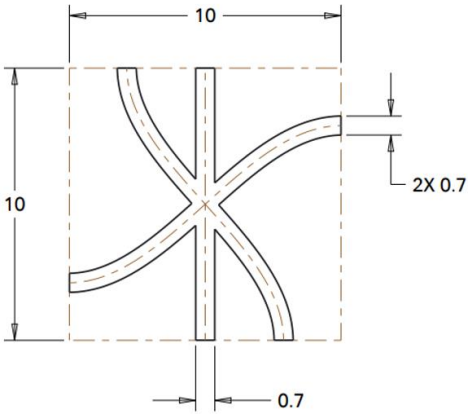


Figure 2.39 Unit cell of ımproved geometry 2

After the geometric improvements were completed, structural analysis was performed on both improved geometries using the finite element method to calculate the Poisson's ratio of the lattice structures. Analysis settings are given in detail in the section. All the settings of the analysis performed are the same as the settings of the 15 analyzes made in the first section.

According to the results of the analysis, the Poisson's ratio and masses of the lattice structure before the improvement and the two lattice structures after the improvement are given in Table 2.12.

Table 2.12 Mass and Poisson's ratios of lattice structures

Lattice Structure	**Poisson's Ratio (ν)**	**Unit Cell Mass (g)**
Normal Lattice Structure	-0.70	5.97
Improved Lattice Structure 1	-0.78	5.94
Improved Lattice Structure 2	-0.73	5.97

The geometry with the lowest Poisson's ratio was calculated as the Improved 1st Lattice structure. Then comes the improved 2nd Lattice structure, and the highest Poisson's ratio is that of the normal geometry. Unit cells have the same mass.

The geometry with the lowest Poisson's ratio was calculated as the Improved 1st Lattice structure. Then comes the improved 2nd Lattice structure, and the highest Poisson's ratio is that of the normal geometry. Unit cells have the same mass.

2.3 Comparison of Obtained Lattice Structures with Structural Analysis

2.3.1 Overview

This section includes the examination of three different lattice structures obtained from the previous sections under various forces. An analysis program using the finite element method will be used for this examination.

In the first part, analyzes were made according to thickness and angle parameters. In the second section, geometric improvements were applied to the lattice structure with the lowest Poisson's ratio. In total, three different lattice structures were obtained.

Comparisons will be made by applying various analyzes to the lattice structures obtained. First, the static analysis will be completed by applying equivalent forces with the Static Structural module to examine the behavior of three different lattice structures under static force. Then, modal analysis will be performed with the aim of calculating the natural frequencies of the structures and finding their modes. Finally, collision analysis will be performed with the explicit analysisys module to calculate the shock absorption.

2.3.2 Analysis Settings

A total of three different structural analyzes will be applied to the three different lattice structures to be analyzed. This section contains the common settings of the different analyzes to be applied. Settings other than common settings are given in detail in the subsections.

2.3.2.1 Analysis Geometry Information

A total of three different analyzes, Modal, Static Structural and Explicit Dynamics, were run for three different unique lattice structures determined. The details of the analyzed unit cell are given in Figure 2.40.

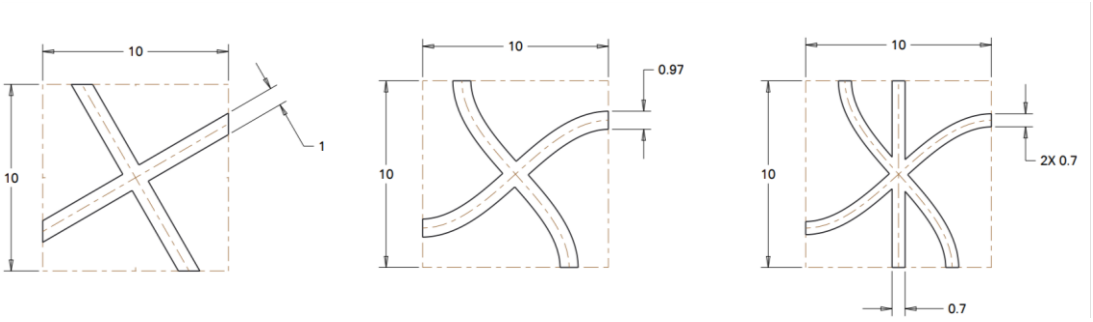


Figure 2.40 Structural analysis unit cell details

2.3.2.2 Solid Model Information

The unit cells that form the lattice structure used in the three completed analyzes are given in detail in section 2.3.2.1. The same solid model was used for static structural and modal analysis. All three solid models consist of a total of 24 lattice structures (96 unit cells) and two grap bars (Figure 2.41.). The outer dimensions of the model are 80×160×10 mm with the grab bar.

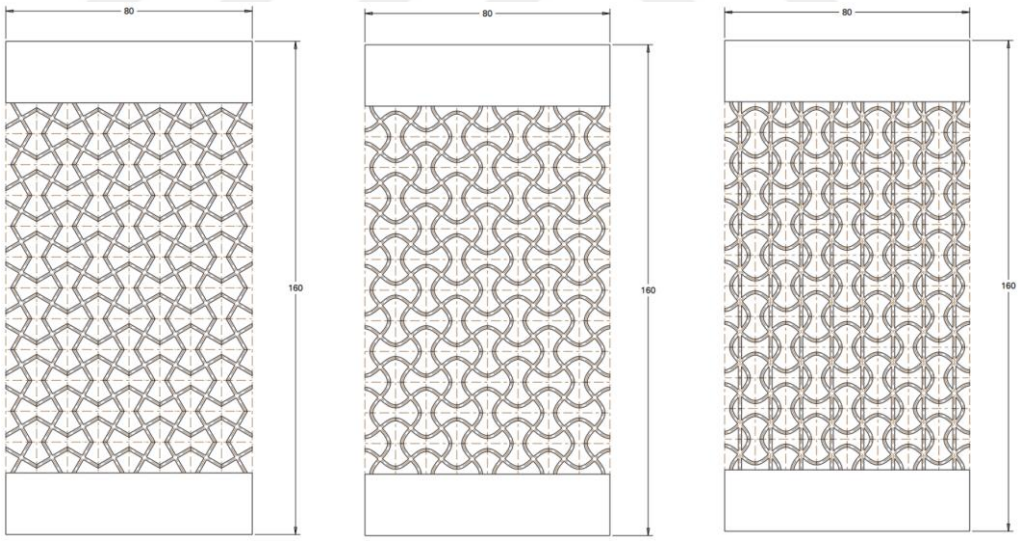


Figure 2.41 Static structural and modal analysis solid models

However, due to the Explicit dynamic solution time, the solid model used in the analysis consists of 12 lattice structures (48 unit cells) and two grap bars (Figure 2.42.). The dimensions of the analyzed solid model are 80×60×10 mm.

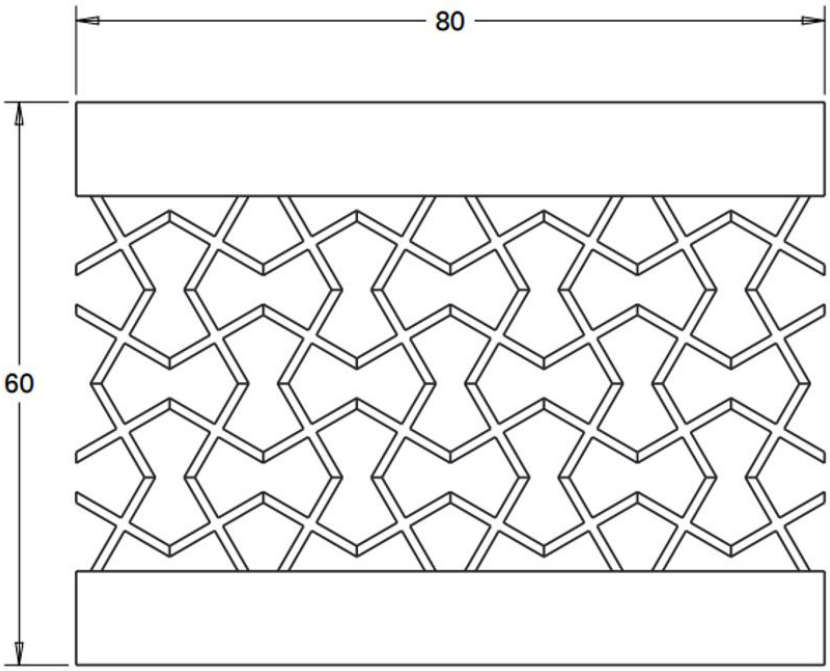


Figure 2.42 Explicit dynamics analysis matrix of normal geometry

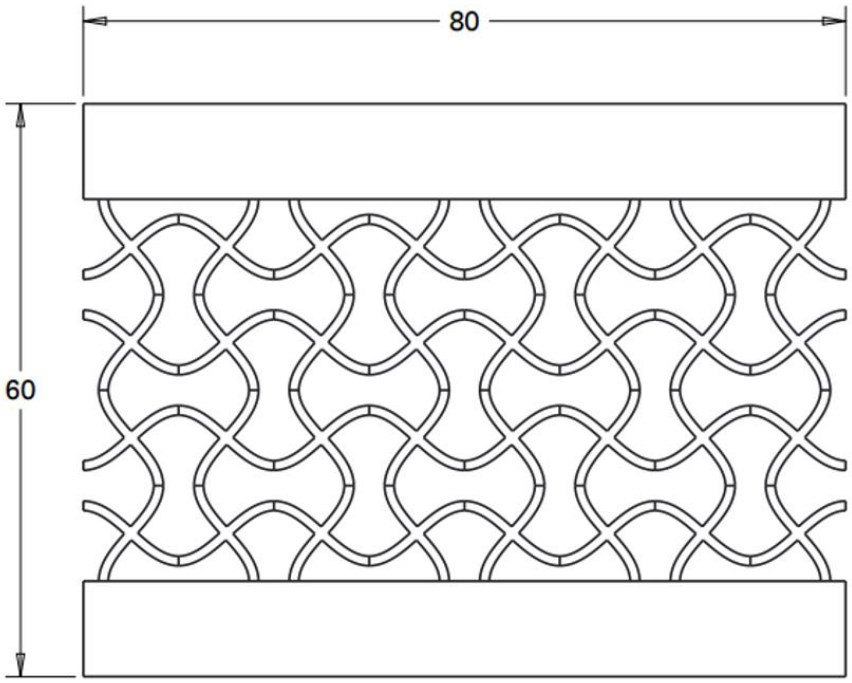


Figure 2.43 Explicit dynamics analysis matrix of improved geometry 1

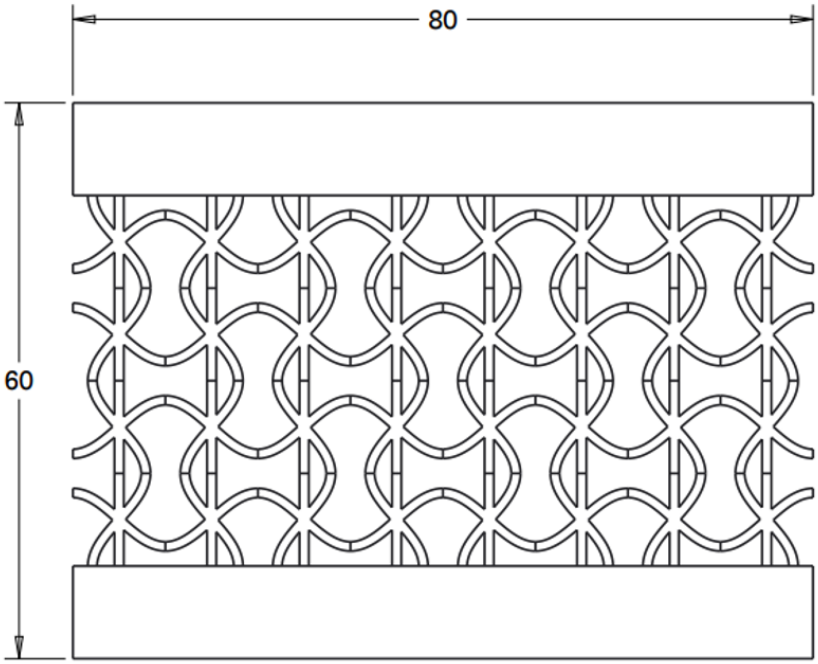


Figure 2.44 Explicit dynamics analysis matrix of improved geometry 2

2.3.2.3 Material Properties

AL6061-T6 used in all previous analyzes was used in all three completed analyzes. The mechanical properties of the material are given in Table 2.2.

2.3.2.4 Contact Algorithms

All the parts that come into contact with each other are connected to each other by an inseparable connection "bonded". Other settings are the default settings in the program.

2.3.2.5 Mesh Details

The prepared Static structural/Modal analysis solid model and Explicit Dynamics analysis solid model mesh structure are different from each other. No method has been assigned to any model. However, a maximum size of 2 mm for grab bars and 0.5 mm for all unit cells was defined for the static structural/modal analysis solid models as mesh dimensions. For the Explicit Dynamics analysis floor model, all elements were set to a maximum size of 1 mm using the “sizing” tool.

In order to control the mesh quality, Aspect Ratio and Element Quality values in Mesh Metric were checked in this section, as in the previous sections. Mesh details are given in Table 2.13.

Table 2.13 Mesh details

Analysis Model	Node Number	Element Number	Element Quality (m)	Aspect Ratio (max)
Normal Lattice Structure (Static Structural /Modal)	1477018	282400	0.78689	1.755
Normal Lattice Structure (Explicit Dynamics)	56155	39680	0.88071	2.244
Improved Lattice Structure 1 (Static Structural /Modal)	1094554	190240	0.92719	1.307
Improved Lattice Structure 1 (Explicit Dynamics)	47707	32000	0.99505	1.189
Improved Lattice Structure 2 (Static Structural/Modal)	1456666	251680	0.88399	2.047
Improved Lattice Structure 2 (Explicit Dynamics)	55099	35520	0.96249	2.362

2.3.3 Modal Analysis for Geometries

Modal analysis was performed to see the vibration characteristics in various boundary conditions. Thus, at which frequencies the system can resonate and the deformation orientation have been determined.

2.3.3.1 Modal Analysis Settings

During the modal analysis, no pre-stress or loading was applied to the models. As a boundary condition, fixed support was assigned from the 5 surfaces of the lower grap bar. An example free body diagram is given in Figure 2.45. The maximum number of modes to be calculated is set to 6.

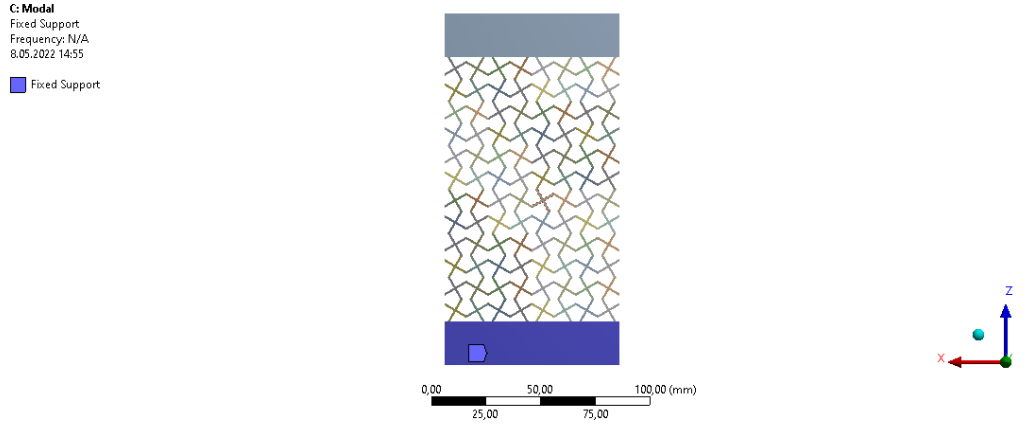


Figure 2.45 Modal analysis free body diagram

2.3.3.2 *Modal Analysis Results*

In the analysis, a total of 6 different mode values and the deformation according to these modes were calculated. The mode frequencies obtained for all three solid models according to the analysis results are given in Table 2.14.

Table 2.14 Modal analysis frequencies

Mode Number	Normal Geometry	Improved Geometry 1	Improved Geometry 2
Mode 1	61.466	52.964	153.73
Mode 2	208.46	175.89	220.77
Mode 3	342.89	346.81	429.83
Mode 4	537.54	464.76	902.84
Mode 5	848.34	729.75	1308
Mode 6	946.19	770.34	1796.4

Normal Geometry Results

For normal geometry, the first mode was found to be 61.47 Hz, the mode shape (the state before deformation is shown with the wireframe) is shown in Figure 2.46.

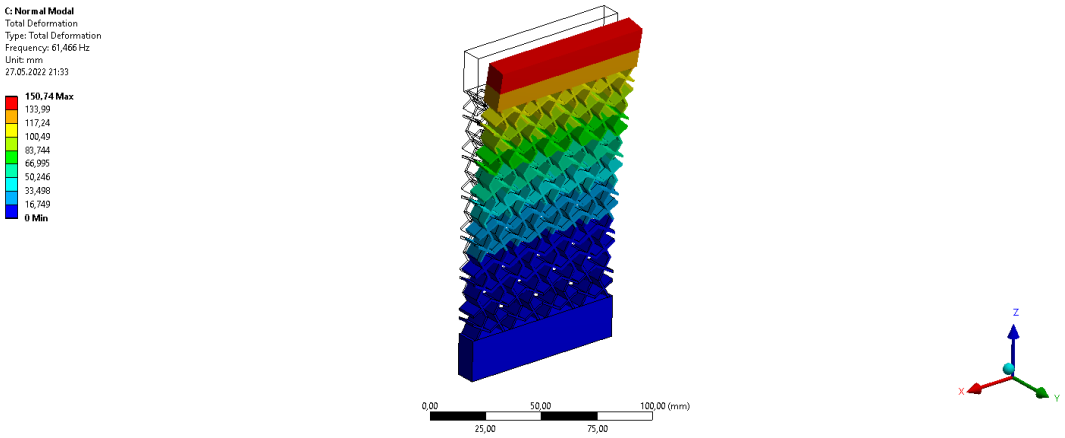


Figure 2.46 Normal geometry mode 1 deformation

However, it is one of the most important mode shapes because of the 6th mode deformation. In this mode, the geometry is deformed axially (Figure 2.47) and the frequency value is 946 Hz.

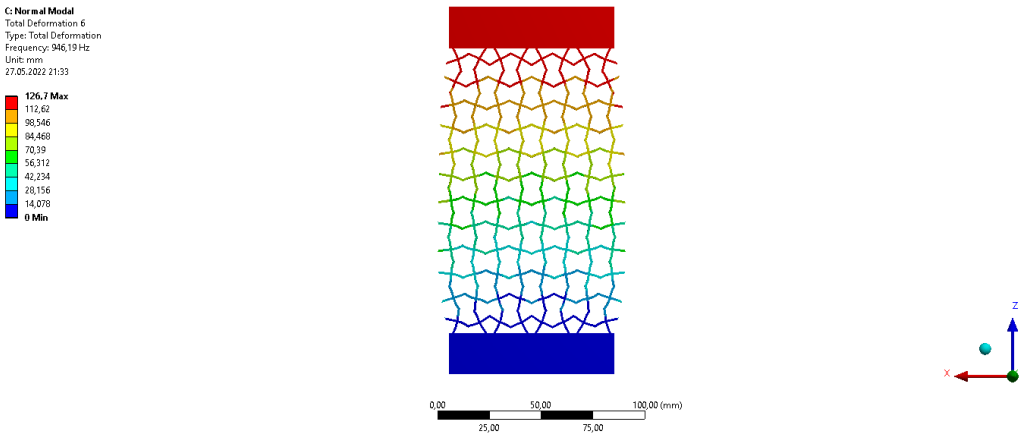


Figure 2.47 Normal geometry mode 1 deformation

Improved 1. Geometry Modal Analysis Results

According to the geometry analysis result created by the first improvement, the 1st Mode value was calculated as 53 Hz. Mode deformation is similar to normal geometry (Figure 2.48.).

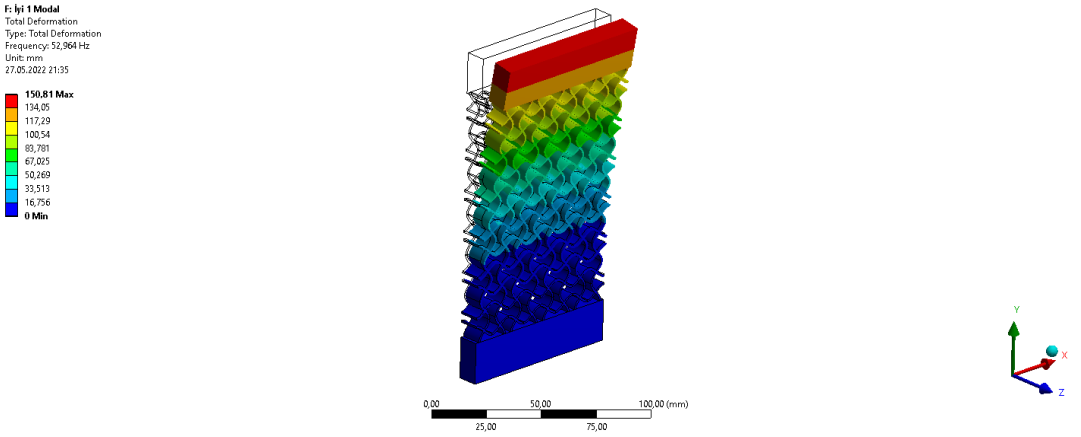


Figure 2.48 Improved geometry 1 mode 1 deformation

The mode with axial deformation for the improved 1st geometry is the 6th mode with 770 Hz (Figure 2.48.).

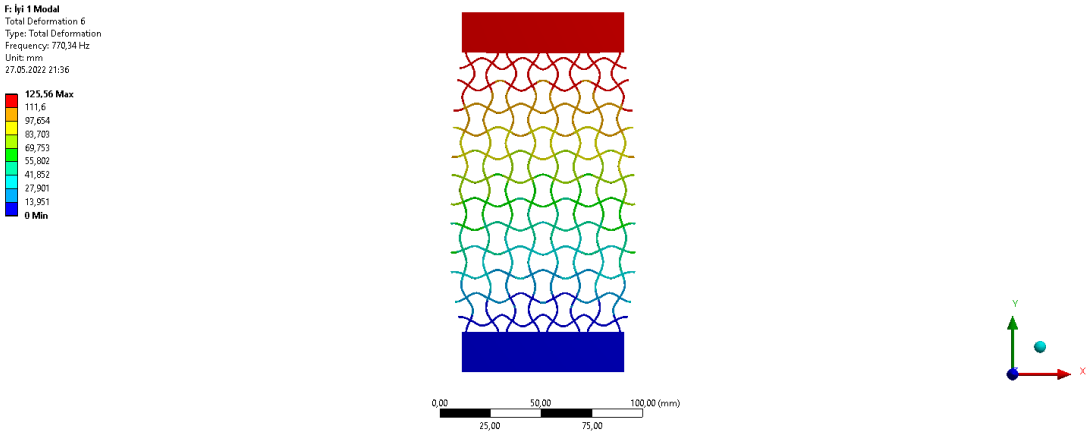


Figure 2.49 Improved geometry 1 mode 6 deformation

Improved 2. Geometry Modal Analysis Results

According to the modal analysis results of the lattice structure created by adding a support column, the 1st mode value is 153.7 Hz. In Figure 2.50, its deformed state (as a wireframe) is given as it was before it was deformed.

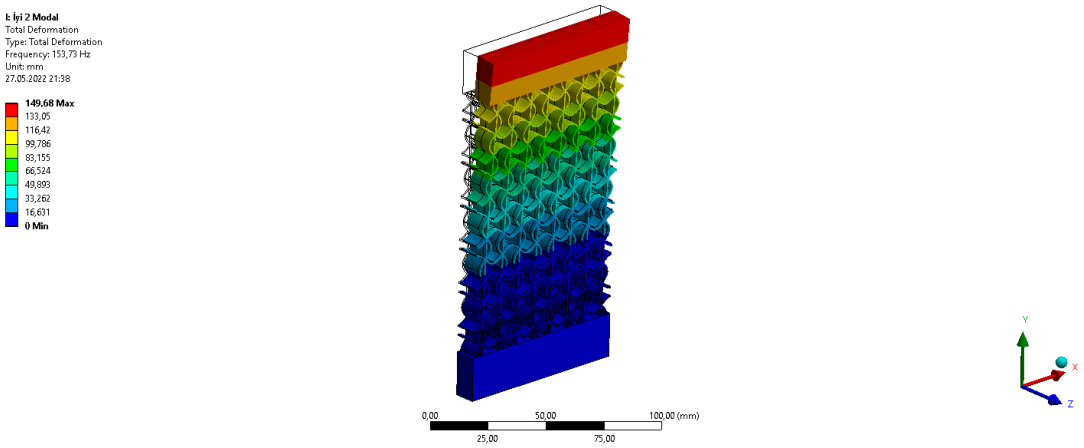


Figure 2.50 Improved geometry 2 mode 1 deformation

Due to the support column added in addition to the other lattice structures, axial deformation was observed at 3428.3 Hz in the 10th mode.

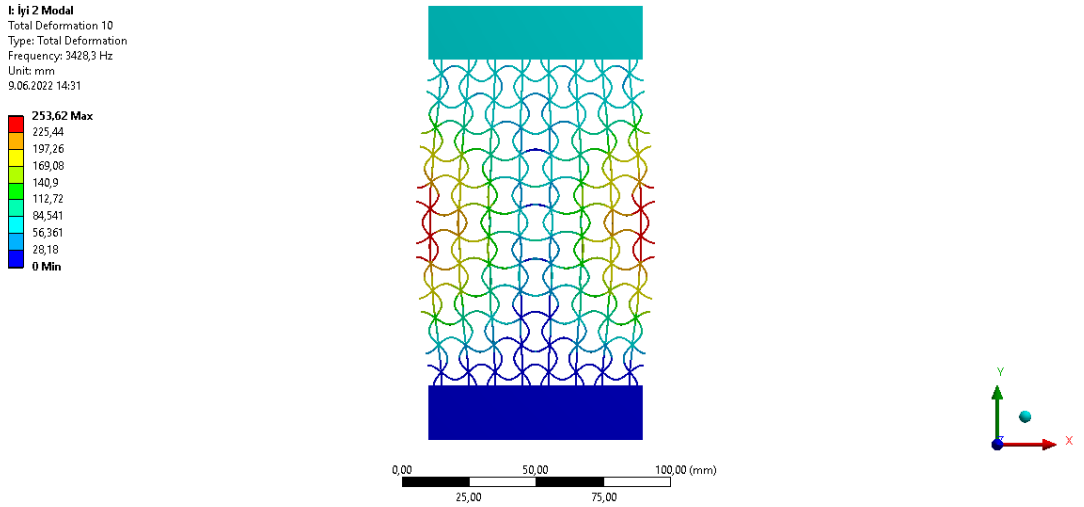


Figure 2.51 Improved geometry 2 mode 10 deformation

2.3.4 Static Structural Analysis for Geometries

Structural static analyzes were carried out in order to see the deformation and stress level that may occur as a result of a loading on the determined lattice structures. According to the results of the analysis, the reaction of the lattice structure against these loads will be shown under constant loading.

2.3.4.1 Static Structural Analysis Settings

Settings related to material assignment, mesh form and contact algorithms are given in section 2.3.2. Boundary conditions and loadings were applied from the bars as in the previous analyses. Boundary conditions and loadings are the same for all three analysis models. Fixed Support was applied from the 5 surfaces of the lower grap bar as a boundary condition and a force of 200 N was applied to the upper grap bar as a loading. The sample free body diagram of the analyzes made in this section is given in Figure 2.52.

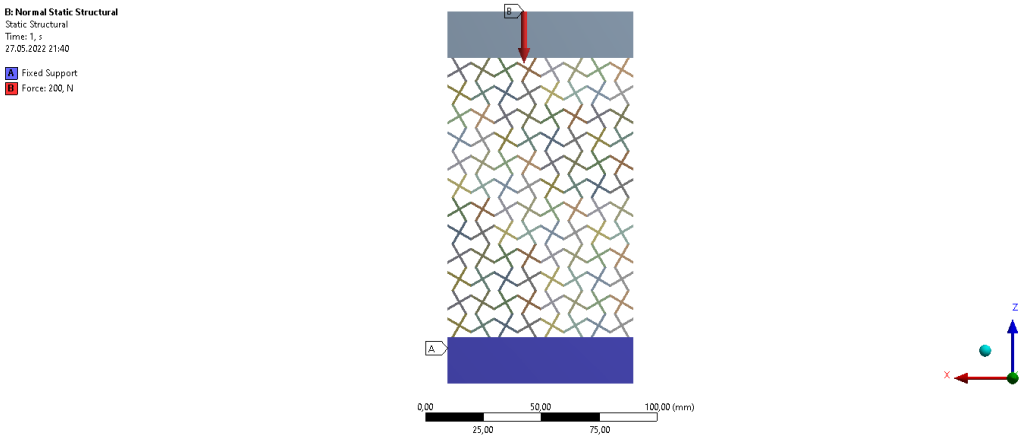


Figure 2.52 Static analysis free body diagram

2.3.4.2 Static Structural Analysis Results

According to the completed static analysis results, total deformation and stress level results were obtained. The displacement and equivalent stress values obtained for all three analyzes are given in Table 2.15.

Table 2.15 Equivalent stress and total displacement results

Analysis Model	Equivalent Stress (MPa)	Total Deformation (mm)
Normal Lattice Structure	41.28	0.088296
Improved Lattice Structure 1	35.643	0.13162
Improved Lattice Structure 1	8.4588	0.0059012

Normal Geometry Static Analysis Results

The equivalent stress level of the normal geometry was found to be higher than the other two models. The stress zone is the sharp corners where transitions occur. The maximum stress was calculated as 41.28 MPa. The maximum deformation was calculated as 0.088 mm. However, this value was formed at the corner of the lattice structure. Therefore, the maximum deformation should be taken as the displacement in the upper bar. The maximum average deformation of the upper grap bar was calculated as 0.083 mm (Figure 2.54).

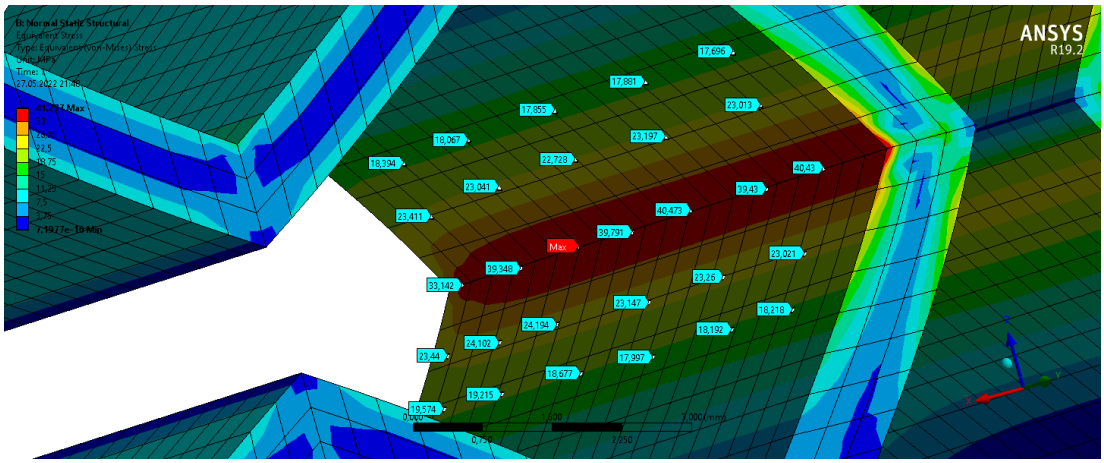


Figure 2.53 Normal geometry equivalent stress

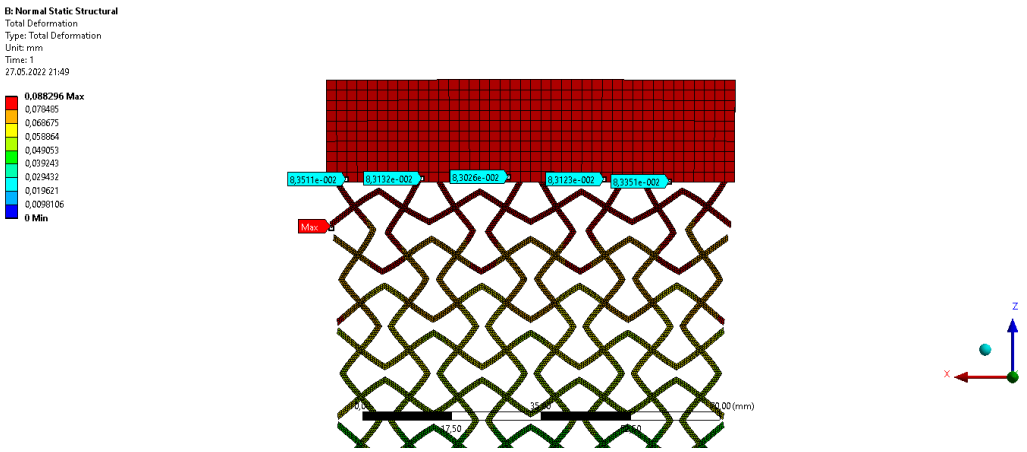


Figure 2.54 Normal geometry equivalent stress

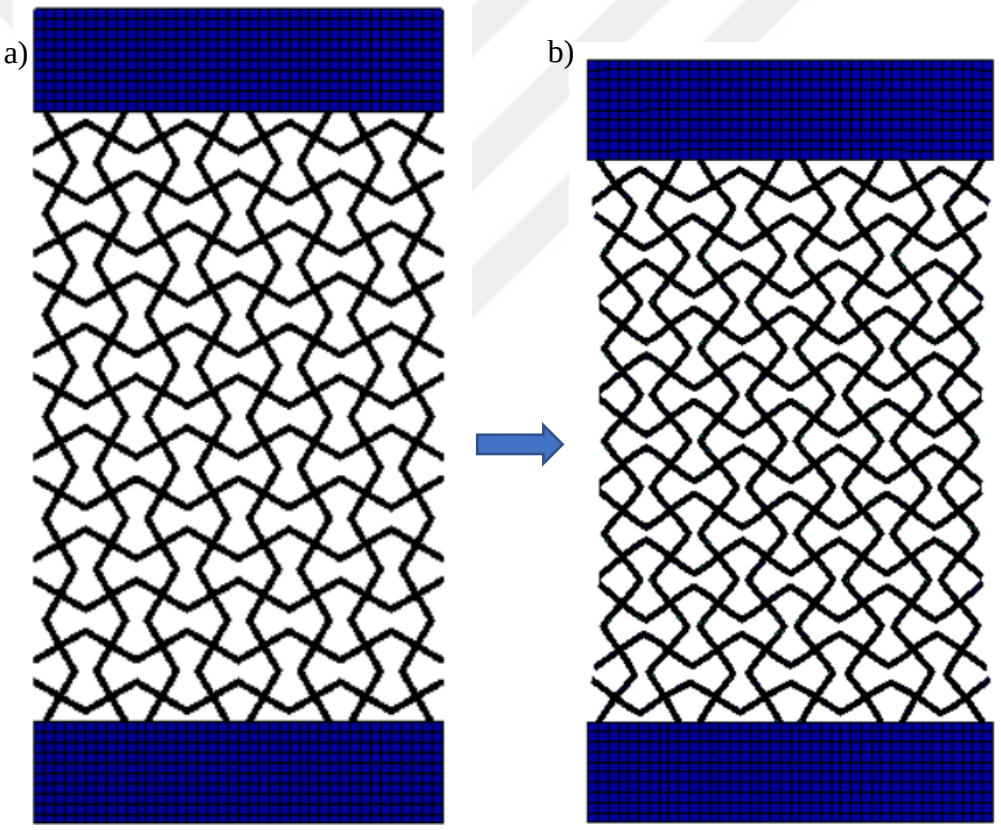


Figure 2.55 Before deformation (a), after deformation (b)

Improved 1. Geometry Static Analysis Results

Sharp corners are eliminated in the optimized geometry and the lattice structure is constructed according to the equation shown in the previous sections. According to the

completed static structural analysis, the maximum equivalent stress was calculated as 35.64 MPa. The average displacement of the upper bar was accepted as the displacement. Thus, the maximum deformation was calculated as 0.125 mm (Figure 2.57.).

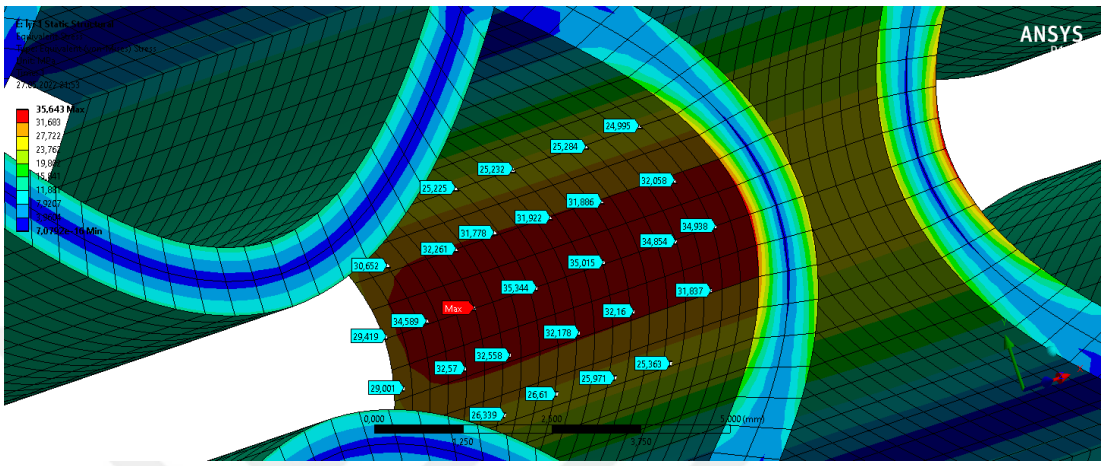


Figure 2.56 Improved geometry 1 equivalent stress

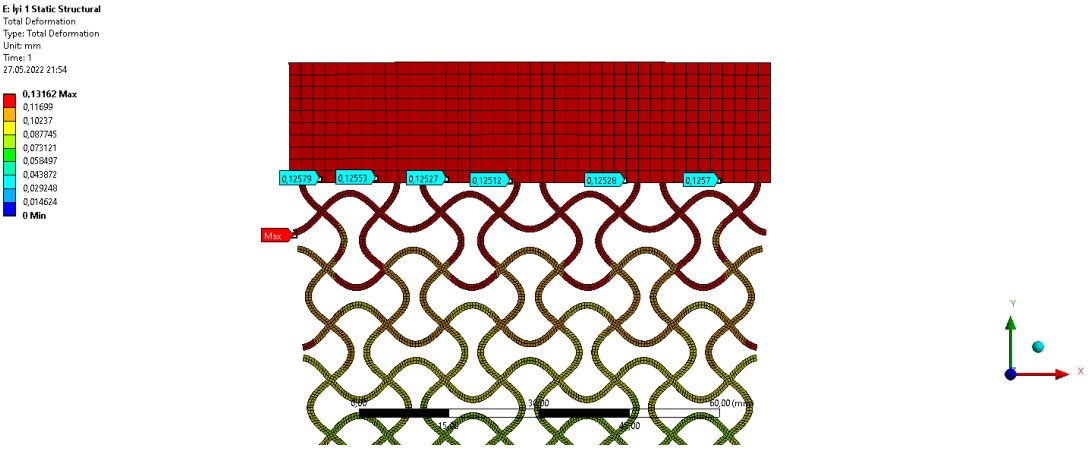


Figure 2.57 Improved geometry 1 equivalent stress

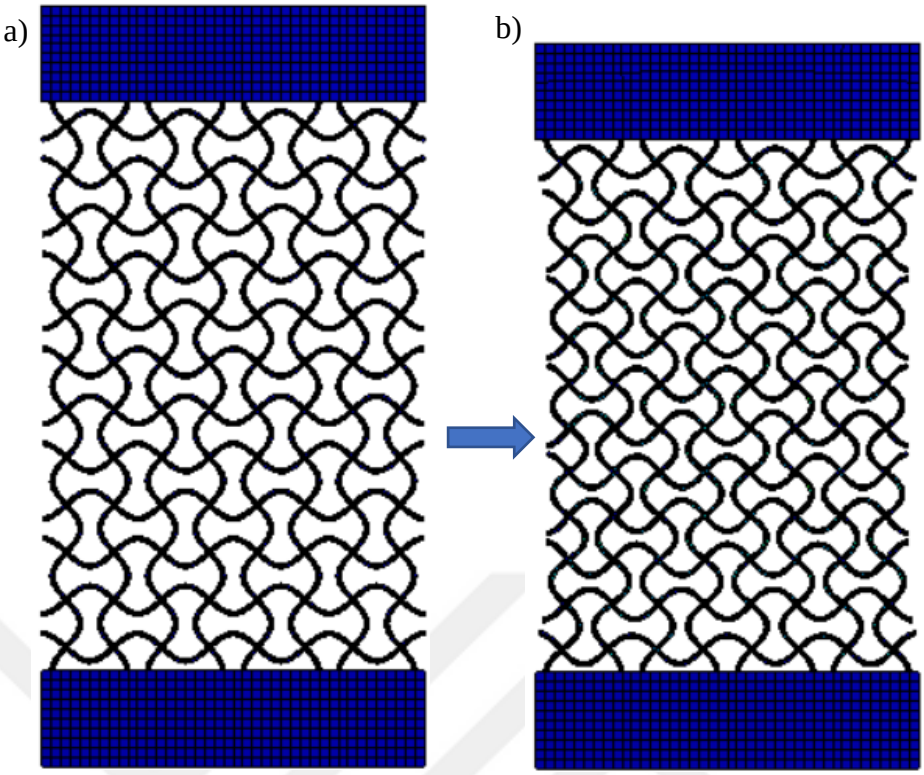


Figure 2.58 Before deformation (a), after deformation (b)

Improved 2. Geometry Static Analysis Results

Thanks to the support columns added in the improved 2nd geometry, the stress level and deformation have decreased significantly. The maximum equivalent stress was calculated as 8.46 MPa. The deformation was found to be 0.00537 mm when the upper grap bar was taken as reference.

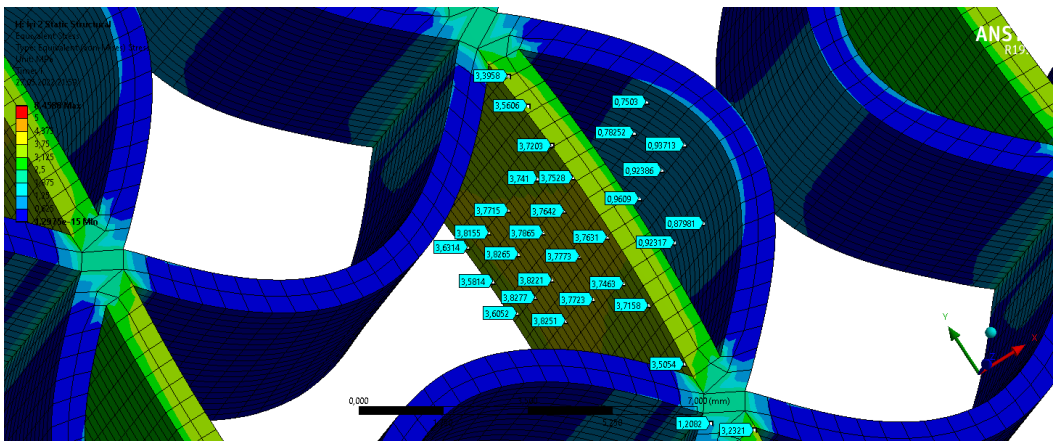


Figure 2.59 Improved geometry 2 equivalent stress

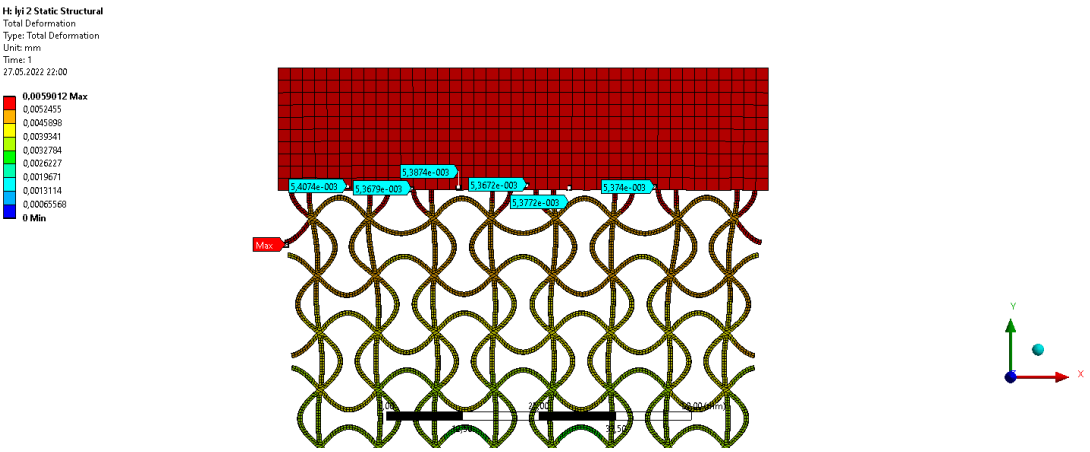


Figure 2.60 Improved geometry 2 equivalent stress

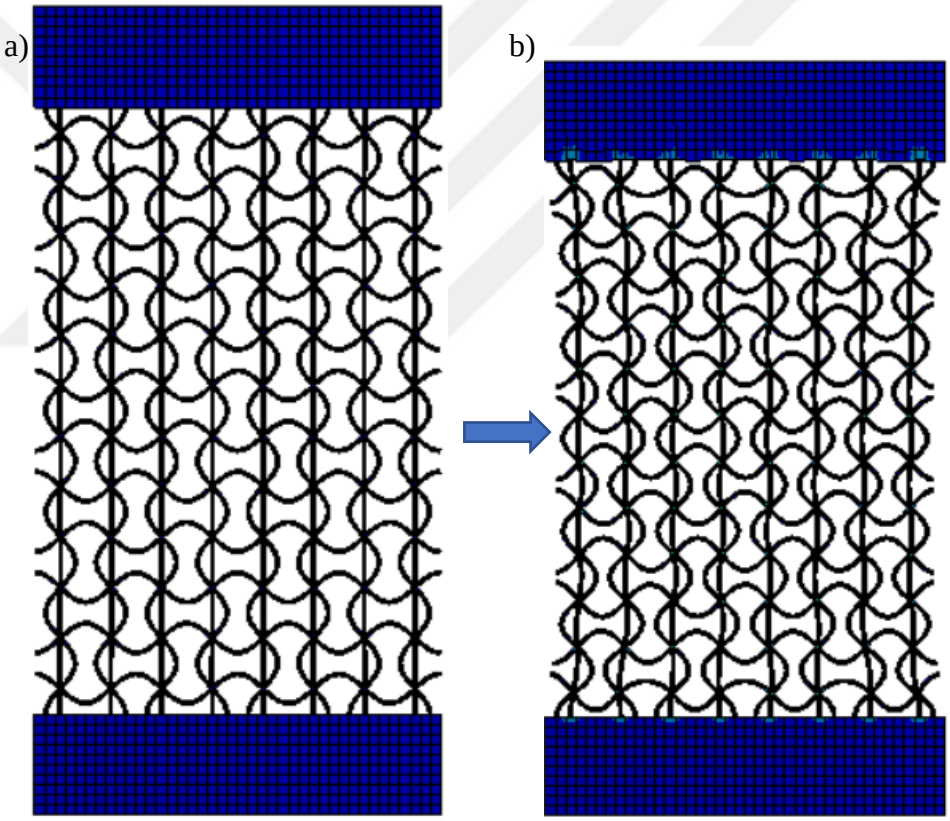


Figure 2.61 Before deformation (a), after deformation (b)

2.3.5 Explicit Dynamics Analysis for Geometries

Explicit Dynamics analyzes were carried out to calculate the shock forces that will act on the lattice structures. With this analysis, the capacity to absorb the shock force of

the lattice structures against the shock effects such as impact/fall applied on the lattice structures will be calculated.

2.3.5.1 Explicit Dynamics Analysis Settings

The basic settings are explained in detail in the previous section while performing the explicit analysis. However, unlike other analyzes completed in contact algorithms, Body Interaction is used. The reason for this may be the contact change on the parts against the instantaneous shock effect. Body Interaction has been adjusted so that new contact formations are automatic.

Fixed Support has been assigned to 5 surfaces of the bottom bar as a boundary condition. In order for the deformation to be observed as a result of loading to be in the desired axis, free displacement is allowed only in the vertical and lateral axes. In order to fully simulate the shock/impact effect, a part of the same size and characteristics as the bar hits the upper bar at a speed of 20000 mm/s. No additional download has been made. The collision time was determined as 0.00005 s.

2.3.5.2 Explicit Dynamics Analysis Resutls

Total deformation, maximum equivalent stress and internal energy change were calculated in Explicit Dynamics analysis results. The obtained values are given in Table 2.16.

Table 2.16 Explicit dynamic analysis results

Analysis Model	Equivalent Stress (MPa)	Total Deformation (mm)	Internal Energy (J)
Normal Lattice Structure	340.35	0.4861	2.4
Improved Lattice Structure 1	128.45	0.48413	1.6
Improved Lattice Structure 2	168.4	0.6156	3.75

Normal Geometry Explicit Dynamics Analysis Results

The equivalent stress level of the normal geometry was found to be very high compared to the other two models. The stress region is concentrated at sharp corners as in the static structural analysis. The maximum stress was calculated as 340 MPa. The total deformation is 0.486 mm. The deformation image is given in Figure 2.63.

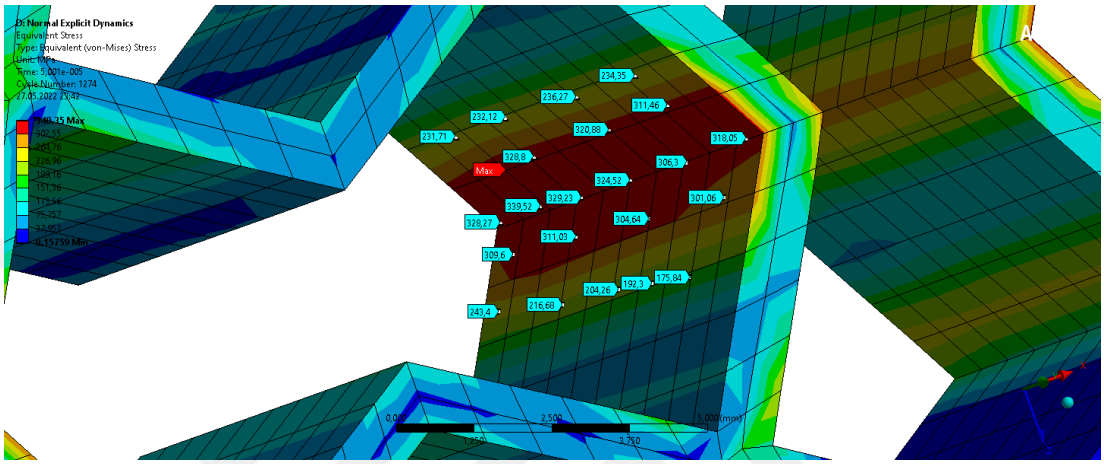


Figure 2.62 Normal geometry equivalent stress details

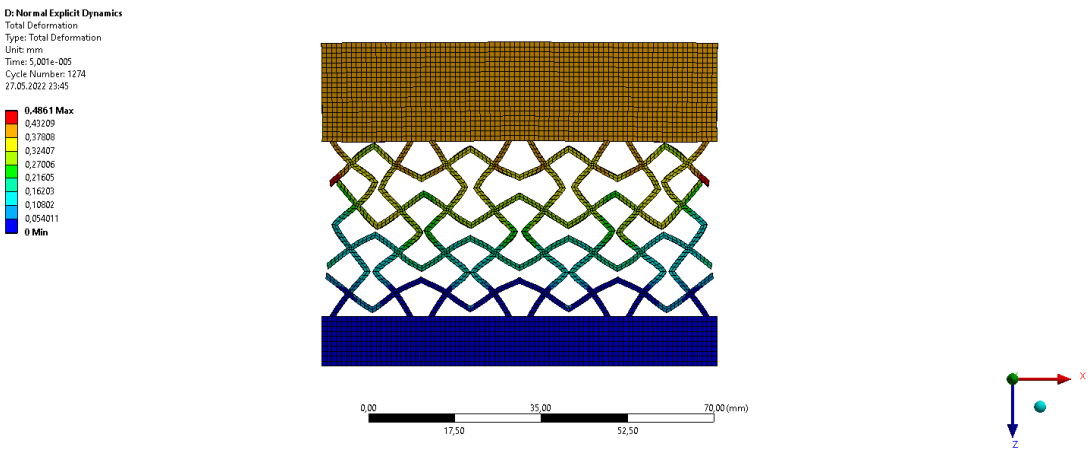


Figure 2.63 Normal geometry deformation

Improved Geometry 1 Explicit Dynamics Analysis Results

The equivalent stress level of the improved 1st geometry was calculated to be approximately 128 MPa. As in Static Structural analysis, the resulting stress is lower than normal geometry. The total deformation is 0.484 mm. This value is close to normal geometry. However, it is higher than the improved 2nd Geometry.

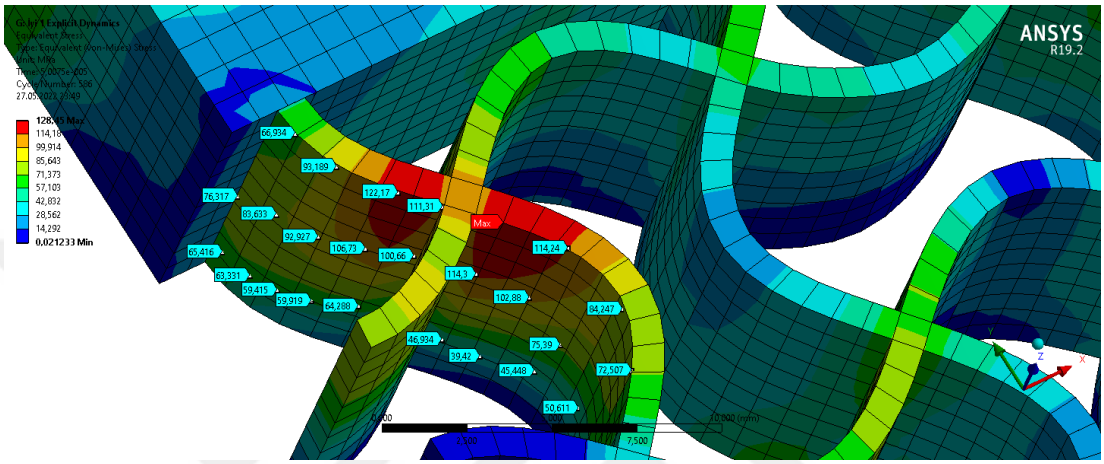


Figure 2.64 Improved geometry 1 equivalent stress

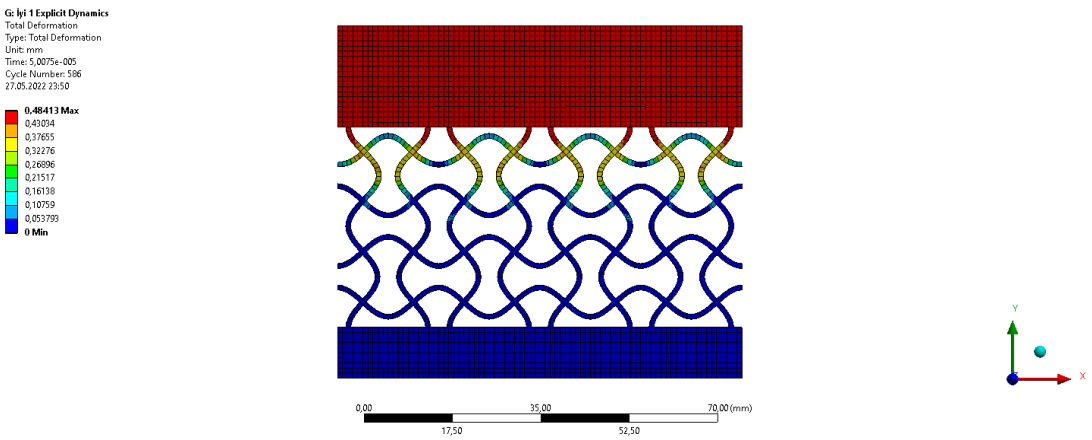


Figure 2.65 Improved geometry 1 deformastion

Improved 1. Geometry Explicit Dynamics Analysis Results

The equivalent stress level on the lattice structure has been improved. It is more than the 1st geometry, it is lower than the normal geometry. A stress of approximately 168

MPa occurs in the lattice twists. The total deformation obtained is a little higher than the other two geometries.

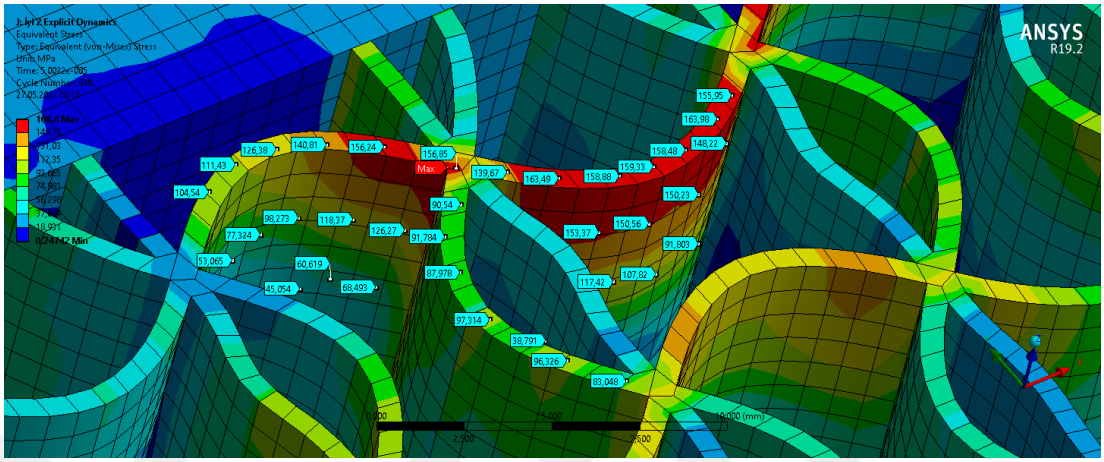


Figure 2.66 Improved 2. geometry equivalent stress

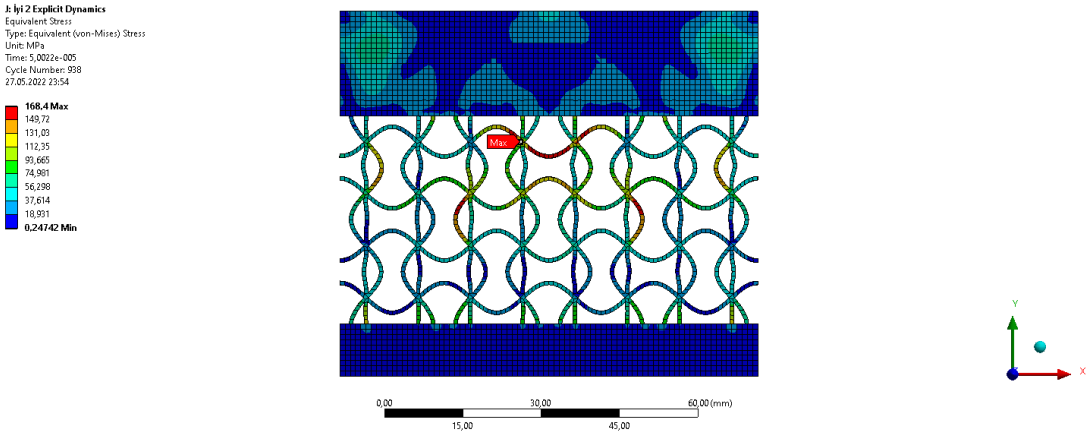


Figure 2.67 Improved 2. geometry deformation

2.3.6 Section Evaluation

Two different geometric improvements were made to a lattice structure determined in the previous section. With these changes, improvements were made in Poisson's ratio and lattice structure strength. In this section, three different structural analyzes of the lattice structures created with the improvements made, Static Structural, Modal and Explicit Dynamics, have been completed.

As a result of the first analysis, the 1st mode value of the lattice structure, which was improved by adding columns, is significantly higher than the other lattice structures. Mode values and mode shapes of the 1st geometry improved with normal geometry are very close to each other.

After the modal analysis, static structural analysis was performed for all three structures. A compression force of 200 N acted on all three lattice structures. The highest stress amount occurred in normal geometry with 41.28 MPa, while 35.64 MPa stress occurred in the improved 1st geometry. In the improved 2nd geometry, the equivalent stress amount is calculated very low compared to the others.

Finally, Explicit Dynamics analysis was performed to calculate the behavior of unique lattice structures against shock effects. According to the results of the analysis, the highest absorption capacity is in the improved 2nd geometry, and the lowest shock absorption capacity is in the normal geometry. The calculated equivalent stress and total deformation results are approximately the same.

CHAPTER 3

RESULTS AND DISCUSSION

In this section, finding the optimum unique lattice structure according to the variable parameters presented in the methodology section, geometric improvement of the optimum lattice structure and numerical models of the improvements, and finally, the results of the structural analysis for new unique lattice structures with geometric improvement will be shared and these results will be evaluated.

3.1 Calculation of Poisson's Ratio of Lattice Structure According to Variable Parameters

Firstly, a unique lattice structure was created, inspired by the figures and geometries examined in the literature. In order to calculate the lowest Poisson's ratio of the formed lattice structure, evaluation was made according to various parameters. Before the evaluation, the lattice structure that combined by the unit cells were determined so that the parameters could be applied at a basic level. Two different parameters, the thickness, which is thought to have an effect on the Poisson's ratio, and the angle made with the nominal axis, were applied on the original lattice structure.

The outer dimensions of the unit cell are determined as 10×10×10 mm to form a cube. Angle and thickness parameters are applied on the unit cell. A total of three different thicknesses, 1, 2 and 3 mm, were taken as reference. As an angle; A total of 5 different values, 0, 10, 20, 26.52, and 30°, were taken as reference. 15 different unit cells were created for the unique lattice structure created.

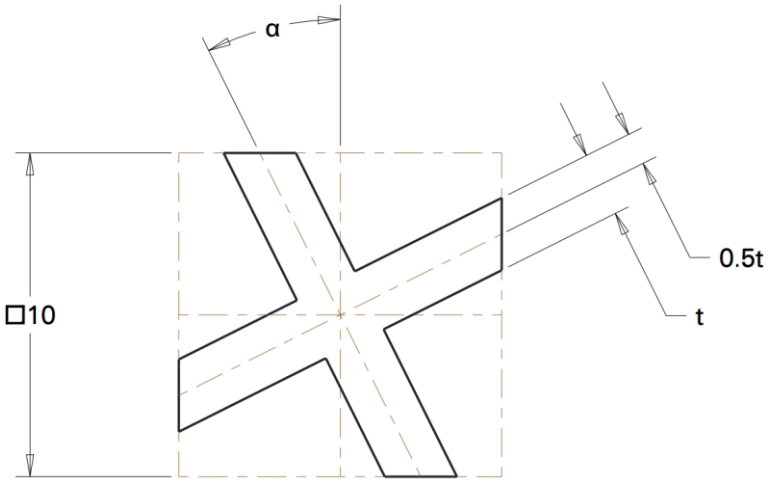


Figure 3.1 Parameters of unit cell

The lattice structure is formed by combining 4 unit cells. In order to calculate the Poisson's ratio of the lattice structure, the matrix geometry was formed by combining the lattice structures. Poisson's ratio analyzes and calculations were made on matrix geometry.

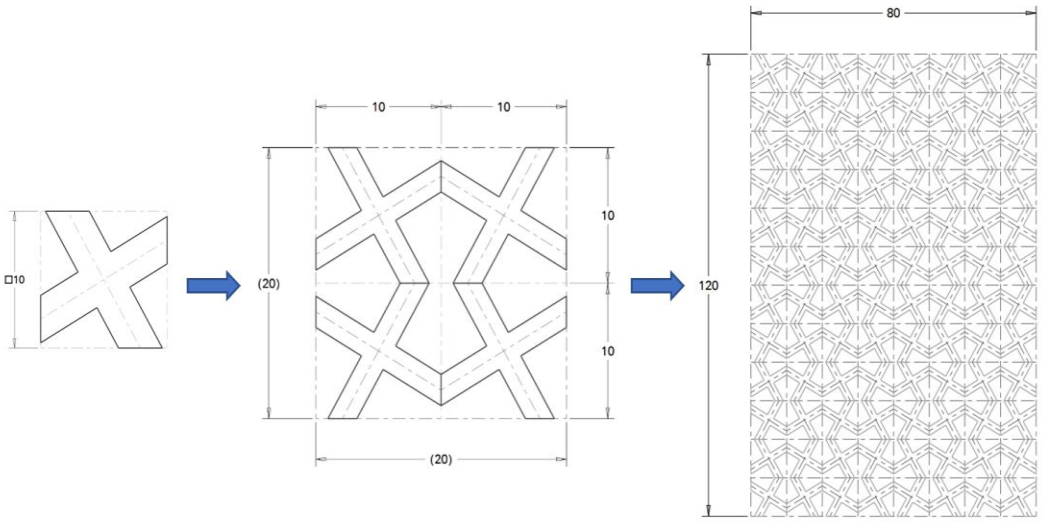


Figure 3.2 Unit Cell, lattice structure and matrix geometry

While calculating the Poisson's ratio, the analysis program Ansys 19.2, which works with the finite element method, was used. Poisson's ratio calculations were made statically for all structures. While performing the analyses, no force or pressure was

given due to the different thicknesses and angles of the unit cells, displacement was given as loading. In this way, all analyzes were completed within the elastic deformation region of the material used.

Table 3.1 Results of analysis for Poisson's ratio calculation

Analysis No	ΔL_y	L_{y_1}	ΔL_x	L_{x_1}	v
1	0.10	120	-0.0013	50	0.03
2	0.10	120	0.0186	50	-0.45
3	0.10	120	0.0269	50	-0.65
4	0.10	120	0.0287	50	-0.69
5	0.10	120	0.0293	50	-0.70
6	0.10	120	-0.0030	50	0.07
7	0.10	120	0.0073	50	-0.18
8	0.10	120	0.0193	50	-0.46
9	0.10	120	0.0240	50	-0.58
10	0.10	120	0.0258	50	-0.62
11	0.10	120	-0.0048	50	0.12
12	0.10	120	0.0014	50	-0.03
13	0.10	120	0.0115	50	-0.28
14	0.10	120	0.0174	50	-0.42
15	0.10	120	0.0202	50	-0.48

While calculating the Poisson's ratio, the deformation probe and directional deformation tools in the program were used. These tools give the displacement in the desired axis according to the results of the analysis. In order not to be affected by the free movement of the unit cells on the edges of the matrix geometry, the unit cells within one of the edges were taken as reference. The Poisson's ratio calculation method is shown in detail in section 2.1.3.1.

Table 3.2 Equivalent stress of analyzes

Analysis No	Equivalent Stress (MPa)	Analysis No	Equivalent Stress (MPa)	Analysis No	Equivalent Stress (MPa)
1	151.41	6	212.13	11	256.65
2	122.05	7	182.07	12	245.19
3	79.66	8	147.29	13	233.48
4	58.91	9	127.63	14	206.06
5	49.92	10	115.01	15	135.92

According to the results of the completed analysis, the lowest Poisson's ratio is the unit cell number 5 with a thickness of 1 mm and an angle of 30°, and the Poisson's ratio was found to be -0.70.

3.2 Geometric Improvement of Lattice Structure with the Lowest Poisson's Ratio

The lowest Poisson's ratio was calculated as -0.70 according to the results of the analysis completed according to various parameters of the unique lattice structure created. The lowest Poisson's ratio is obtained with a thickness of 1 mm and a unit cell of 30°.

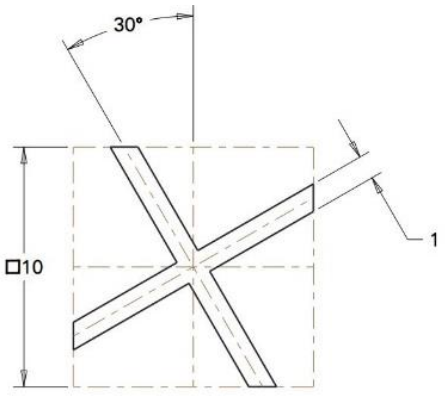


Figure 3.3 Optimum unit cell demonstration

In this section, the geometrical improvement of the lattice structure with the lowest Poisson's ratio has been made and the mathematical models of these improvements have been created.

As a result of the improvements made, the mass was kept constant so that the unit cells could be compared more meaningfully. In order to keep the masses constant, the thickness of the unit cells was revised after the improvement was made.

In total, two different geometric improvements were applied. First, the removal of sharp corners formed by combining unit cells; the second is the addition of a support column. In both methods, it is aimed to increase the strength of the lattice structure without worsening the Poisson's ratio.

The lattice structure is formed by the union of the unit cells. Therefore, while applying the first method, the center and edge points of the unit cells are kept constant. Thus, the original of the determined lattice structure was preserved. A sinus curve is formed by keeping the center and edge points of the unit cell constant.

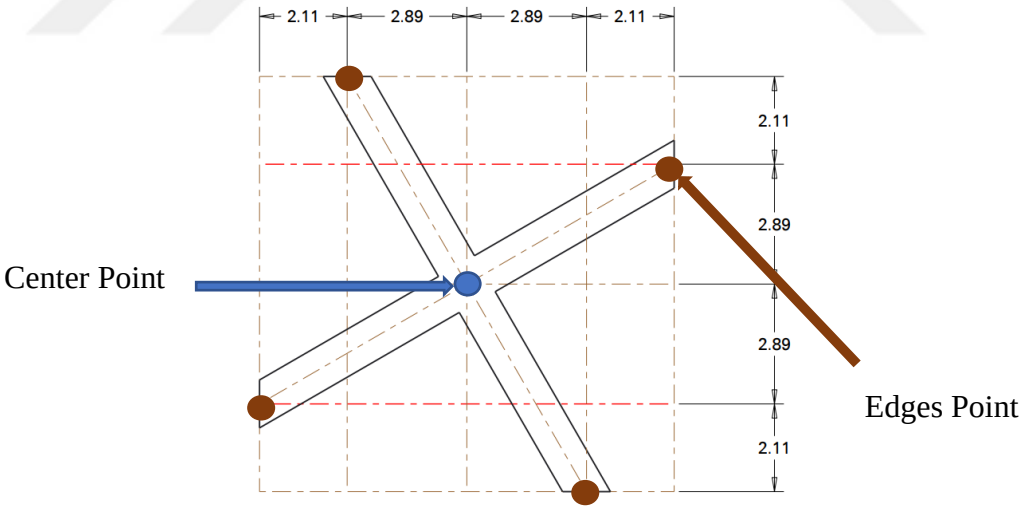


Figure 3.4 Center and edge points are fixed

The edge points form the maximum and minimum values of the unit cell. The coefficient in front of the sinus is taken as 2.89, which is the peak, for the unit cells to combine with each other tangentially. Thus, when sinus = 1, it equals 2.89mm, which is the junction of the lattice structure.

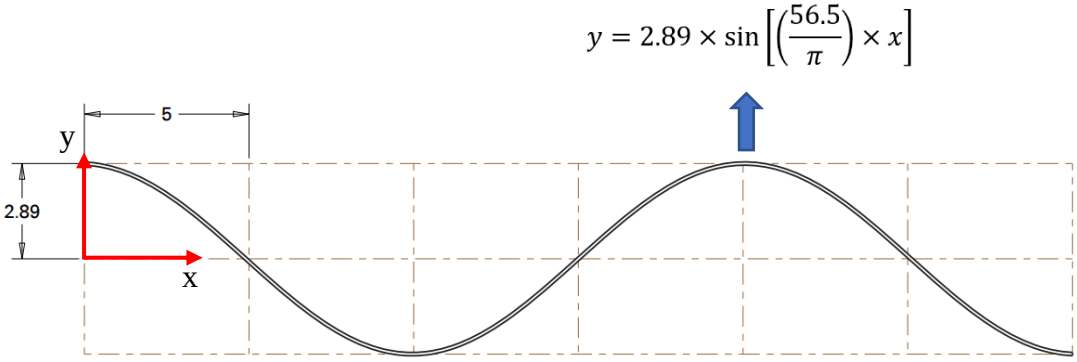


Figure 3.5 Improvement equation demonstration

The convergence method was used while creating the inside of the sinus curve. As the first iteration, the values between 0 and 90 were increased by 10 points and the calculation was made for the whole. According to the results of the first iteration, the coefficient in the sinus was determined to be between 50 and 60.

For the second iteration, the values between 50 and 60 were increased by 1 point and the same calculation was made again. According to the results of the second iteration, the coefficient is between 56 and 57.

In the third iteration, the values between 56 and 57 were increased by 0.1 points and recalculations were completed. According to the calculations, if the coefficient is 56.5, the result is 2.89. Thus, the equation converged 100%.

As a result of the first method, only the unit cell was formed with the obtained equation. The thickness is taken as 0.97 mm so that the mass is the same as the normal unit cell.

In the second method, in addition to the first method, a support column is added to the axis of the lattice structure that is exposed to the force. The mass was kept constant by taking the thickness of 0.7 mm.

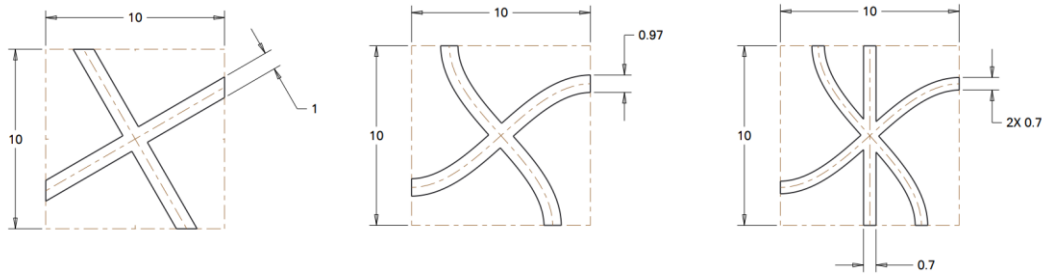


Figure 3.6 Unit cells demonstraions

The masses of the formed unit cells were found to be 5.97g for the first and third unit cells, and 5.94g for the second unit cell. There is a negligible 0.5% difference between the unit cells with the highest and lowest mass.

Table 3.3 Poisson's ratio and unit cell volume change

Analysis Model	V_{UC}	ΔV	**Poisson Ratio (ν)**
Normal Geometry	220.9	0%	-0.70
Improved Geometry 1	219.6	-0.5%	-0.78
Improved Geometry 2	220.9	0%	-0.73

In order to observe the effect of the completed geometric improvements, the analyzes made in the first section were applied exactly. According to the results of the analysis obtained, the Poisson's ratio of the lattice structure with only the first improvement was calculated as -0.78, and the Poisson's ratio of the lattice structure with both geometric improvements was calculated as -0.73.

Table 3.4 Results of Analysis for Poisson's ratio calculation

Analysis Model	ΔL_y	L_{y_1}	ΔL_x	L_{x_1}	v
Normal Geometry	0.1	120	0.0293	50	-0.70
Improved Geometry 1	0.1	120	0.0326	50	-0.78
Improved Geometry 2	0.1	120	0.0299	50	-0.73

3.3 Comparison of Obtained Lattice Structures with Structural Analysis

As a result of two different geometric improvements applied to the unit cells, a total of three different lattice structures were formed. Static structural, modal and explicit Dynamics analyzes were completed on the matrix geometries created to compare the mechanical properties of these lattice structures.

The lattice structure measurements obtained from the unit cell and unit cells are the same in all analyses. However, since the solution times are very long in explicit Dynamics analysis, the matrix geometry of this analysis is 4×2 lattice structure. In the matrix geometry of the static structural/modal analysis, a 6×4 matrix was created as in the previous analyses. Other analysis settings are presented in the corresponding analysis settings sections.

First, the modal analysis is completed. According to the modal analysis results, the first mode was calculated as the lattice structure with the highest matrix structure at 153.73 Hz, in which both improvements were applied. This value is much higher than other lattice structures. Then comes the original geometry with 61.47 Hz. The lattice structure with the lowest first mode value was calculated with 52.96 Hz as the geometry in which only the first improvement was made.

Improved 1st Geometry and 6th Mode shapes of normal geometry exhibit auxetic behavior. No auxetic behavior in the first 6 mods for the improved 2nd Geometry.

Static structural module was used as the second structural analysis. In this analysis, unlike the previous sections, 200 N force is defined for all three matrix structures instead of displacement for loading. The lowest stress is in the improved 2nd geometry with 8.46 MPa, this value is very low compared to other lattice structures. The highest stress amount was found in normal geometry with 41.28 MPa. Improved 1. The stretch of the geometry is 35.64 MPa. There was a 13.66% difference in equivalent stress between the normal geometry and the improved 1st geometry. There was a 79.51% difference between the normal geometry and the improved 2nd geometry.

Table 3.5 Stress change and Poisson's ratio for static analysis

Analysis Model	Equivalent Stress (MPa)	Stress Change	Poisson Ratio
Normal Geometry	41.28	0	-0.7
Improved Geometry 1	35.643	-13.66%	-0.78
Improved Geometry 2	8.4588	-79.51%	-0.73

When the total displacement results are compared, the highest displacement occurred in the 1st Geometry, which was improved by 0.13 mm. The lowest displacement is in the 2nd Geometry, which is improved by 0.0059 mm. The normal geometry is less deformed than the improved geometry 1, but the equivalent stress is higher. Improved Geometry 1 was calculated as the most flexible lattice structure among the compared geometries.

Table 3.6 Stress change and Poisson's ratio for static analysis

Analysis Model	Equivalent Stress (MPa)	Stress Change	Poisson Ratio
Normal Geometry	340.35	0	-0.7
Improved Geometry 1	128.45	-62.26%	-0.78
Improved Geometry 2	168.4	-50.52%	-0.73

Finally, explicit Dynamics analyzes were performed on matrix geometries consisting of lattice structures. In the analysis, the collision event was simulated. An object moving with a speed of 20000 mm/s collides on the matrix geometries. As a result of the collision, the highest stress occurred in normal geometry. As a result of the normal geometry collision, it reached an equivalent stress of 340.35 MPa and passed the breaking strength value and failed. In the improved geometries, the calculated stresses

are within the elastic region, failure did not occur. Improved 1. Geometry is the lattice structure with the lowest equivalent stress with 128.45 MPa due to its elastic structure. The equivalent stress of the improved 2nd geometry is 168.4 MPa and the stress zone is formed in the support columns.

CHAPTER 4

CONCLUSION AND RECOMMENDATIONS

Within the scope of this study, the lowest Poisson’s ratio was found according to various parameters of the unique lattice structure. Two different geometric improvements were made by keeping the mass constant on the lattice structure with the lowest Poisson’s ratio. As a result of these improvements, an improvement in the Poisson’s ratio was observed. Three different structural analyzes, modal, static structural and explicit dynamics, were applied to the lattice structures obtained with the completed geometric improvements.

Static structural analyzes were completed according to the angle and thickness parameters to find the optimum Poisson’s ratio of the unique lattice structure created. According to the results of the completed analysis, the lowest Poisson’s ratio was found to be -0.70. The results obtained from the first section can be listed as follows;

- Poisson's ratio depends on thickness. As the thickness increases, the Poisson’s ratio approaches 0 (zero). As the thickness decreases, the Poisson’s ratio tends to move away from 0. Values between 1 mm and 3 mm were evaluated in the study. When the thickness is more than 3 mm, conflict is seen at the edges of the lattice structures. For this reason, the upper limit was chosen as 3 mm. As the thickness decreases below 1 mm, the production cost increases exponentially. For this reason, 1 mm was chosen as the lower limit.
- Poisson's ratio depends on the lattice angle. The Poisson's ratio moves away from 0 as the angle between the unit cells and the nominal axis increases. In the angle parameter, the limits are set between 0 and 30°. When the angle is desired to be increased more, the corners of the lattice structures merge and the unique structure is distorted.

Geometric improvements were applied to the optimum lattice structure with the lowest Poisson’s ratio obtained as a result of the first analysis. Mathematical models of the improvements were created. As a result of the analysis of the lattice

structures created with mathematical models, the Poisson's ratios were improved and it was concluded that the method was correct. The results obtained from the second part can be listed as follows;

- Geometric improvements can be made by using the numerical method introduced in the literature in different lattice structures. In this study, a mathematical model consisting of 3 lines (combining 3 curves) was created by keeping the edge and center points constant.
- Poisson's ratios usually approach 0 when the support column is added in the literature. However, in the study, it was revealed that the column added on the force axis improved the Poisson's ratio.

Modal, static structural and explicit analyzes were run on lattice structures with geometric improvements. Various results were obtained for all 3 geometries. The results can be listed as follows;

- When the support column is added, the mod value of the lattice structure increases significantly and reduces the risk of resonance.
- The 1st Mode value of the improved 1st Geometry is a bit lower than the normal geometry. The reason for this was interpreted as the improved 1st geometry being more flexible.
- When equivalent stresses were compared in Static Structural analysis, the most durable structure was calculated as the 2nd improved geometry. The support column acted as the main force carrier.
- There is a significant stress difference between the improved 1st geometry and the normal geometry. The effect of the applied numerical method on the lattice structure has been demonstrated.
- According to the displacement results in the static structural analysis, the most improved 1st geometry was deformed due to its flexible structure. However, this deformation is within the elastic region. The least deformation is on the 2nd optimized geometry.

- When comparing the explicit analyzes, the lowest equivalent stress was seen on the improved 1st geometry due to its flexible structure. On the improved 2nd geometry, stress has occurred in the columns. The highest stress is in normal geometry and the lattice structure has ruptured.
- Adding a support column in static loads adds extra strength to the lattice structure. However, the improved 1st Geometry comes to the fore due to its flexible structure in cases such as shock/collision.

REFERENCES

[1] Groover, M. P. Engineering Materials. Fundamentals of modern manufacturing: materials, processes, and systems. USA: Wiley. 2020

[2] Hibbeler, R. C. Mechanical Properties of Materials. Mechanics of materials. Singapore: Pearson. 2014

[3] Callister, W. D. Mechanical Properties. Fundamentals of materials science and engineering. London: Wiley. 2000

[4] Liu, Y., Hu, H. A review on auxetic structures and polymeric materials. Scientific research and essays, 5(10), 1052-1063. 2010

[5] Alderson, A., Alderson, K. L. Auxetic materials. Proceedings of the Institution of Mechanical Engineers, Part G: Journal of Aerospace Engineering, 221(4), 565-575. 2007

[6] Evans, K. E., Nkansah, M. A., Hutchinson, I. J., Rogers, S. C. Molecular network design. Nature, 353(6340), 124-124. 1991

[7] Love, A. E. H. Stress-Strain Relations. *A treatise on the mathematical theory of elasticity*. Cambridge: Cambridge university press. 1892

[8] Dunn, M. L., Ledbetter, H. Poisson's ratio of porous and microcracked solids: Theory and application to oxide superconductors. Journal of Materials Research, 10(11), 2715-2722. 1995

[9] Gunton, D. J., Saunders, G. A. The Young's modulus and Poisson's ratio of arsenic, antimony and bismuth. Journal of Materials Science, 7(9), 1061-1068. 1972

[10] Li, Y., Chung, D. Y. The anisotropic behavior of Poisson's ratio, Young's modulus, and shear modulus in crystals with different symmetries. physica status solidi (a), 46(2), 603-610. 1978

[11] Lakes, R. Foam structures with a negative Poisson's ratio. Science, 235(4792), 1038-1040. 1987

[12] Choi, J. B., Lakes, R. S. Fracture toughness of re-entrant foam materials with a negative Poisson's ratio: experiment and analysis. International Journal of fracture, 80(1), 73-83. 1996

[13] Alderson, A., Alderson, K. L., McDonald, S. A., Mottershead, B., Nazare, S., Withers, P. J., Yao, Y. T. Piezomorphic materials. Macromolecular Materials and Engineering, 298(3), 318-327. 2013

[14] Mir, M., Ali, M. N., Sami, J., Ansari, U. Review of mechanics and applications of auxetic structures. Advances in Materials Science and Engineering, 2014.

[15] Williams, J. L., Lewis, J. L. Properties and an anisotropic model of cancellous bone from the proximal tibial epiphysis. 1982

[16] Veronda, D. R., Westmann, R. A. Mechanical characterization of skin finite deformations. Journal of biomechanics, 3(1), 111-124. 1970

[17] Frolich, L. M., LaBarbera, M., Stevens, W. P. Poisson's ratio of a crossed fibre sheath: the skin of aquatic salamanders. Journal of Zoology, 232(2), 231-252. 1994

[18] Lees, C., Vincent, J. F., Hillerton, J. E. Poisson's ratio in skin. Bio-medical materials and engineering, 1(1), 19-23. 1991

[19] Silva, M. J., Hayes, W. C., Gibson, L. J. The effects of non-periodic microstructure on the elastic properties of two-dimensional cellular solids. International Journal of Mechanical Sciences, 37(11), 1161-1177. 1995

[20] Evans, K. E. Auxetic polymers: a new range of materials. Endeavour, 15(4), 170-174. 1991

[21] Underhill, R. S. Defense applications of auxetic materials. Advanced Materials, 1(1), 7-12. 2014

[22] Scarpa, F. Auxetic materials for bioprostheses [In the Spotlight]. IEEE Signal Processing Magazine, 25(5), 128-126. 2008

[23] Brańka, A. C., Heyes, D. M., Wojciechowski, K. W. Auxeticity of cubic materials. Physica status solidi (b), 246(9), 2063-2071. 2009

[24] Li, Z., Wang, K. F., Wang, B. L. Indentation resistance of brittle auxetic structures: Combining discrete representation and continuum model. Engineering Fracture Mechanics, 252, 107824. 2021

[25] Evans, K. E., Alderson, A. Auxetic materials: functional materials and structures from lateral thinking!. Advanced materials, 12(9), 617-628. 2000

[26] Choi, J. B., Lakes, R. S. Nonlinear analysis of the Poisson's ratio of negative Poisson's ratio foams. Journal of Composite Materials, 29(1), 113-128. 1995

[27] Choi, J. B., Lakes, R. S. Non-linear properties of polymer cellular materials with a negative Poisson's ratio. Journal of Materials Science, 27(17), 4678-4684. 1992

[28] Panico, M., Langella, C., Santulli, C. Development of a biomedical neckbrace through tailored auxetic shapes. Emerging Science Journal, 1(3), 105-117. 2017

[29] Sanami, M., Ravirala, N., Alderson, K., Alderson, A. Auxetic materials for sports applications. Procedia Engineering, 72, 453-458. 2014

[30] Foster, L., Peketi, P., Allen, T., Senior, T., Duncan, O., Alderson, A. Application of auxetic foam in sports helmets. Applied Sciences, 8(3), 354. 2018

[31] Yang, W., Li, Z. M., Shi, W., Xie, B. H., Yang, M. B. Review on auxetic materials. Journal of materials science, 39(10), 3269-3279. 2004

[32] Yang, H., Wang, B., Ma, L. Mechanical properties of 3D double-U auxetic structures. International Journal of Solids and Structures, 180, 13-29. 2019

[33] Ranjbar, M., Boldrin, L., Scarpa, F., Neild, S., Patsias, S. Vibroacoustic optimization of anti-tetrachiral and auxetic hexagonal sandwich panels with gradient geometry. Smart Materials and Structures, 25(5), 054012. 2016

[34] Li, X., Wang, Q., Yang, Z., Lu, Z. Novel auxetic structures with enhanced mechanical properties. Extreme Mechanics Letters, 27, 59-65. 2019

[35] Yang, C., Vora, H. D., Chang, Y. Behavior of auxetic structures under compression and impact forces. Smart Materials and Structures, 27(2), 025012. 2018

[36] Gao, Q., Liao, W. H. Energy absorption of thin walled tube filled with gradient auxetic structures-theory and simulation. International Journal of Mechanical Sciences, 201, 106475. 2021

[37] Alomarah, A., Masood, S. H., Sbarski, I., Faisal, B., Gao, Z., Ruan, D. Compressive properties of 3D printed auxetic structures: experimental and numerical studies. Virtual and physical prototyping, 15(1), 1-21. 2020

[38] Lee, W., Jeong, Y., Yoo, J., Huh, H., Park, S. J., Park, S. H., Yoon, J. Effect of auxetic structures on crash behavior of cylindrical tube. Composite Structures, 208, 836-846. 2019

[39] Wang, X. T., Wang, B., Wen, Z. H., Ma, L. Fabrication and mechanical properties of CFRP composite three-dimensional double-arrow-head auxetic structures. Composites Science and Technology, 164, 92-102. 2018

[40] Alomarah, A., Masood, S. H., Ruan, D. Out-of-plane and in-plane compression of additively manufactured auxetic structures. Aerospace science and technology, 106, 106107. 2020

[41] Johnston, R., Kazancı, Z. Analysis of additively manufactured (3D printed) dual-material auxetic structures under compression. Additive Manufacturing, 38, 101783. 2021

[42] Rad, M. S., Hatami, H., Alipouri, R., Nejad, A. F., Omidinasab, F. Determination of energy absorption in different cellular auxetic structures. Mechanics & Industry, 20(3), 302. 2019

[43] Shepherd, T., Winwood, K., Venkatraman, P., Alderson, A., Allen, T. Validation of a finite element modeling process for auxetic structures under impact. physica status solidi (b), 257(10), 1900197. 2020

[44] Najafi, M., Ahmadi, H., Liaghat, G. Experimental investigation on energy absorption of auxetic structures. Materials today: proceedings, 34, 350-355. 2021

[45] Subramani, P., Rana, S., Oliveira, D. V., Fangueiro, R., Xavier, J. Development of novel auxetic structures based on braided composites. Materials & Design, 61, 286-295. 2014

[46] Kaya, F. Afyonkarahisar minareleri. Taşpınar Dergisi, 5, 40-50. 2010

[47] ANSYS Classic 11.0 and ANSYS Workbench 11.0 Help Manual

CURRICULUM VITAE

PERSONAL INFORMATION

Name Surname **:** İbrahim AKSOY
Date of Birth **:**
Phone **:**
E-mail **:**

EDUCATION

High School **:** Samanyolu Anatolian High School / ANKARA (2010-2014).

Bachelor **:** Ankara Yıldırım Beyazıt University, Faculty of Engineering and Natural Sciences, Mechanical Engineering / ANKARA (2014-2019)

Master Degree **:** Ankara Yıldırım Beyazıt University / Graduate School Of Natural And Applied Sciences / ANKARA (2019-continued)

WORK EXPERIENCE

Mechanical Design Engineer: Promec Engineering Co. Ltd. / (2020-continued)

TOPICS OF INTEREST

- Negatif Poisson’s ratio and auxetic structures
- Kaizen philosophy and continuous improvement methods
- Gear and transmission system designs
- Nitrogen gas purging systems

PRESENT ORGANIZED SOURCES / PRESENTATION

I. Aksoy, İ., & Toktaş İ. Mathematical modeling of geometric improvement to reduce stress without increasing the mass and Poisson ratio of the lattice structure. 7. International Congress on Engineering and Technology Management. 2022.

II. Alparslan, C., Aksoy, İ., & Toktaş, İ.Toplam kalite yönetiminde ahilik ve kaizen felsefesi. 9. International Symposium on Innovative Technologies in Engineering and Science. 2021.

III. Aksoy, İ., & Şengül, H. Azot gazı ile yapılan arındırma işlemlerinde vakum özelliğinin işlem süresi ve kuru gaz sarfiyatı üzerine etkisinin deneysel araştırılması. 9. International Congress on Engineering, Architecture and Design. 2022.

IV. Mazıbaş F., Şengül, H., & Aksoy, İ. Sikloid dişli kutusu. 9. International Congress on Engineering, Architecture and Design. 2022.